NOTE TO USERS

MICROTUBULE AND F-ACTIN INTERACTION IN THE CYTOSKELETAL SYSTEM OF NON-MAMMALIAN ERYTHROCYTES AND THROMBOCYTES

by

KYENG GEA LEE

A dissertation submitted to the Graduate Faculty in Biology

in fulfillment of the requirements for the degree of

Doctor of Philosophy, The City University of New York

2004

INFORMATION TO USERS

The quality of this reproduction is dependent upon the quality of the copy submitted. Broken or indistinct print, colored or poor quality illustrations and photographs, print bleed-through, substandard margins, and improper alignment can adversely affect reproduction.

In the unlikely event that the author did not send a complete manuscript and there are missing pages, these will be noted. Also, if unauthorized copyright material had to be removed, a note will indicate the deletion.

ProQuest Information and Learning Company
300 North Zeeb Road
P.O. Box 1346
Ann Arbor, MI 48106-1346

This manuscript has been read and accepted for the Graduate Faculty in Biology in satisfaction of the dissertation requirement for the degree of Doctor of Philosophy.

5/27/04
Date

William D. Cohen
Chair of Examining Committee,
Dr. William D. Cohen, Hunter College

6/1/04
Date

Richard L. Chappell
Executive Officer,
Dr. Richard L. Chappell

Jesus G. Angulo
Dr. Jesus Angulo, Hunter College

Peter Lipke
Dr. Peter Lipke, Hunter College

Dr. Dan Eshel, Brooklyn College

Ray Gavin
Dr. Ray Gavin, National Science Foundation

Babette Weksler
Dr. Babette Weksler,
Weill Medical College of Cornell University

Supervising Committee

The City University of New York

Abstract

MICROTUBULE AND F-ACTIN INTERACTION
IN THE CYTOSKELETAL SYSTEM OF
NON-MAMMALIAN ERYTHROCYTES AND THROMBOCYTES

by

KYENG GEA LEE

Adviser: Professor William D. Cohen

Interaction between microtubules and actin filaments may be crucial for common cell processes such as cytokinesis and for the specific functions of differentiated cells. Microtubules and actin filaments are known to have different mechanical properties, and proper distribution of these elements can provide cells with distinctive characteristics. This work focuses on functional and structural interaction of microtubules and actin filaments in nucleated erythrocytes and thrombocytes. The cytoskeleton of the nucleated erythrocytes contains a peripheral or marginal band of microtubules responsible for cell shape maintenance. Confocal fluorescence microscopy shows that the marginal band colocalizes with a band of F-actin in non-mammalian vertebrate erythrocytes. Functionally, the F-actin band is implicated in maintaining the ellipsoidal shape of the marginal band as revealed by studies using proteases. Also, hyperstabilization of the F-actin band protects against low temperature-induced disassembly of marginal band microtubules, showing that microtubule stability in the marginal band is dependent on the

F-actin band. Studies using pointed erythrocytes, induced by temperature cycling, show that hyperstabilization of the F-actin band reduces the number of pointed cells generated. Since these cells contain pointed or fractured marginal bands, this indicates that increased stabilization of the F-actin band increases stability of the marginal band. In contrast, thrombocytes exhibit a different form of microtubule and F-actin interaction. In unactivated thrombocytes, which are flattened, ovoid cells, marginal band microtubules colocalize with a band of F-actin in a pattern similar to that of erythrocytes, except that the F-actin band is thinner and localized only at the periphery. Unlike erythrocytes, thrombocytes undergo drastic shape changes when activated by various stimuli. In activated thrombocytes with altered shape, typical F-actin-microtubule colocalization in the marginal band is lost, and F-actin has an outward distribution while microtubules remain central, possibly remodeling the nucleus. Functionally, marginal band microtubules in unactivated thrombocytes are found to be cold labile and their disappearance alters cell shape. Pre-exposure of unactivated thrombocytes to F-actin disassembly-promoting agents blocks normal activation-induced shape change. These findings indicate that thrombocyte microtubules are responsible for maintaining unactivated cell shape, while F-actin is the major driving force for post-activational cell shape changes.

ACKNOWLEDGMENTS

I would like to thank Dr. William D. Cohen for his great mentorship. He has gone out of his way to make it possible for me concentrate in my graduate studies. In moments of trouble, he was there to support me emotionally, materially, and in any other way he could. In moments of excitement, such as those happening from successful experiments, he was there to celebrate with me. I have learned many things from him. Most importantly, however, I have learned through him how to look at the world with a big heart, one that resides in optimism.

This dissertation would not have been possible without his incessant guidance. I just hope that I could be one tenth as good of a teacher as he in my upcoming times.

I would also like to thank Ruben Pinkhasov for his assistance in thrombocyte temperature cycling experiments; Anthony Williams for his help in pointed erythrocyte temperature cycling experiments; Todd Miller for cooperating in thrombocyte shape change experiments; Louie Kerr for technical advice and training on Zeiss laser scanning confocal microscopy; Rudi Rottenfusser for technical advice and training on Zeiss light and fluorescence microscopy; and Dr. Phong Tran for conceptual advice on thrombocyte experiments.

TABLE OF CONTENTS

CHAPTER 1: **Introduction**

1. Overview: microtubule-actin filament interaction

The study of structural and functional synergy between microtubules and actin filaments is in its "infancy" (Gavin, 1997). Representative structural examples include microtubules (MTs) and microfilament networks organized in the basal body fibrillar network complex of ciliated epithelia, neurosensory epithelia, and ciliated protozoa such as *Tetrahymena* or *Paramecium* (Reed *et al.*, 1984; Arikawa and Williams, 1989; Gavin, 1977). Functional interaction between these cytoskeletal elements is well documented in cell division and development. In cell division, centrosome movement requires proper interaction of microtubule and actin as revealed by inhibitor studies (Euteneur and Schliwa, 1985). In cell development, the direction of cortical flow is determined by the distribution of actin microfilaments in the cytoskeleton, which in turn, is determined by the orientation of the microtubules in the spindle (Hird and White, 1993). Similarly in animal cytokinesis, it is well established that location of cleavage furrow is determined by spindle orientation (Strome, 1993). Other examples of microtubule-actin interaction include cytokinesis and nuclear migration in plant cells, cytoplasmic streaming observed in ring canals or cytoplasmic bridges of in *Drosophila* germ line cells, mobility of growth cones in nerve cells, and spindle-associated chromosome movements in crane-fly spermatocytes (Eleftheriou and Palevitz, 1992; Mineyuki and Palevitz, 1990; Kadota and Wada, 1995; Riparbelli and Callaini, 1995; Lin and Forscher, 1993; Forer and Pickette-Heaps, 1998).

More recently, functional interaction between microtubules and actin filaments has been demonstrated for organelle transport. In the giant squid axon, actin filaments have been found abundantly distributed in parallel to long, longitudinal microtubules by confocal microscopy (Bearer and Reese, 1999; Bearer *et al.*, 1999). At the EM level, longitudinal thin sections of extruded axoplasm showed fine microfilaments interwoven among the microtubule bundles. In cross sections, these filaments appeared as 6-8 nm diameter dots distributed on the periphery of a single microtubule or between several microtubules. Furthermore, S1 decoration confirmed that these were actin filaments and showed that the filaments could contact the microtubules in both polarities. Based on these findings, Bearer and Reese (1999) proposed that actin filaments might be structural components within microtubule bundles involved in vesicle transport, and that they might directly function in the transport of vesicles within and outside of MT bundles.

Microtubules and actin filaments are major cytoskeletal elements of many systems, as noted above. The interaction between these two may be crucial for proper occurrence of common cell processes such as cytokinesis and also for the specific function of a particular cell type. Microtubules and actin filaments are known to have different mechanical properties (Janmey *et al.*, 1991) and proper distribution of these elements can provide a cell with flexural rigidity or other mechanical characteristics. For instance, both the nucleated erythrocytes and thrombocytes addressed in this work are subject to constant flow in bloodstream. Such cells are in constant collision with other cells and with the blood vessel, and thus sufficient rigidity is necessary to prevent deformation. However such cells also require sufficient flexibility in order to maneuver through narrow capillaries or through abrupt turns in the blood stream. Therefore, it is

conceivable that microtubules and actin filaments in these cells are arranged in a pattern that would give cell needed flexural rigidity and other mechanically relevant properties.

2. Nucleated Erythrocytes

The cytoskeleton of non-mammalian vertebrate (nucleated) erythrocytes has been a useful model system in previous work. It consists principally of the marginal band (MB) of microtubules (MT), the membrane skeleton (MS), and the intermediate filaments (Figure 1-1). MBs are normally obscured by hemoglobin and treatment of cells with detergents such as Triton X-100 results in a state in which the MB, the nucleus, and the membrane skeleton are visible under phase contrast (Cohen, 1978).

In dogfish, exposure of red cells to 0 °C results in disappearance of the MB, but not the MS, indicating that MB microtubules are cold labile (Cohen *et al.*, 1982). While disassembly of the MB by low temperature does not lead to change of cell shape per se, exposure of cells lacking MBs to mechanical stress results in cell shape deformation (Joseph-Silverstein and Cohen, 1984). This indicates that the function of the MB is to maintain the flattened, biconvex ellipsoidal shape of nucleated erythrocytes. That the function of the MB is to maintain cell shape is further supported by studies of the singly- or doubly-pointed dogfish erythrocytes that occur as anomalous cell types upon prolonged exposure to room temperature. Detergent treatment reveals that these pointed cells contain corresponding pointed marginal bands (Joseph-Silverstein and Cohen, 1984). Furthermore exposure of cells lacking MBs to hyperosmotic conditions results in cell collapse, while those with intact MBs resist. Therefore the MB can be considered as a flexible frame that can deform or support the cell surface from within (Joseph-Silverstein

and Cohen, 1984). This is supported by measurements of extensional and flexural rigidities of protease-isolated MB, which shows that the MB is nearly inextensible and resistant to bending relative to the cell membrane (Waugh *et al.*, 1986; Waugh and Erwin, 1989). For circulating cells, shape deformability is certainly a crucial trait for proper functioning.

In mammalian systems, MBs are implicated in primitive erythrocyte biogenesis. In newly born animals or fetuses of the Tammar Wallaby (*Macropus eugenii*) and the Opposum (*Monodelphis domestica*), the bloodstream is populated by relatively large, nucleated primitive erythrocytes (Cohen *et al.*, 1990). These cells were flattened discoids or ellipsoids containing the marginal band of microtubules enclosed in the membrane skeleton, in a pattern analogous to non-mammalian vertebrate erythrocytes. With the development of the animal, erythrocytes that are newly formed in other tissue, such as the liver, become anucleate and lack the MBs (Cohen *et al.*, 1990).

Presence of MBs is also reported in several invertebrate blood cell types such as amebocytes and coelomocytes of certain Arthropod species and erythrocytes of blood clams such as *Anadara transversa*. Interestingly, MBs in blood clams are found in association with a pair centrioles, suggesting that centrioles may be the MB organizing centers. Such structural association can conceivably be extended to investigate vertebrate erythrocyte and platelet MB biogenesis (Cohen and Nemhauser, 1980).

MBs can be isolated by selective removal of the membrane skeleton using a mixture of SDS and Triton X-100 (Sanchez *et al.*, 1990). Such isolated MBs consist mainly of microtubule bundles with some associated material as revealed when negatively stained for the TEM or critical-point dried for the SEM. Immunofluorescence labeling of the

isolated MBs shows that one of the components of the associated material is tau, a microtubule-associated protein (Sanchez *et al.*, 1990). In vitro studies using microtubules extracted from dogfish erythrocytes shows that tau is necessary for both MT reassembly and bundling (Sanchez and Cohen, 1994b).

In addition to tau, isolated dogfish and chicken erythrocyte MBs are found to have an associated band of actin as revealed by phalloidin binding. However, this association has been the subject of relatively little study and the nature of structural and functional interaction with MB microtubules has not been explored (Sanchez and Cohen, 1994a; Kim *et al.*, 1987). In addition, the mechanism and stages by which this association occurs during terminal cell differentiation remains to be determined.

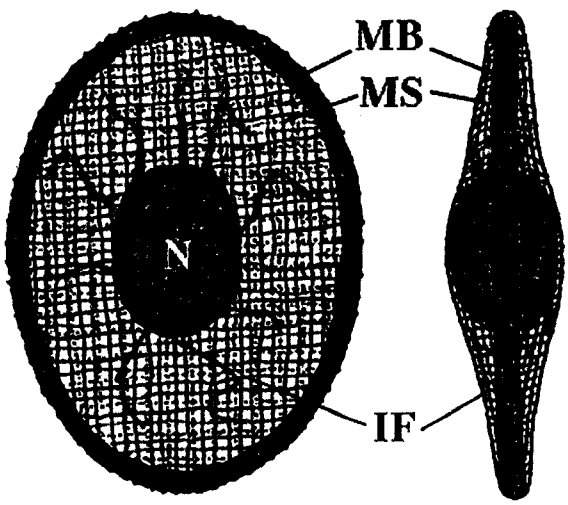

Figure 1-1. A general model of the nucleated erythrocyte cytoskeleton. (components highly diagrammatic).
MB = marginal band;
MS = membrane skeleton;
IF = intermediate filament

3. Nucleated Thrombocytes

Thrombocytes play a vital role in vertebrate wound healing and innate immunity. Mammalian thrombocytes, i.e., blood platelets, have been the subject of innumerable studies, and their structural and physiological properties are well known (e.g., White, 1971; Allen *et al.*, 1979; Kowit *et al.*, 1988; Bearer *et al.*, 2002). In contrast, though their properties are generally assumed to be similar to those of platelets, non-mammalian vertebrate thrombocytes have received relatively little attention. Morphologically, the two cell types are quite distinct: unactivated platelets are highly flattened, minute (~ 3 μm diameter), anucleate discoids, whereas fish, amphibian, reptilian, and avian thrombocytes are thicker nucleated ellipsoids of more typical eucaryotic size (~10 μm or greater long axis; Mainwaring and Rowley, 1985; Shepro *et al.*, 1966). Despite these differences in size and shape, unactivated non-mammalian thrombocytes, referred to hereafter as nucleated thrombocytes, have two highly distinctive structural features in common with platelets: a "canalicular" membrane system just beneath their surface (White and Clawson, 1980; Daimon and Uchida, 1985), and a prominent marginal band of microtubules (MB) in their plane of flattening (Fawcett and Witebsky, 1964; Rowley *et al.*, 1988; Schwer *et al.*, 2001; Lee *et al.*, 2002). In addition, the cortical cytoskeleton of resting bovine platelets contains actin filaments densely arrayed in parallel with the marginal band of microtubules (Takeuchi *et al.*, 1990).

Upon activation of both nucleated thrombocytes and platelets, cellular aggregation, adhesion, and morphological alterations are observed. Aggregation of both cell types can be induced by agents such as ADP and thrombin (Haslam, 1964; Aledort, 1971; O'Toole *et al.*, 1994; Pica *et al.*, 1990), and activation of both appears to involve an integrin-like

surface protein complex and eicosanoid signaling pathways (Hill *et al.*, 1999; Lloyd-Evans *et al.*, 1994; Passer *et al.*, 1997; Wang and Herman, 1997). For activated platelets the morphological changes include membrane protrusions, pseudopod formation, and spreading on a surface (Allen *et al.*, 1979), and these activities are correlated primarily with the assembly of F-actin rather than MB reorganization (Debus *et al.*, 1981; Nachmias, 1980).

Although it has been shown that nucleated thrombocytes are similar to platelets with respect to structure and activation signaling, neither their post-activation stages nor their related cytoskeletal changes have been demonstrated (Table 1). Dogfish thrombocytes can be employed as a model system because they exhibit typical nucleated thrombocyte morphology, are readily obtained (Cohen *et al.*, 1997), and have been the subject of two previous studies (Shepro *et al.*, 1966; Mainwaring and Rowley, 1985).

TABLE 1

PROPERTY	PLATELET (MAMMALIAN)	NUCLEATED THROMBOCYTE (birds, reptiles, amphibians, fish)
UNACTIVATED		
Shape	highly flattened discoid	somewhat flattened ellipsoid
Cell Size	rel. small (~3 μm diameter)	rel. large (usually >10 μm long axis)
Nucleus	absent (anucleate)	present (nucleated); large % cell vol.
Cytoskeletal system: -microtubular band (MB) -MB-associated F-actin	 present (thin) present (Debus *et al.*, 1981)	 present (thick) UNKNOWN (addressed, this study)
Canalicular Membrane System	present	present
Granules	present (rel. small size, 0.2 ~ 0.3 μm)	some evidence (Mainwaring and Rowley, 1985)
ACTIVATED		
Aggregation, adhesion	observed upon activation	observed upon activation
Early activation morphological change	rounding up and formation of pseudopods	UNKNOWN (addressed, this study)
Late activation morphology	"pancake" flattening on surface	"pancake" flattening on surface
Cytoskeletal rearrangements	microtubule move to interior	UNKNOWN (addressed, this study)
Phagocytosis	some evidence (Endo *et al.*, 1984; Mantur *et al.*, 1986; White and Clawson, 1982)	some evidence (Bertram *et al.*, 1998; DaMatta *et al.*, 1998; Pellizon and Lunardi, 2000; Hill and Rowley, 1998)
Production of phagocytosis activators	some evidence (Sakamoto *et al.*, 2000)	UNKNOWN
Nuclear "lobulation" or "fragmentation"	not relevant (no nucleus)	some evidence

4. Objectives

The general objective of this work was to investigate the nature of F-actin-microtubule interaction from both structural and functional perspectives in mature nucleated erythrocytes and in both activated and unactivated nucleated thrombocytes. Detailed experimental objectives are summarized as following:

To investigate F-actin and microtubule interaction in erythrocytes at structural level, the detailed experimental objectives were to determine: (a) whether a band of F-actin is a constant feature of erythrocyte marginal band in different vertebrate classes; (b) the strength/extent of its colocalization with the microtubules in the MB; and (c) the pattern of F-actin organization with respect to microtubules in the marginal band at the ultrastructural level.

For the study of functional interaction in erythrocytes, the objectives were to determine: (a) the function of F-actin band* by its removal; (b) whether it is sensitive to low temperature as the microtubule band; (c) whether its hyperstabilization affects low temperature induced microtubule band disassembly and reassembly; and (d) the effect of F-actin hyperstabilization in the formation of anomalously pointed erythrocytes, which have pointed microtubule bands.

***Notes on terminology:** Study of the F-actin band as a separate structure entailed revision of relevant terminologies. That is, before establishing the F-actin band as a discrete structure, marginal band was a terminology synonymous to the band of microtubules. For conceptual clarification, the MB will be referred to as a structure composed of the F-actin band and the microtubule band from this point on.

To investigate F-actin and microtubule interaction in thrombocytes at structural level, the experimental objectives were to determine: (a) whether a band of F-actin was present in unactivated thrombocytes; (b) the pattern of colocalization with the microtubule band in unactivated thrombocytes; (c) sequence of shape change induced by activation; (d) the corresponding changes in the cytoskeleton, particularly that of F-actin band and the microtubule band.

For the study of functional interaction in thrombocytes, these were to determine: (a) whether the F-actin band and the microtubule band in unactivated thrombocytes are sensitive to low temperature as in erythrocytes; (b), and if so, the effect of removing microtubule band in unactivated thrombocytes on cell shape; (c) reversibility of temperature-induced microtubule band disassembly in unactivated thrombocytes; (d), in activated thrombocytes, the function of F-actin on cell shape change by exposure to F-actin disassembly promoting agents; and (e) whether nucleated thrombocytes truly resemble platelets functionally by progressing through post-activation stages based on F-actin reorganization.

To facilitate the mentioned studies, new methodologies were devised with the following objectives: (a) to immobilize both erythrocytes and thrombocytes that exist in vivo as cells in suspension for microscopic studies using protein fibers; (b) to develop an improved and faster method of fixation/permeabilization and labeling, particularly for the study of thrombocyte cytoskeleton during activation-induced shape change.

CHAPTER 2: **F-Actin-Microtubule Structural Interaction in Erythrocytes**

RESULTS:

1. A band of F-actin is present and colocalizes with the marginal band (MB) of microtubules in mature dogfish erythrocytes.

Dogfish erythrocyte cytoskeletons were prepared within fibrin clots prepared as described in Lee *et al.* (1998b) and labeled for actin and tubulin. To assess the extent of cross signal contamination, actin and tubulin were singly labeled with Texas-Red phalloidin (red: em. 608 nm) and FITC (green: em. 510 nm) conjugated tubulin antibodies (figures 2-1 and 2-2). No significant signal bleeding was observed between the red and the green channels. F-actin was distributed in high intensity along the marginal band (shown in DIC image) and diffusely in the region of the membrane skeleton, with occasional patches. When cytoskeletons were double labeled, actin and tubulin showed overlapping colocalization in the marginal band as represented by extensive yellow color in figure 2-3d.

A more intact preparation was attempted in which cells were first fixed and then detergent permeabilized (figure 2-4). Although cells retained relatively unchanged morphology (very similar to their natural state), detection of the F-actin band was considerably diminished due to background fluorescence of hemoglobin (which emits in the red range). Detection of tubulin was not significantly altered by this method. In fact, the marginal band retained its elliptical shape since the cell was first fixed (figure 2-4b).

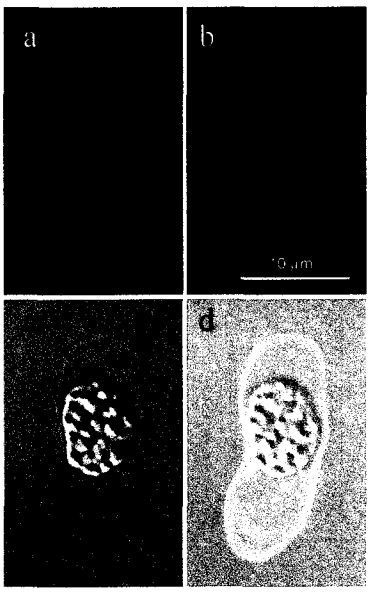

Figure 2-1. Localization of F-actin in the dogfish erythrocyte cytoskeleton trapped in fibrin clot: (a) F-actin visualized by Texas Red-phalloidin This optical (confocal) section shows a distinct band of F-actin with somewhat less pronounced membrane skeleton; (b) FITC (abs. 488 nm/ em. 510 nm) channel. The blank field shows that Texas Red emission is not bleeding into the FITC channel; (c) DIC image of the same field; (d) superimposition of (a), (b) and (c).

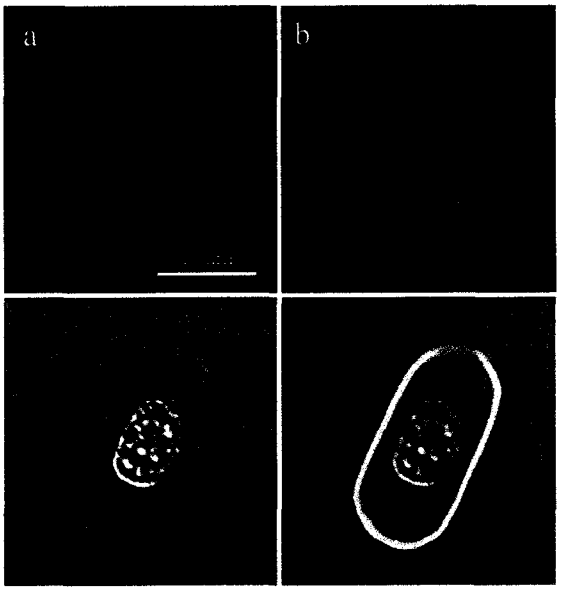

Figure 2-2. Localization of tubulin in the dogfish erythrocyte cytoskeleton (clot method): (a) Texas Red detecting channel (abs.591 nm/ em. 608 nm) The blank field shows that the FITC fluorescence is not bleeding into the 608 nm channel; (b) FITC channel, indirect immunofluorescence showing tubulin distribution in the MB; (c) DIC image; (d) superimposition of all channels.

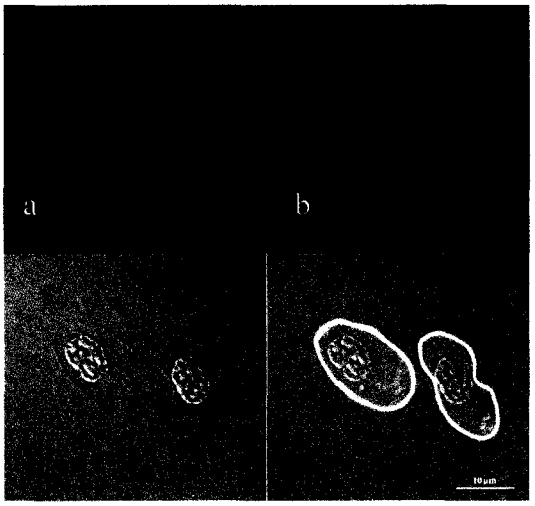

Figure 2-3. Double labeled dogfish erythrocyte cytoskeletons (clot method): (a) F-actin distribution; (b) Tubulin distribution; (c) DIC field; (d) Superimposition of all three channels. The bright intensity in the ring indicates extensive colocalization of F-actin and tubulin in the MB.

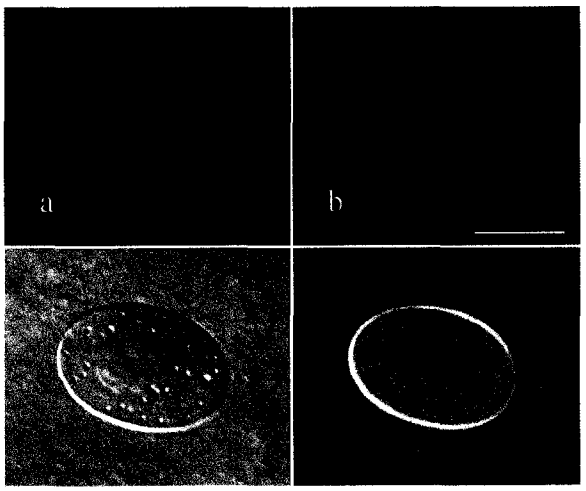

Figure 2-4. Double labeled dogfish erythrocyte prepared by pre-fixation/clot method. (a) F-actin distribution. The F-actin band appears thinner compared to preparation by "post-fixation method". Hemoglobin is retained in the cell, but produces a negligible background fluorescence in this channel (not shown); (b) Tubulin distribution. The majority of specimens prepared by this method preserved the MB microtubules as shown; (c) DIC image; Note that MB is not visible in a pre-fixed cell (compare with figures above); (d) superimposition of all three channels.

2. The F-actin band is also present and colocalizes with the microtubule band in mature newt erythrocytes.

Colocalization of F-actin with the MB microtubules was also assessed in Eastern spotted newt erythrocytes, which measure ~40 μm in the long axis and possess considerably thicker marginal bands (~0.5 μm), a thickness greater than the lateral resolution limit of a confocal microscope using a high N.A. objective lens. As in dogfish erythrocytes, the newt erythrocytes exhibited a clear and intense F-actin signal in the MB region (fig. 2-5). Since cytoskeletons tend to adhere to the glass surface in a flat manner, 3D projections were constructed from ~30 optical sections and rotated to examine colocalization in the digital cross section of MBs (figs. 2-6 and 2-7). A perfect match of the green and red signal at the cut end was observed, in both non-twisted and twisted cytoskeletons.

Figure 2-5. Cytoskeletons newt erythrocyte prepared by standard polylysine adhesion method: (a) tubulin distribution (FITC); (b) F-actin distribution (Texas-Red); (c) superimposition of (a) and (b). Note: The membrane skeleton does not appear as obvious as in previous figures because the red channel sensitivity was reduced to avoid bleed through from the intense green channel.

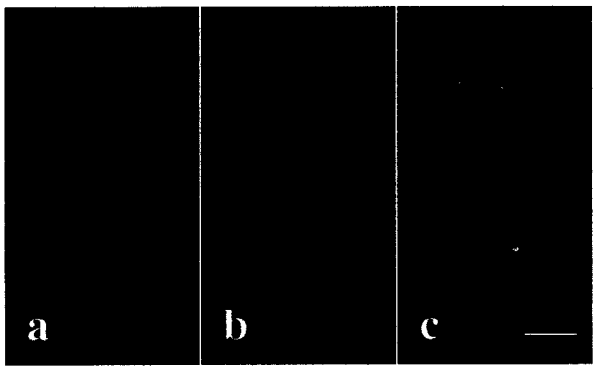

Figure 2-6. 3D reconstructed image of a cytoskeleton, after digital rotation and cutting. (a) tubulin distribution, viewed at an oblique angle; (b) corresponding view in the red channel; (c) superimposition of (a) and (b).

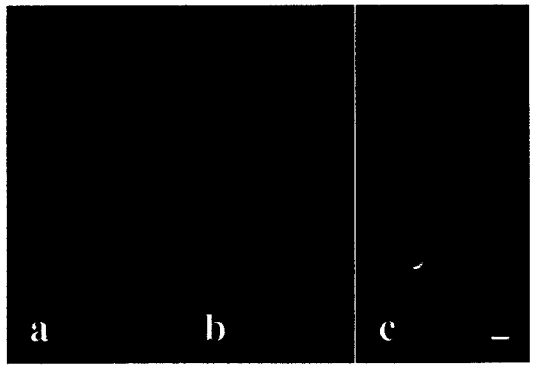

Figure 2-7. 3D reconstructed image of a twisted cytoskeleton, after rotation and cutting. (a) tubulin distribution, viewed at an oblique angle; (b) corresponding view in the red channel (F-actin); (c) superimposition of (a) and (b). The two signals match point to point at the cut surface. Note: In "standard method" preparations, approximately 10% of the MBs become twisted after lysis in the manner shown in this figure. Although the mechanism of twisting is unknown, twisted cytoskeletons are useful for co-localization studies.

3. Disappearance of the MT band correlates with the disappearance of F-actin band, and F-actin is present throughout the length of broken MT bands.

Occasionally, cytoskeletons with bent and broken MBs were observed (fig. 2-8). Colocalization of F-actin with the MB microtubules was maintained even in these cases, suggesting an intimate link between the two bands, the nature of which is still to be explored. This is also supported (in rare occurrences) by cytoskeletons with missing MBs (fig. 2-9). The band of F-actin in these cytoskeletons was absent, indicating that the interaction between the F-actin band and the MB microtubules was stronger than the interaction between the F-actin band and the membrane skeleton.

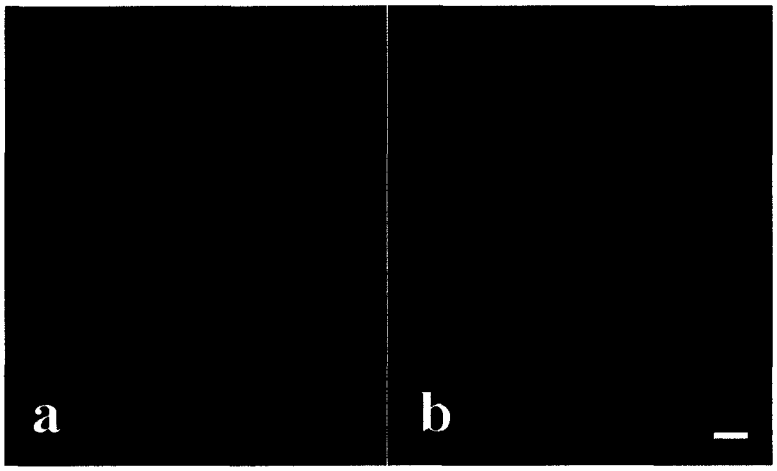

Figure 2-8. Newt erythrocyte cytoskeletons with bent and broken MBs (observed occasionally). (a) tubulin distribution; (b) F-actin distribution. Note: Even after breakage of the MB MB tubulin and Factin colocalize. Fragments of the membrane skeleton are still associated with the MB in (b).

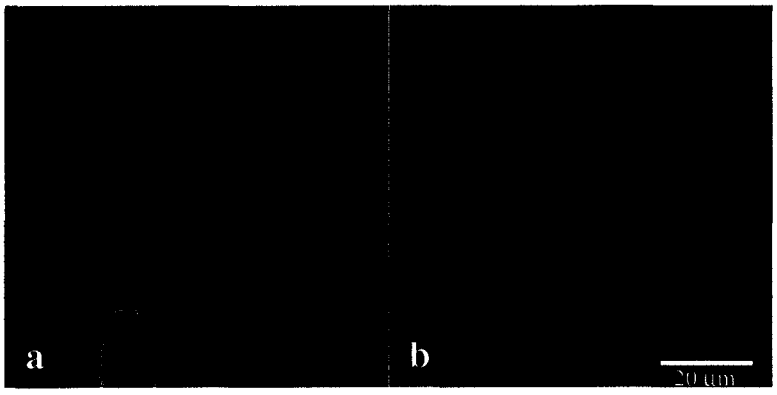

Figure 2-9. Newt erythrocyte cytoskeletons with missing MBs (observed rarely). (a) the green channel; (b) the red channel, showing the MS of two cytoskeletons missing MBs. In (b), no F-actin signal remains in the region of the MB, indicating that F-actin is closely associated with microtubules or other components of the MB.

4. HMM and S1 binding also reveal the presence of the F-actin band in isolated dogfish marginal bands.

HMM and S1 can be used to tag F-actin. HMM (fig 2-10, a and b) and S1 (fig 2-10, c and d) fragments of skeletal myosin were applied to detergent-isolated, and fixed, dogfish marginal bands. These myosin fragments were then probed with skeletal anti-myosin as the primary antibody, and a corresponding secondary antibody tagged with FITC. Although the signal emitted was weaker compared to Texas-Red phalloidin (fig 3-1a), the binding pattern corresponded to that of actin. Problematic nuclear fluorescence was produced due to glutaraldehyde fixation, but the bands emitted no signals when the actin probes were omitted (fig 2-10, e and f).

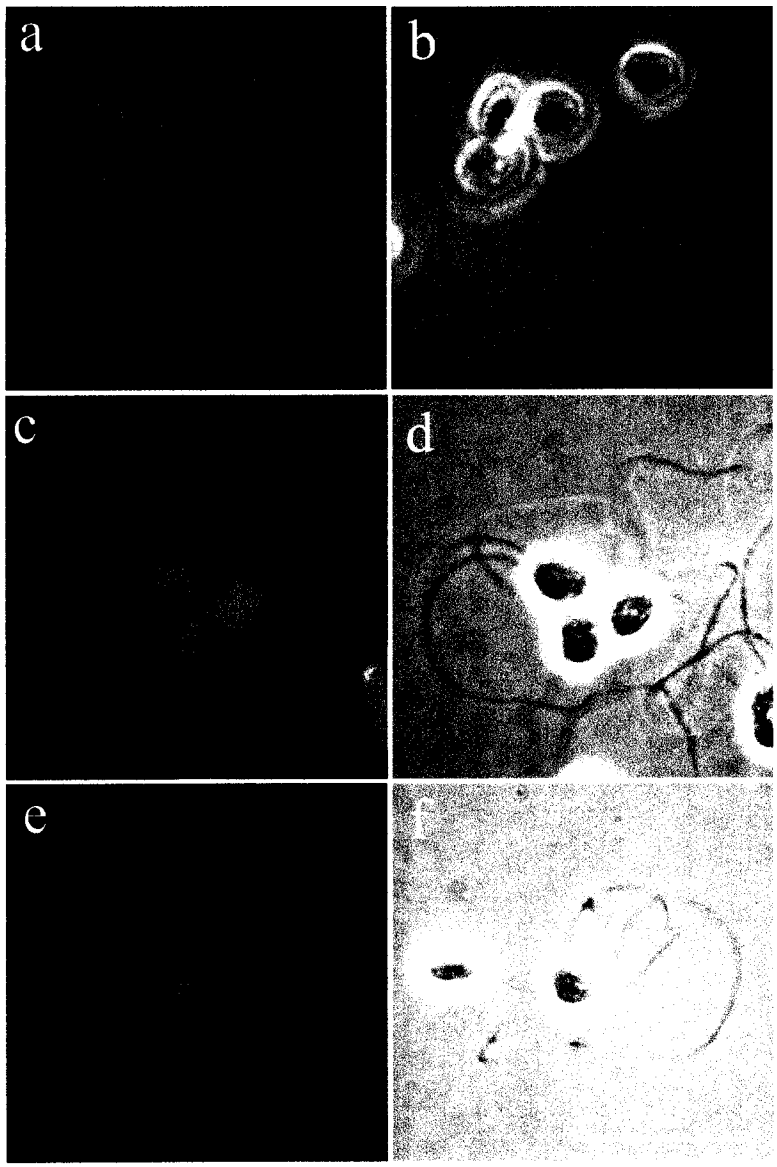

Figure 2-10. Localization of F-actin revealed by HMM and S1 fraction of skeletal myosin in dogfish isolated bands: (a) HMM binding pattern; (c) S1 binding pattern; (e) control with no probe; (b), (d), and (f) phase contrast images of (a), (c), and (e), respectively

5. Atomic force microscopy is suitable for general examination of cytoskeleton, but not sufficient for determining F-actin organization at the ultrastructural level.

A recent study showed that actin filaments could be imaged down to monomeric scale using an atomic force microscope (AFM). In this study, actin filaments were created by surface-induced polymerization of G-actin on a fresh mica surface (Weisenhorn, 1990). AFM analysis revealed that these unfixed filaments were ~5 nm in

diameter, arranged in a helical pattern, consistent with the generally accepted model of F-actin. At the cellular level, dynamic actin filaments were resolved in the lamellipodia and filopodia of living glial cells derived from *Xenopus laevis* retinal neuroepithelium. This study demonstrated that an AFM could image structures internal to the cell membrane, despite the fact that AFM is a surface-scanning device. According to the proposed explanation, this was possible when the cell membrane conformed to the shape of the underlying actin filaments, or when the scanning probe actually penetrated the cell membrane, depending on the forces used. Disappearance of filaments by treatment with cytochalasin B and fluorescence imaging after AFM imaging verified that the imaged filaments were actin (Henderson, 1992).

AFM imaging of single microtubules has also been reported (Vinckier, 1995). In this study, microtubules isolated from pig brains were fixed and covalently immobilized on a silicon wafer by 4-aminobutyldimethylmethoxysilane and glutaraldehyde. By this method, the height (diameter) of a single microtubule was 10 nm in buffer solution and 15 nm in air, a smaller measurement when compared to ~25 nm by TEM. Differences in measurements obtained in buffer and in air were attributed to the differing softness of microtubules in air and liquid.

Although relatively little has been achieved to date using AFM on cytoskeletal systems and it was not considered to be critical part of this work, it potentially offered certain advantages that deserved exploration. For instance, this technique required no dehydration or drying, a treatment that could lead to distortion of structures under study (actin filaments and microtubules). Secondly, lack of staining requirement could yield

more constant results over a larger area, as compared with negative staining for TEM, which can produce quite variable visibility of structures over large areas.

Whole, fixed cytoskeletons of newt erythrocytes (fig. 2-11) were examined by atomic force microscopy in a demonstration by technicians of Digital Instruments Inc. Detection of individual microtubules was possible through the membrane skeleton both in tapping mode and non-tapping mode.

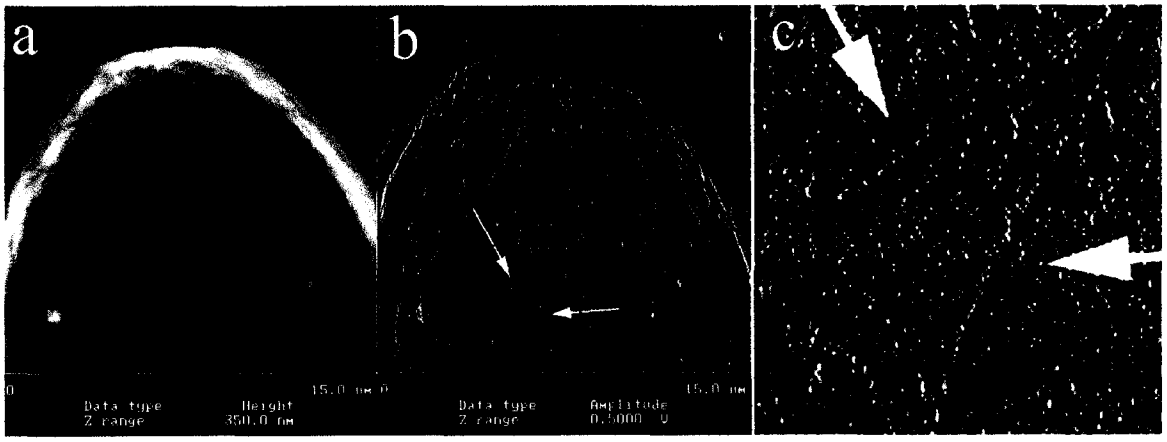

Figure 2-11. Cytoskeleton of a newt erythrocyte (AFM): (a) image produced by tapping mode; (b) image produced by non-tapping mode; arrows point at single microtubules; (c) Enlarged view of the boxed region in (b)

To investigate the organization of the actin band, in-vitro polymerized F-actin and microtubules were examined as standard samples under the AFM with various settings. However, scans of these samples constantly produced inaccurate width and height measurements of the filament and the tubule, parameters critical in distinguishing one from the other. Especially, the error in the measurement of F-actin width seemed to be built-in since the scanning probe tip collided with the specimen, many times moving it out of place. Therefore, it appears that atomic force microscopy is useful for general

survey of the cytoskeleton in the "wet state", while determination of the F-actin band arrangement is impaired by technical limitations.

6. Post-embedding gold labeling of F-actin exhibited non-specific binding.

Post-embedding immuno-gold labeling of actin has been reported in a variety of systems. In the *Tetrahymena* basal body-cage complex, gold-labeled actin was found in close association with basal body microtubules (Hoey and Gavin, 1992). In rat cerebral cortex, extensive labeling was observed in the dendritic spines, particularly in the postsynaptic density and the subsynaptic web filaments (Cohen RS *et al.*, 1985). And in rat seminiferous tubules, actin was identified in the subacrosomal space of spermatids during spermiogenesis, in studies that also demonstrated that the extent of post-embedding immuno-gold labeling of actin was dependent on the fixatives and the embedding resins utilized (Kann and Fouquet, 1989).

In an additional approach to localize F-actin at the EM level, newt erythrocyte cytoskeletons were whole-mounted on carbon-coated grids. Gold particle conjugated avidin-biotin phalloidin was used as the probe on these samples. However, the labeling pattern lacked specificity despite continued attempts.

Secondly, whole cells, detergent-produced cytoskeletons, and detergent-isolated marginal bands were trapped in fibrin clots and embedded in both hydrophilic (LR White and Lowicryl K4M) and hydrophobic (Epon) resins. F-actin was labeled with/without prior etching (metaperiodate + HCl) using available probes (e.g., gold particle conjugated avidin-biotin phalloidin and polyclonal, and monoclonal actin antibodies with gold

particle conjugated secondary antibody). However, no clear pattern of F-actin labeling was observed even at the fluorescence light microscopic level.

DISCUSSION:

7. F-actin band is present in all non-mammalian vertebrate classes and it colocalizes with the microtubule band.

F-actin has been found to be present in the plane of flattening in chicken erythrocytes, but it has not been resolved whether it resides at the MB-membrane skeleton interface or occupies the same cortical region as the MB microtubules (Kim *et al.*, 1987). As a means of answering this question, preparations of dogfish (*Mustelus canis*) and Eastern newt (*Notophthalmus viridescens*) erythrocyte cytoskeletons were double labeled with anti-tubulin and rhodamin- or Texas Red-phalloidin for confocal fluorescence microscopy. These erythrocytes are comparatively larger than those of chickens, with thicker marginal bands (0.3 μm for dogfish and 0.5 μm for newt vs. 0.1 μm), facilitating structural survey at the light microscopic level.

Labeling result in dogfish and newt erythrocyte cytoskeleton indicates that the F-actin band is present in all non-mammalian vertebrate classes. The thickness of the band appears to be identical to the microtubule band at the limit of resolution of confocal microscope, and both structures colocalize on a point-by-point basis. The "tightness" of such association is evidenced in broken marginal bands where both F-actin and microtubule are clearly labeled. Furthermore, absence of the F-actin band in membrane skeletons that have lost the microtubule band indicates that the F-actin band-microtubule band association is stronger than that of F-actin band-membrane skeleton association.

8. Suggested experiment: Negative staining of whole cytoskeletons and isolated marginal band labeled with HMM and S1 may reveal detailed F-actin arrangement.

Heavy meromyosin (HMM) can both identify and reveal the polarity of actin filaments by a "herringbone" pattern (Huxley, 1963). Actin has been localized by HMM or S1 subfragment decoration in many systems, such as in the microvilli of intestinal epithelial cells, in the secretory system of lactating guinea pig mammary gland alveolar cells, and in the cleavage furrow of rat kangaroo (PtK2) cells (Mooseker and Tilney, 1975; Amato and Loizzi, 1981; Sanger and Sanger, 1980, respectively).

HMM or S1 labeling revealed presence of F-actin in isolated MBs under fluorescence LM as shown above. These can also be used on whole cytoskeletons or isolated marginal bands to localize and reveal the arrangement of F-actin with respect to microtubules by negative EM staining.

SUMMARY OF FINDINGS:

(A) F-actin band is present in erythrocytes of other vertebrate classes (i.e., newt and dogfish) by confocal imaging.

(B) F-actin band colocalizes tightly with the marginal band microtubules (MT) since:

(i) disappearance of MT band correlates with the disappearance of F-actin band.

(ii). F-actin is present throughout the length of broken MT bands.

CHAPTER 3: F-Actin-Microtubule Functional Interaction in Erythrocytes

RESULTS:

1. The F-actin band resists the effects of common F-actin disassembly promoting agents.

Different F-actin disassembly promoting agents were tested to observe the effect of F-actin band removal. Detergent-isolated marginal bands (from Eastern newt) were perfused with physiological concentrations of latrunculin B, cytochalasin D, gelsolin, and mycalolide B under a coverslip for time-lapse observation. None of these inhibitors caused significant change in the distribution of F-actin at least over a period of 1 hour (table 1). This indicated that the MB associated F-actin band was highly stable, or protected by stabilizing molecules that prevented the disassembly promoting effects of tested agents.

TABLE 1: Preliminary results using actin perturbing agents

F-ACTIN INHIBITORS	**MECHANISM OF ACTION**	**CONC.**	**EXPOSURE TIME**	**EFFECT**
LATRUNCULIN-B	severing, capping, nucleating (Spector *et al.*, 1989)	0.35 μg/ml	> 60 min.	NONE
CYTOCHALASIN D	severing, capping, nucleating (Selden *et al.*, 1980)	5 μg/ml	> 60 min.	NONE
GELSOLIN	severing, capping, nucleating (McGough, *et al.*, 1998)	50 μg/ml	> 60 min.	NONE
MYCALOLIDE-B	Severing (Saito et al, 1994; Takakuwa *et al.*, 2000)	10 μM	> 60 min.	NONE

2. Removal of the F-actin band by elastase correlates with circularization of isolated marginal band.

Newt erythrocyte cytoskeletons were pre-labeled with Texas-Red phalloidin and treated with Triton-SDS solution to isolate the band. The isolation reaction was stopped at the elliptical stage by addition of excess Triton as indicated by Sanchez and Cohen (1990). The MB actin remained labeled after isolation with a distribution pattern similar to that of cytoskeleton before marginal band isolation (3-1a). Application of elastase, however, led to dissociation of actin from the marginal band as a diffuse cloud (3-1c). Interestingly, this dissociation correlated with the transformation of elliptical marginal band to a much more circular shape as shown by the phase contrast micrograph (3-1b →3-1d).

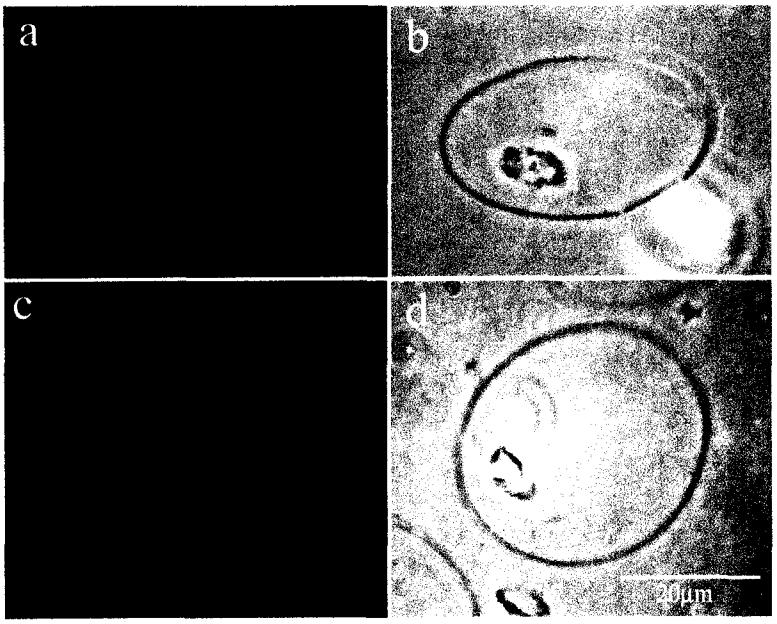

Figure 3-1. Effect of elastase on isolated newt erythrocyte MBs: (a) MB isolated from Texas-Red phalloidin pre-labeled cytoskeleton; (b) phase-contrast image of (a); (c) isolated MB such as (a) exposed to 0.5 u/ml of elastase; (d) phase image of (c)

3. F-actin band is resistant to low temperature treatment

Normal dogfish erythrocyte cytoskeletons prepared at 22 °C exhibit strict colocalization of MB microtubules with a band of actin filaments (Fig. 3-2). This colocalization was lost when erythrocytes are incubated for sufficient time (here, 16 hours) at 0 °C. Most MB microtubules became disassembled and tubulin was detected as patchy/disorganized clusters (Fig. 3-2a). The actin cytoskeleton, however, did not show the same extent of disassembly. While it is possible that there was some reorganization, the actin membrane skeleton appeared relatively intact, and the F-actin band was much more prominent than the MB microtubules (Fig. 3-2b).

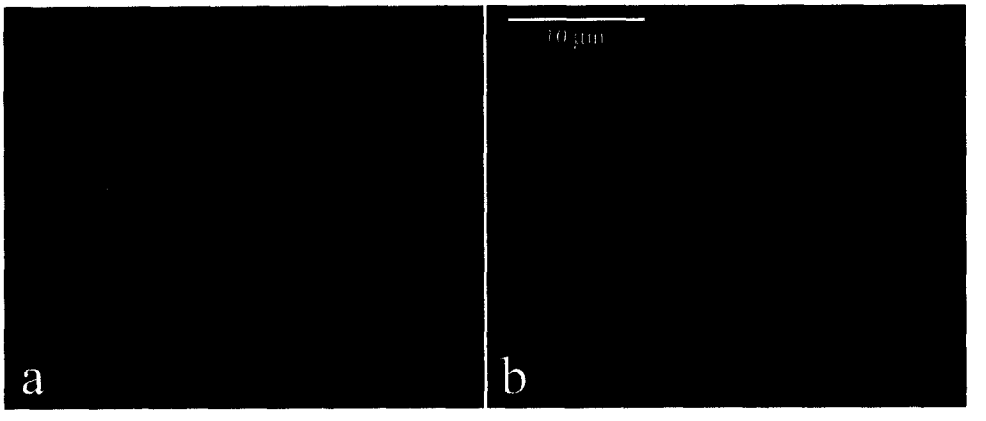

Figure 3-2. Loss of tubulin and F-actin colocalization at 0 °C (16 hours). (a) Extensively disassembled MB microtubules; (b) Relatively intact F-actin membrane skeleton and the F-actin band.

4. Hyperstabilization of F-actin results protects the MT band from low temperature induced disassembly (Lee et al., 2001).

Jasplakinolide is a cell-permeable F-actin stabilizing cyclopeptide from the marine sponge *Jaspis johnstoni*, with the same binding site as phalloidin (Bubb *et al.*, 2000; Senderowicz *et al.*, 1995). Cells exposed to 1 mM jasplakinolide in Elasmobranch

Ringer's solution for 15 hours show minimal labeling with Texas-red phalloidin compared to methanol controls (fig 3-3). Decreasing concentrations of jasplakinolide result in increased binding of Texas-red phalloidin.

MB microtubules of cells pre-treated with 1 μM jasplakinolide and incubated at 0 °C undergo reduced disassembly compared to solvent controls (Fig. 3-4a vs. 3-4d). In treated cells, most microtubules are restricted to the peripheral region of the cytoskeleton, with the major bundles still localized in the MB. In controls, no such bundles are visible in the MB. The actin in the membrane skeleton and the peripheral band appear to be better preserved in the treated than the control cytoskeletons (even despite the weak Texas-Red phalloidin labeling, Fig. 3-4b vs. 3-4e). These initial observations indicate that stabilization of actin cytoskeleton by jasplakinolide can indirectly stabilize MB microtubules against 0 °C-induced disassembly.

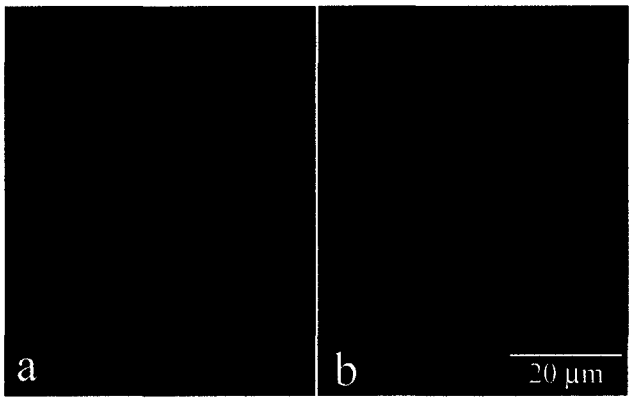

Figure 3-3. Competitive binding of Jasplakinolide and Texas-Red phalloidin. Jasplakinolide is cell permeable and competes with phalloidin for the same binding site in F-actin. (a) Cytoskeleton of cells treated 1μM jasplakinolide and labeled with Texas-Red phalloidin; (b) Cytoskeleton of cells treated with 0.3% MeOH (the solvent for jasplakinolide) and labeled with Texas-Red phalloidin

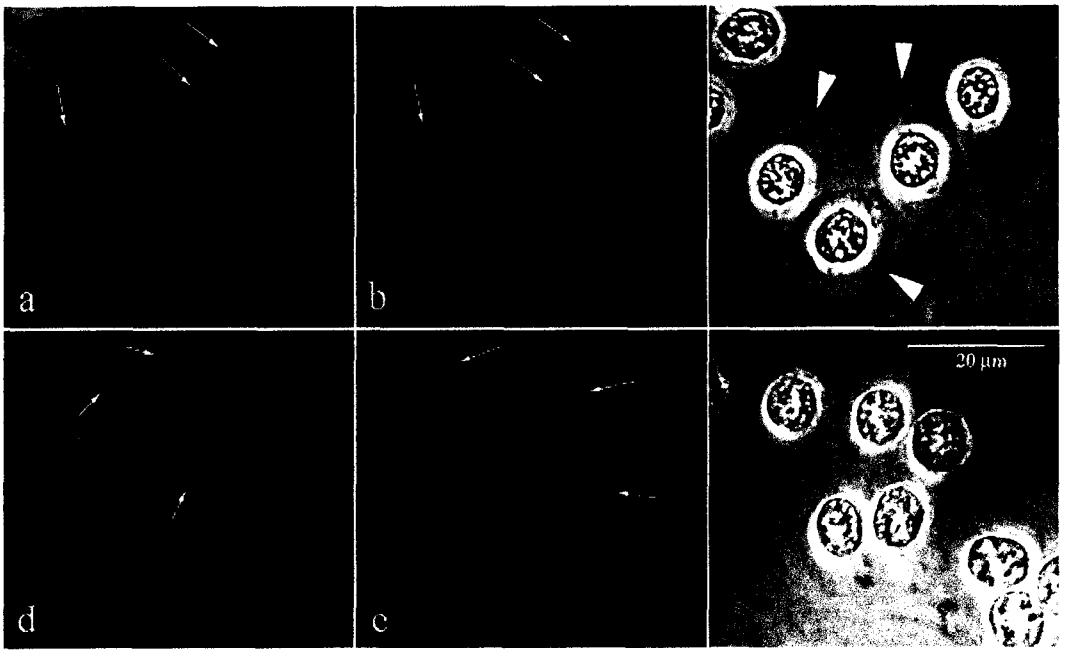

Figure 3-4. (a)~(c), Increased MB microtubule stability at 0 °C by 1 mM jasplakinolide pre-treatment. (a) Tubulin distribution. MB microtubules exhibit partial disassembly, with major bundles still visible in the MBs (arrows); (b) F-actin distribution in the same cytoskeleton. F-actin bands are weakly visible (arrows, signal digitally enhanced to make them visible); (c) Phase-contrast. cytoskeletons supported by the MB, although thinner than normal (arrowheads). (d)~(f), Extensively disorganized MB microtubules in cells exposed to control solution (0.3% MeOH) only. (d) Tubulin distribution; (e) F-actin distribution. Note that Texas-Red signal is much brighter here than when treated with jasplakinolide (b, above). Arrows in (d) and (e) indicate lack of actin and tubulin colocalization; (f) Phase-contrast. cytoskeleton and MB is not as obvious as in (c).

5. Hyperstabilization of F-actin has no effect on temperature induced MB reassembly (Lee et al., 2001).

Temperature-induced (0 °C → 22 °C) reassembly of MB microtubules is not affected by jasplakinolide pre-treatment. Most microtubule bundles of either jasplakinolide or methanol pre-treated cells are localized in the MB, with minor bundles near the MB (fig. 3-4). The actin cytoskeleton in both cases appears normal and similar to fig. 3-3b.

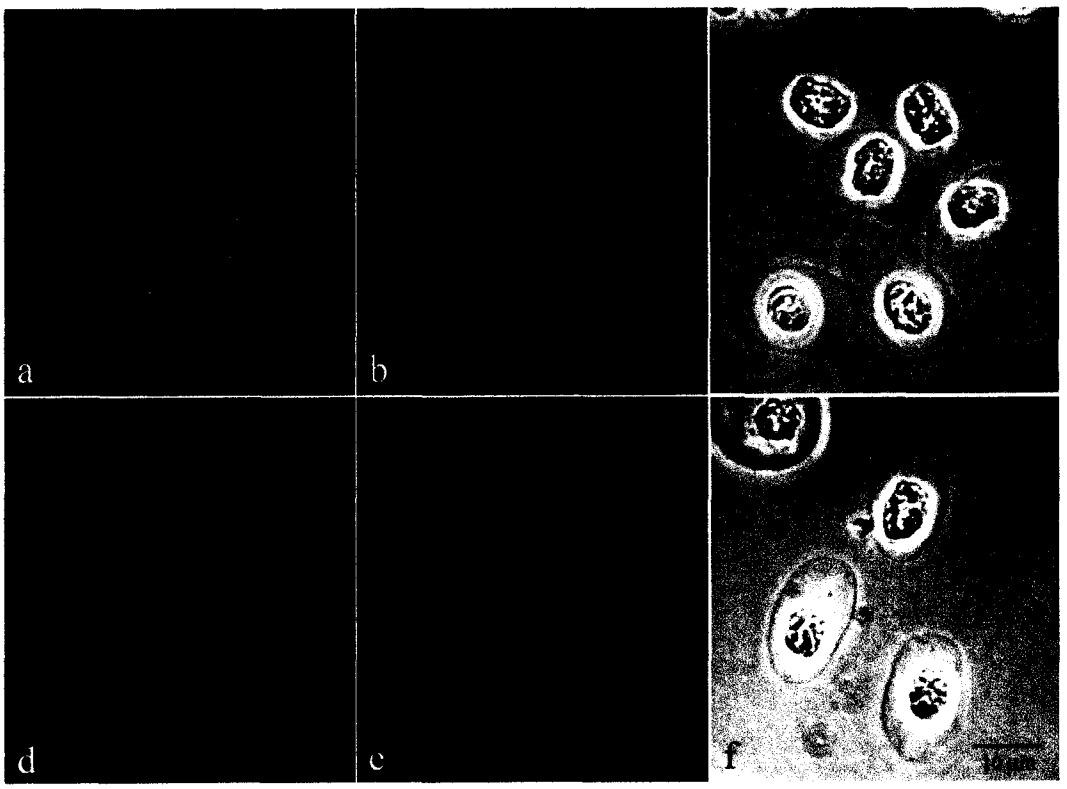

Figure 3-4. (a)~(c), Lack of effect of 1 μM jasplakinolide treatment on MB microtubule reassembly at 22°C. (a) Tubulin distribution. Major microtubule bundles are localized in the MB, while some minor bundles are fraying off the major bundles; (b) F-actin distribution. F-actin band is discernable despite the low signal intensity; (c) Phase-contrast view. (d)~(f), Reassembly in control solution (0.3% MeOH), (d) Tubulin distribution. MB microtubules are localized very similar to (a), but most bands are thinner; (e) F-actin distribution. F-actin band colocalizes with the major MB microtubule bundles; (f) Phase-contrast. As in (c), MBs are relatively clear.

6. F-actin-microtubule colocalization is partially lost in anomalously pointed dogfish erythrocytes.

In previous work, anomalous pointed cells (fig. 3-5) had been observed to form in relatively small numbers in populations of initially normal, smoothly curved ellipsoidal cells, after several hours of incubation in dogfish Ringer's solution. New experiments showed that both singly- and doubly-pointed morphology could be generated in a substantial percentage of cells several hours after first temperature-cycling the cells to

induce MB reassembly. Anti-tubulin immunofluorescence labeling showed that these cells contained MBs that were disorganized into discontinuous and more highly linearized microtubule bundles, suggesting microtubule linearization and subsequent pressure against the MS as a relatively simple mechanical mechanism for the generation of pointed cells. In these pointed cells, F-actin retained co-localization with some of the major microtubule bundles that were no longer restricted to the cell periphery, but lost co-localization with others. Taken together these results suggest that there is close structural and functional interaction between F-actin and MB microtubules in this system, and that anomalous formation of pointed cells might involve loss of such interaction.

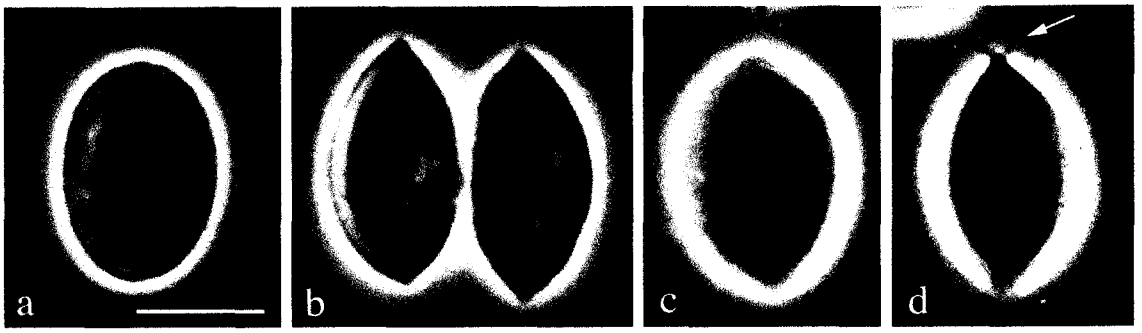

Figure 3-5. Dogfish erythrocytes (phase-contrast). (a) normal ellipsoid morphology; (b) double-pointed cells, (c) subtly-pointed cell, (d) point with extensions (arrow). Bar = 10 μm

Given a means for producing the pointed cells in considerable numbers (see the next section), it was possible for the first time to obtain good preparations of pointed cell cytoskeletons for fluorescence localization of the major cytoskeletal proteins. As shown for two of these cytoskeletons in figure 3-6, major microtubule bundles are still present, converging at the pointed end(s) of the cells (fig. 3-6 a,d). Some bundles remain curved at the periphery, but others are internal and are now in a more linear state than in normal

cells. F-actin (fig. 3-6 b,e) is still associated with some microtubule bundles, but in general it has lost colocalization with them as compared with normal MBs (e.g., fig. 2-3). The dense elements seen in phase contrast (fig. 3-6 c,f) correspond to microtubule bundles (fig. 3-6 a,d), not to actin filament bundles (fig 3-6 b,e)

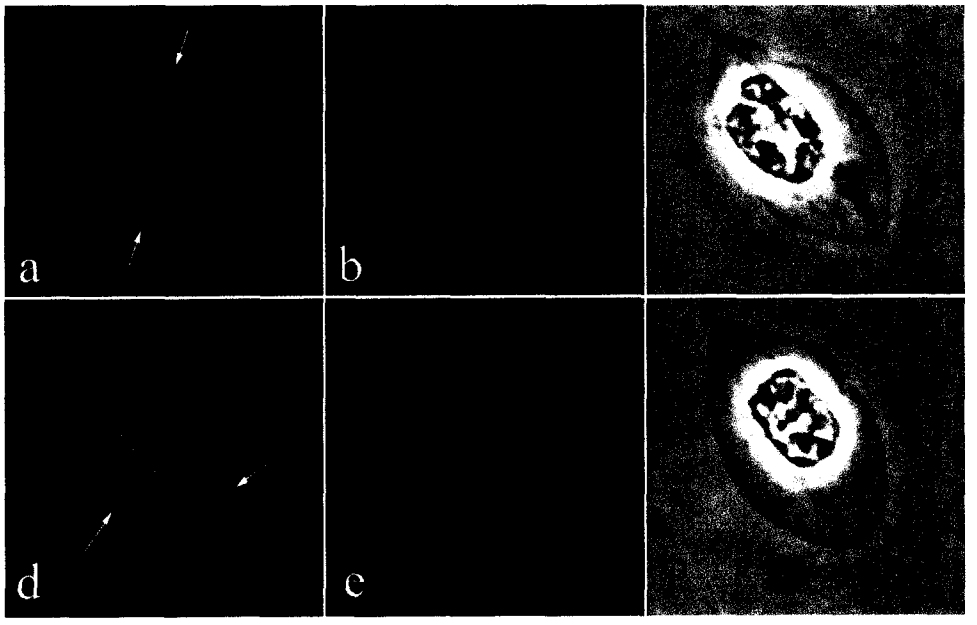

Figure 3-6. Cytoskeletons of doubly pointed, (a)~(c), and singly pointed erythrocytes, (d)~(f), formed by the standard method, labeled with (a) and (d) FITC-anti-tubulin, (b) and (e) Texas-red phalloidin. (c) and (f) Phase-contrast. Major microtubule bundles converge at pointed ends of cell. Many microtubules reside in areas other than the classical MB. Microtubules are more stringently associated with F-actin in normal cytoskeletons (figure 2-3), and they colocalize with actin in very few places (e.g., arrow in a and d)

7. Pointed cells can be produced in large quantities by temperature cycling.

Initial attempts to produce large numbers of pointed erythrocytes by simple incubation for several hours at ~22 °C were unsuccessful. However, it was found that if incubation at 0 °C preceded the ~22 °C incubation period, both singly-pointed and doubly-pointed cells were produced in readily countable numbers (fig. 3-7). Variation of

0 °C incubation time showed that 2 or 4 hours were quite effective (usually 5%,or more pointed cells; fig. 3-8). However, relatively few pointed cells were present after 2 hours at ~22 °C, as compared with 5 hours rewarming (fig. 3-8). Based on these results, a standard procedure of 2 or 4 hours incubation at 0 °C followed by 5 hours rewarming was adopted. Insertion of an extra cycle of 2 hours 0 °C - 2 hours ~22°C before the standard cycle had only a minor effect on % pointed cells produced (fig. 3-9), and mechanical agitation of cells by fluxing through fine capillary tubes also had only a minor effect (Fig. 3-10).

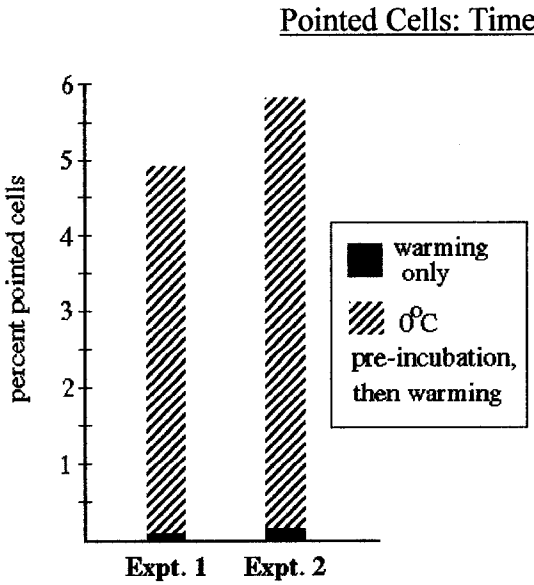

Figure 3-7. Primary variable: + or - pre-incubation at 0 °C
Warming: 5 hrs. at 22 °C

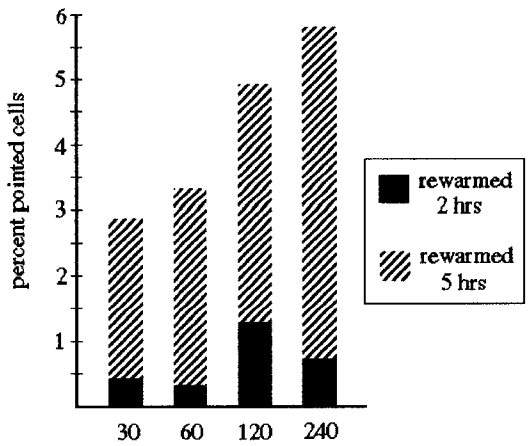

Figure 3-8. Primary variable: time at 0 °C
Rewarming: 2 hrs vs. 5 hrs
NOTE: % pointed at 0 °C (before rewarming) ≈ 0

Pointed Cells: Temperature Cycling and Agitation

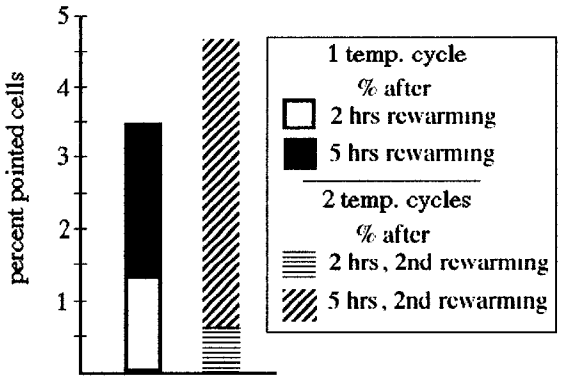

Figure 3-9. Primary variable: no. of temperature cycles.
1 cycle = 2 hrs 0 °C, 5 hrs 22 °C
2 cycles = 2 hrs 0 °C, 2 hrs 22 °C;
2 hrs 0 °C, 5 hrs 22 °C
NOTE: % pointed at 0 °C
(before rewarming) ≈ 0.2

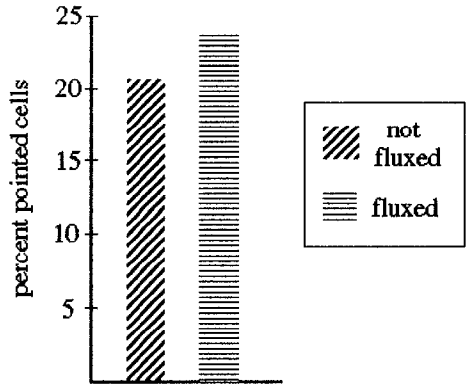

Figure 3-10. Primary variable: + or - mechanical agitation after rewarming (fluxing through 10 µl capillary tubes)
Incubations: 0 °C 2 hrs, rewarming: 5 hrs
NOTE: % pointed at 0 °C
(before rewarming) = < 0.5

8. Jasplakinolide treatment prior to chilling reduces pointed cell formation.

Earlier work established that pointed MBs were the causal agent for pointed, cell formation (Joseph-Silverstein and Cohen, 1984), and therefore the % pointed cells in a given preparation can be used as an indication of MB integrity in the cell population. Given the association of F-actin with the MB in normal cells, the next question was whether jasplakinolide perturbation of F-actin in living cells might have a secondary effect on microtubular MB integrity and pointed cell formation. The simplest hypothesis was that stabilization of the F-actin might stabilize MB microtubules.

Results of first experiments on this question are presented in figures 3-11 and 3-12. Pre-incubation of living erythrocytes with 1 µM jasplakinolide for 4 hrs, followed by the

temperature-cycling procedure, yielded only about half the number of pointed cells as did controls (fig. 3-11). In contrast, addition of jasplakinolide to cells after 4 hrs at 0 °C, just prior to rewarming, produced the opposite effect: an increased % of pointed cells (fig.3-12).

In perspective, presumed hyperstabilization of F-actin prior to MT disassembly at low temperature results in at least some stabilization of MB microtubules, inhibiting pointed cell formation. Jasplakinolide addition after MT disassembly does not have that effect, and may even interfere with normal MB reassembly such that more pointed cells are produced. It should be noted, however, that these results require repetition before publication.

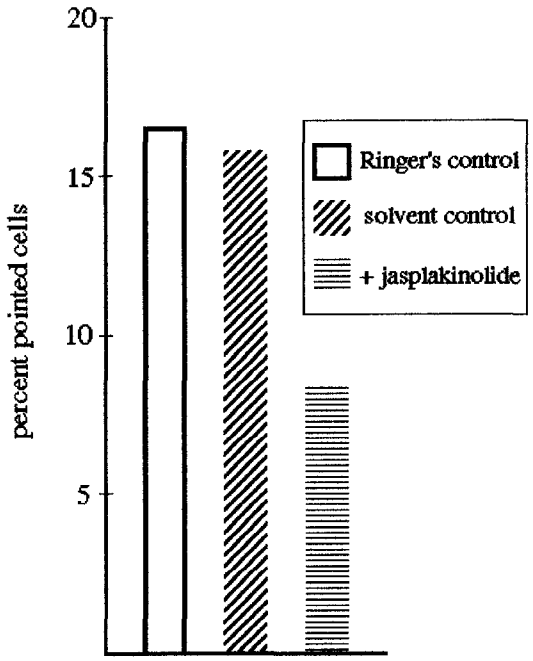

Figure 3-11. Jasplakinolide addition before low temperature incubation (jasplakinolide pre-incubation 4 hrs; 0 °C 4 hrs; rewarming 5 hrs)

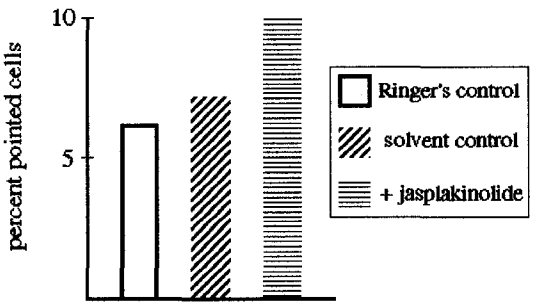

Figure 3-12. Jasplakinolide addition after low temperature incubation (0 °C 4 hrs; addition just prior to rewarming 5 hrs)

DISCUSSION:

9. The F-actin band is a highly stable structure that maintains the elliptical state of the microtubule band.

Latrunculin B, cytochalasin D, gelsolin, and mycalolide B are known to sever actin filaments. While the first three inhibitors also have capping and nucleating capability to some extent, mycalolide B is known to act only as a severing agent (Saito et al, 1994). However, the mechanisms by which these agents affect F-actin are targeted on dynamic systems. These agents failed to remove or detach the F-actin band from the marginal band, strongly indicating that the F-actin band is in non-dynamic state. Its increased stability may be due to various F-actin binding proteins.

MBs can be isolated when cytoskeletons are treated with combined SDS-triton solution. Such isolated MBs are initially elliptical, but become circular when exposed to these treatments for a prolonged period of time (Cohen et al, 1998). Labeling of F-actin (by phalloidin) in the isolated MB followed by circularizing treatment with elastase revealed that F-actin is responsible for maintaining the elliptical MB morphology

10. The F-actin band in erythrocytes protects microtubule band from low temperature induced disassembly.

The MB microtubules of certain species like smooth dogfish are cold labile; they disassemble at 0 °C and reassemble upon re-warming at physiological temperature (Behnke, 1970; Cohen *et al.*, 1982; Nemhauser *et al.*, 1983; Cohen, 1991). Low temperature treatment of living cells in suspension for 16 hours, followed by immediate cytoskeleton preparation and fixation (so that the MB microtubules will not reassemble)

showed that the F-band was still present, although in buckled conformations. This showed that the F-actin band was more resistant to low temperature treatment than the microtubule band. Taken a step further, hyperstablization of the F-actin in low temperature experiment showed decreased microtubule band disassembly. Therefore, data indicate that the function of F-actin is maintenance of both the shape and stability of the microtubule band.

11. Stability of F-actin band is may be required to prevent fracture of the microtubule band.

A fracture in the microtubule band is the causative agent of pointed cell shape (Joseph-Silverstein and Cohen, 1984; fig. 3-6). It was shown above that typical F-actin band-microtubule band colocalization is lost in these cells. Also, hyperstabilization of the F-actin with jasplakinolide diminished the number of temperature-cycle induced pointed cells. These results indicate that F-actin band stability and its association with the microtubule band are required for the integrity of the latter.

SUMMARY OF FINDINGS

(A) F-actin contributes in maintaining the ellipsoidal shape of the MT band.

(B) F-actin bundle is stable at 0 °C whereas the MT band disassembles.

(C) Hyper-stabilization of F-actin retards low temperature induced MT band disassembly.

(D) Normal F-actin band-microtubule band association is lost in pointed erythrocytes.

(E) Hyperstabilization of F-actin reduces the number of pointed cells generated as a result of fractured marginal band.

CHAPTER 4: **F-Actin-Microtubule Structural Interaction In Thrombocytes**

RESULTS:

1. Unactivated thrombocytes are ovoid in shape and possess a prominent nucleus.

Non-mammalian vertebrate thrombocytes are functional equivalents of mammalian platelets, implicated in coagulation and inflammation responses. Unactivated thrombocytes were ovoid and somewhat flattened in shape and 14~16 μm in length (fig. 4-1). The cell contour appeared smooth and the nucleus, also flattened and ovoid, occupied a large proportion of cell volume. The peri-nuclear region was characterized by granular bodies, visible under both phase-contrast and DIC.

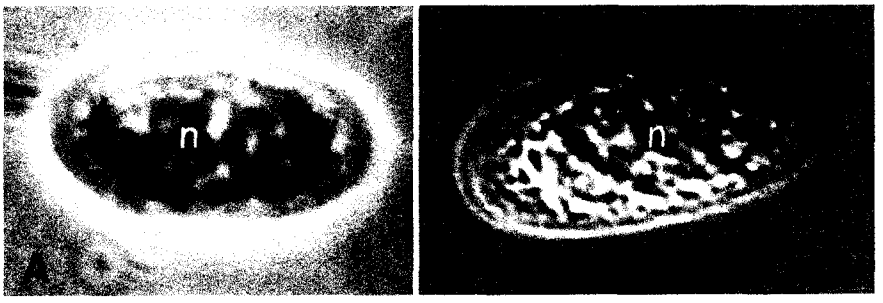

Figure 4-1. Unactivated dogfish thrombocytes: (A) phase-contrast; (B) DIC. n = nucleus. Bar, 10 μm

2. The microtubule band and the canalicular system are two prominent identifying features of unactivated thrombocytes.

Previous studies of the ultrastructure of thrombocytes reported a band of microtubules in the cell periphery (Fawcett and Witebsky, 1964; Rowley and Ratcliffe, 1988).

In thin sections, the resting thrombocyte exhibited relatively smooth cell-contour and a proportionally large nucleus. The nucleus was irregular in shape and characterized by an invagination (fig. 4-2a). A system of uniformly distributed vacuoles was found flanking the nucleus. In most unactivated cells, these vacuoles appeared spherical and were not interconnected. Dense bodies were found in regions between the CS vacuoles and the nucleus. Clusters of cross-sectioned MB microtubules were located at the poles of the cell sectioned either through the short or the long cell-axis (fig. 4-2b). Also, in grazing sections (near cell surface) perpendicular to the cell equator, MB microtubules were distributed in parallel, flanked by CS vacuoles (fig. 4-3). In all samples examined, microtubules of resting thrombocytes were strictly confined to the MB, i.e., absent in other cell regions. Among the white cell types in dogfish blood, MB microtubules and the CS vacuoles were present only in thrombocytes and, thus, these features served as markers for identifying resting and activated thrombocytes from other cell types.

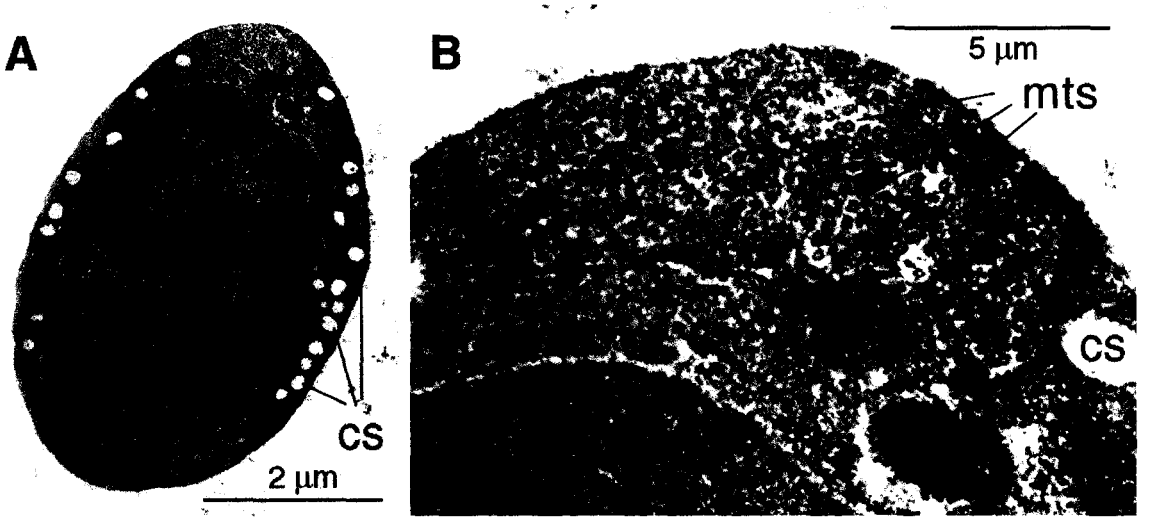

Figure 4-2. Unactivated thrombocyte, thin section in TEM: (A) Cross-section through the short axis of the cell, showing canalicular system (CS) along the periphery; (B) Higher magnification of the upper end of (A) with MB microtubules (MTs) in cross-section.

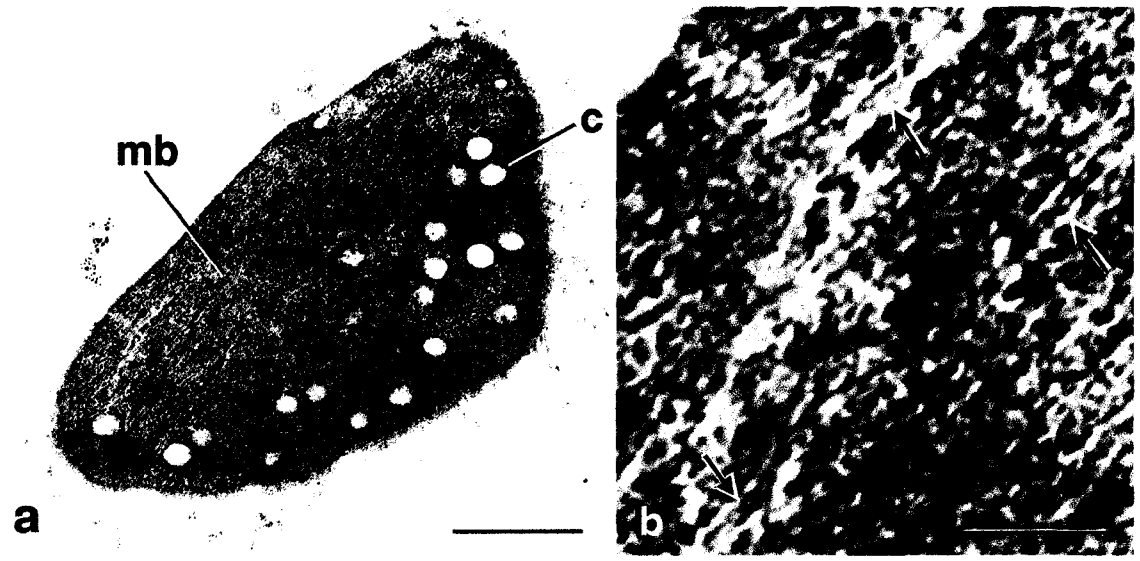

Figure 4-3. Unactivated thrombocyte. (a) A grazing section through the peripheral cell region showing MB microtubules (mb) and the canalicular system. Bar = 1 μm; (b) Higher magnification view of the MB microtubules (arrows) in (a). Bar = 200 nm

3. Unactivated thrombocytes posses a band of F-actin colocalizing with microtubule band.

As observed by immunofluorescence microscopy, resting dogfish thrombocytes exhibited a prominent circumferential microtubule bundle (fig. 4-4A) in the plane of flattening, i.e., a thick marginal band (MB), with few microtubules elsewhere. Confocal image analysis showed that a band of F-actin also existed in the cytoskeleton of the unactivated thrombocytes, and that it co-localized with MB microtubules (figs. 4-4 and 4-5). However, the F-actin band was thinner (~0.5 μm) than the microtubular MB (~1.4 μm), and was restricted to the peripheral MB region (fig. 4-4C). Edge-on views confirmed the presence of the F-actin band and its colocalization with the outer MB microtubules (fig. 4-5).

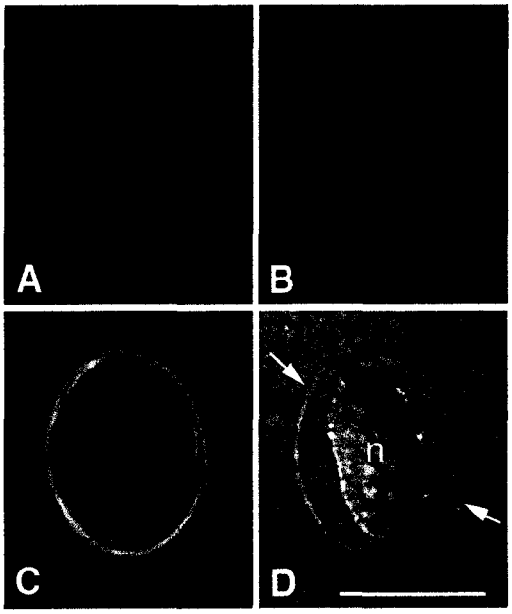

Figure 4-4. Cytoskeleton of unactivated, double-labeled thrombocyte (confocal): (A) FITC-labeled tubulin distribution; note multiple microtubule bundles in the MB and single microtubules or minor bundles internal to the MB; (B) Texas-Red phalloidin; a band of F-actin colocalizes with the MB, but is thinner than that of microtubules. Network-like F-actin also appears in the interior except for the central dark region where the cell cortex is out of optical plane; (C) Superimposition of (A) and (B). The orange overlap is pronounced at the MB periphery, whereas streaks of microtubule signal appear at the MB inner edge; (D) DIC image of the same cytoskeleton, in which bundles of microtubules are distinguishable (arrows). n = nucleus. Bar, 10 μm

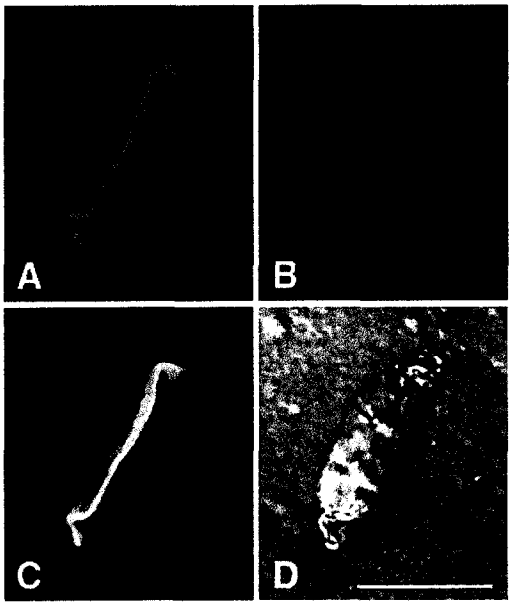

Figure 4-5. Edge-on view of double-labeled thrombocyte cytoskeleton (confocal): (A) tubulin distribution, near-planar band; (B) F-actin; the MB region displays the highest density of F-actin in a band thinner than that of tubulin in (A). A network of F-actin is also present above and below the MB plane; (C) Superimposition of (A) and (B); (D) DIC. Bar, 10 μm.

F-actin was also observed elsewhere in the cytoskeleton. Optical sectioning showed that most of it was localized to the cell cortex in mesh-like form (fig. 4-6A, C), with occasional dense patches. The region deeper into the interior was largely devoid of F-

actin (fig. 4-6B, D). Mid-optical sections through cells oriented on their edge revealed that the MB was enclosed by, and abutting against, the cortical F-actin (fig. 4-6E).

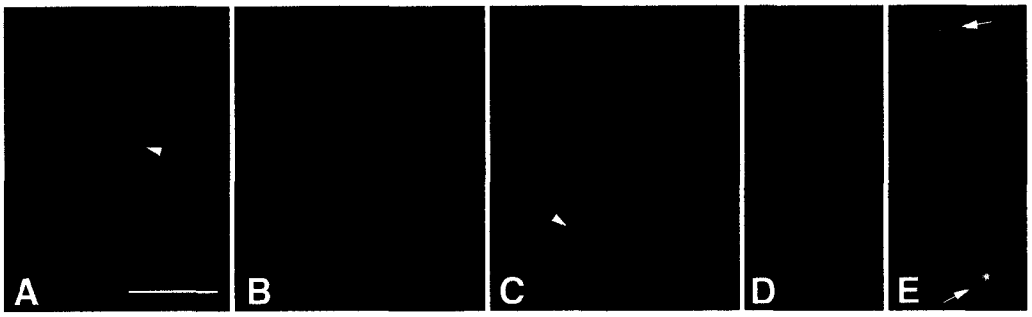

Figure 4-6. F-actin in the cortex (confocal): (A) optical section through one cortical region of unactivated cell in flat orientation; note the meshwork-like pattern of F-actin with a patchy region of high intensity (arrowhead); (B) section through the mid-region showing F-actin in a band and lack of internal signal; (C) section through the opposite cortical region (relative to A), with similar F-actin distribution as in (A, arrowhead: patch); (D) optical section through mid-Z axis of another cell viewed on edge, exhibiting F-actin in the cortical region; (E) composite of (D) with tubulin distribution, showing location of MB cross-sections (arrows) at opposite extremities of the cortical network. Bar, 5 μm.

4. Thrombocytes undergo shape changes as a response to activating agents.

Although nucleated thrombocytes were known to undergo shape changes post-activation, the sequence of stages had not been determined previously. To do this, perfusion with thrombin was used to induce activation of individual pre-selected thrombocytes while they were observed continuously under the coverslip (fig. 4-7). Overall, cell morphology changed from the elongated, somewhat flattened ovoid, to a refractile spheroid, and then to a highly flattened, relatively circular spreading "pancake"-like form. Thrombocytes in initial stages of activation (fig. 4-7A) adhered to the slide and resisted being dislodged by the perfusion flow (fig. 4-7B). Shortly after activation, the cell developed a point at one end of its long axis (fig. 4-7C) and within ~10 seconds

became spheroidal (fig. 4-7E). Blebs and pointed projections were constantly protruding and contracting from the spheroid and, in ~1 minute, sheet-like extensions emanated in a circular pattern (fig. 4-7F). At ~3.5 minutes, cytoplasmic protrusions were evident and the nucleus appeared to be lobed (fig. 4-7G). Subsequently, with further cell spreading, the nucleus became lobulated and appeared to be fragmented (fig. 4-7H, I). Note: A movie of the described sequence is available. The sequence reported in fig. 4-7 was verified by more than 50 perfusion experiments and observation of several hundred individual cells.

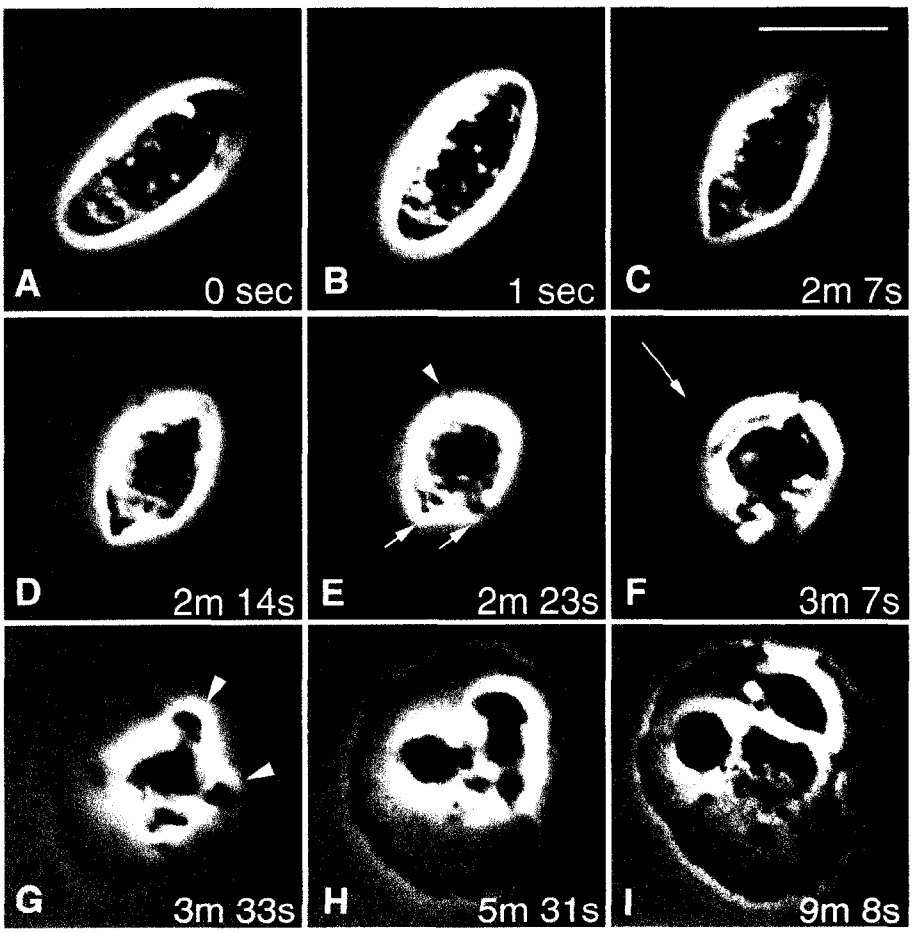

Figure 4-7. Stages following thrombocyte activation by thrombin perfusion (phase-contrast): (A-B) initial stage; cell has adhered to the slide; (C-D) pointed stages; (E) spheroidal stage (arrows: blebs; arrowhead: spike); (F) transition to pancake stage (arrow: edge of spreading cell); (G) developing pancake with cytoplasmic protrusions (arrowheads, focus on upper surface); (H-I) late pancake stages exhibiting nuclear lobulation. Bar, 10 μm

5. In spontaneously activated thrombocytes with altered shape, typical F-actin-microtubule colocalization in the marginal band is lost.

Thrombocytes activated spontaneously, though somewhat asynchronously, when whole blood was spread on coverslips. When cells were fixed within 15 minutes of blood withdrawal, various stages of early activation were observed, corresponding to those induced by thrombin (fig. 4-8B vs. fig. 4-7A - E). MB shape in these cells corresponded very closely to the cell surface contours in different morphological stages of activation (fig. 4-8A vs. 4-8B).

In the pointed stage, the number and location of points in the MB matched that of points in the cell (fig. 4-8, cell 3), whereas in the spheroidal stage, the entire MB was buckled, conforming to cell shape (fig. 4-8, cell 4), which also appeared to be folded relative to the unactivated state (fig. 4-8D).

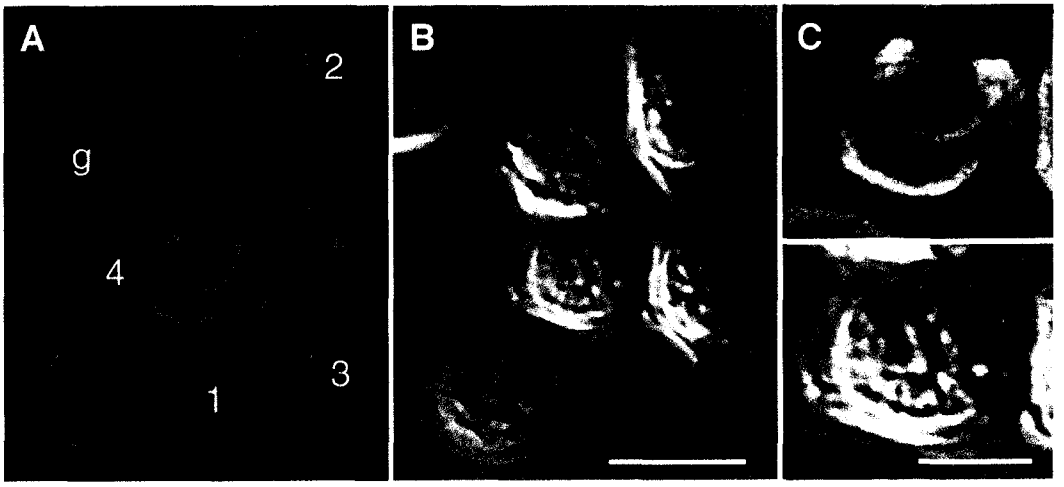

Figure 4-8. Early stages of thrombocyte activation (confocal): (A) tubulin distribution; cell 1: relatively unactivated; cells 2 and 3: pointed stage, corresponding to fig. 4-7C and D; cell 4: spheroidal stage; cell g: a non-thrombocyte spheroidal cell lacking MB (a putative granulocyte); (B) DIC, same field; (C) higher magnification view of cell 4 in (A), showing bent MB (tubulin, green) and F-actin distribution (red). F-actin at this stage has already lost colocalization with outer MB microtubules; (D) DIC view of (C), revealing that nucleus is correspondingly folded. Bars, 10 μm (A & B); 5 μm (C & D)

6. During activation induced shape change, F-actin has an outward distribution while microtubules remain central, possibly remodeling the nucleus.

Confocal sections (stacks) showed that the buckled MB was enclosing the nucleus (fig. 4-9). F-actin, which had colocalized as a band along the entire length of the MB in the unactivated cells, no longer did so in the spheroidal stage cells. However, a significant concentration of F-actin remained in the cortical region and also redistributed into the dynamic surface blebs (fig. 4-9; fig. 4-12). Spheroidal cells of both spontaneously and thrombin-activated preparations exhibited constantly protruding and contracting surface blebs containing F-actin, but not tubulin (fig. 4-10).

Another type of spheroidal cell, with aster-like microtubule distribution instead of a typical MB, was identified as a granulocyte (fig. 4-8, cell G; fig. 4-11). This cell, also containing blebs, was not easily distinguishable from the spheroidal thrombocyte under phase-contrast or DIC. Thus, presence of the MB served to identify activating thrombocytes from other cells.

Subsequently, blebbing spheroidal cells initiated nuclear lobulation, and the nuclear lobes were found to have closely associated microtubules (fig. 4-12A-C). Optical sections through apical regions showed F-actin in several blebs, while basal regions showed F-actin in spike-like projections together with blebs (fig. 4-12D-E). At a transition to the pancake stage, the nucleus was divided into lobes (fig. 4-13B) with microtubule bundles wrapped around the nuclear furrows. These microtubule bundles were disorganized relative to those of MBs and were frequently arranged in a zigzag pattern (fig. 4-13C-D). Computer generated 3D rotation revealed a ring-like structure (fig. 4-13E). Spiky F-actin projections became prominent in the basal region, with few remaining blebs (fig. 4-13F). With constant

extension and retraction, these projections attached to the surface, and regions between them became filled with F-actin sheets in a webfoot-like arrangement.

Early in pancake formation, the nucleus was multi-lobed without marked lobe separation (fig. 4-14A). In most cases, microtubule bundles were associated with each nuclear furrow (fig. 4-14B-C). While blebs and spiky projections were no longer evident, F-actin was found distributed throughout the cell in fibrous arrangements (fig. 4-14D). In full pancake stages, the nucleus of most cells was extensively lobed and sufficiently separated to appear fragmented (fig. 4-15A-B). The microtubule bundles were disorganized to a greater extent than earlier, with many single microtubules or minor bundles projecting from the major ones (fig. 4-15C). When superimposed with nuclear distribution, convoluted MT bundles were found in the gaps between nuclear fragments (fig. 4-15D), with major bundles wrapped around the neck of the lobes (fig. 4-15E). F-actin was now prominent, occupying the entire spreading cell body in the form of stress fibers (fig. 4-15F). Pancakes undergoing nuclear fragmentation exhibited increased stress fiber density in patches near the cell center. However, stress fibers arranged in triangular or quadrilateral geometry were also observed in significant numbers of cells. In these pancakes, there was no apparent nuclear lobulation (fig. 4-16). Similar observations were made in pancakes resulting from spontaneous activation on glass surfaces.

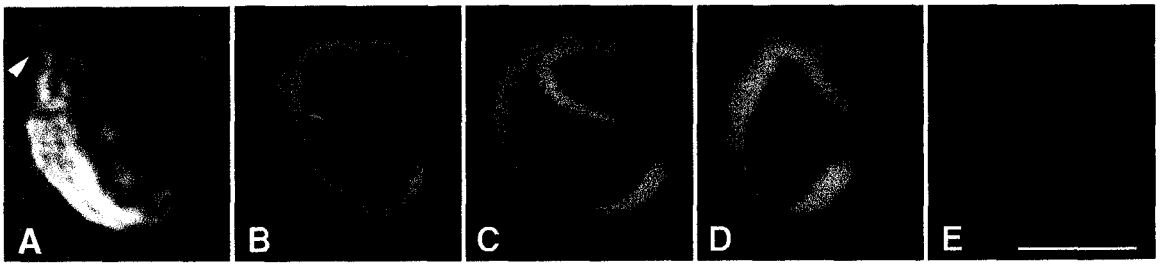

Figure 4-9. MB geometry at the spheroidal stage (confocal): (A) spheroidal cell with a bleb (arrowhead; DIC); (B) composite of DAPI-stained nucleus (blue) and MB microtubules. The MB is bent and encloses the nucleus; (C) 3D computer rotation of (B) by 22.5°;(D) 90°; (E) F-actin distribution. Note: images projected by 3D computer rotation are commonly blurred with increasing angle of rotation such as in (C) and (D). Bar, 5 μm.

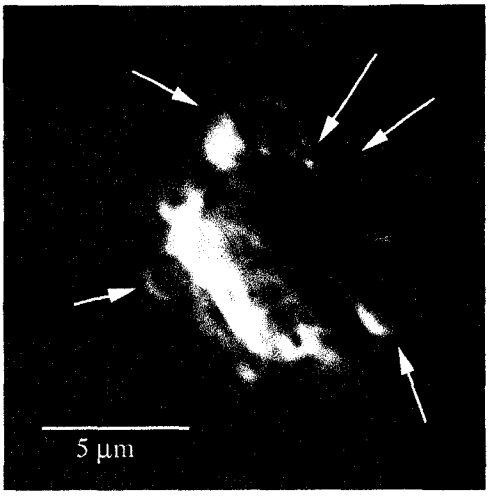

Figure 4-10. Spheroidal stage of activation: At 1~2 minutes of thrombin-induced activation, spheroidal cells develop dynamic blebs such as shown by the white arrows (DIC). Insets: distribution of F-actin in corresponding blebs (confocal).

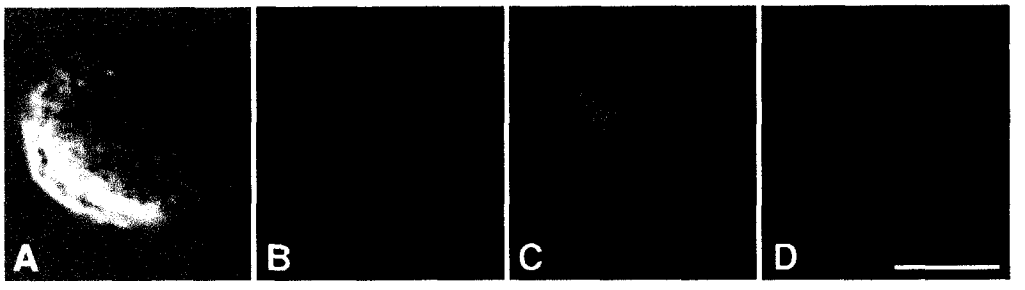

Figure 4-11. Example of a spheroidal cell that is not a thrombocyte (confocal): (A) DIC view; (B) DAPI-stained nucleus; (C) aster-like microtubules (no MB); (D) F-actin distribution, exhibiting irregular surface corresponding to (A). Note: (B)-(D) are stacks. Bar, 5 μm.

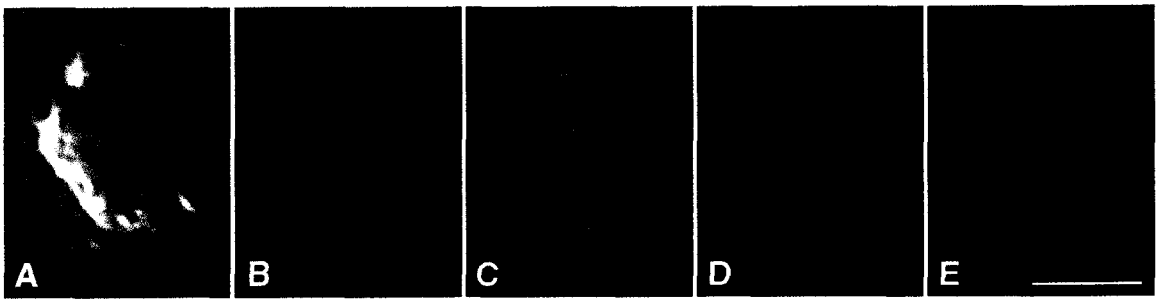

Figure 4-12. Spheroidal cell with blebs and projections (confocal): (A) DIC, showing blebs; (B) nucleus, in two lobes; (C) altered MB; (D) F-actin distribution in an optical section through apical region, exhibiting several blebs; (E) F-actin distribution in a section through basal region, showing both blebs and a projection. Bars, 5 μm.

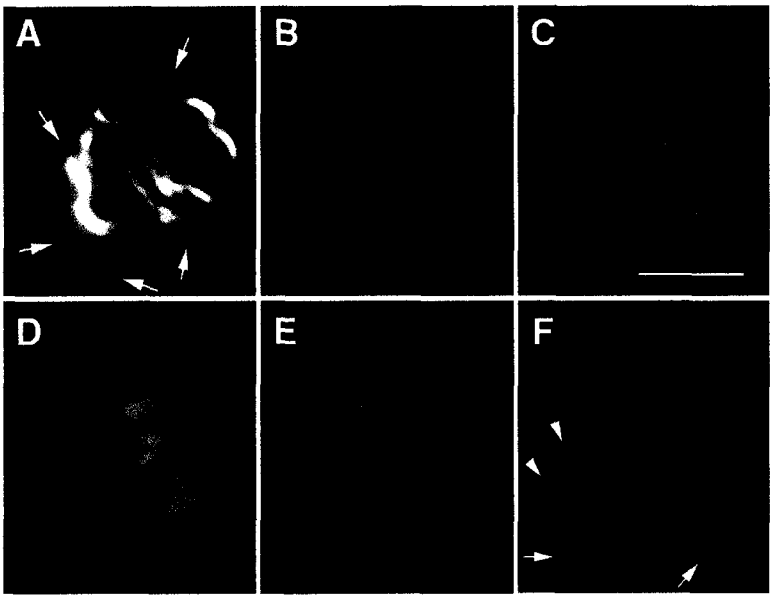

Figure 4-13. Transition from spheroidal to pancake stage (confocal): (A) DIC, showing the spreading cell edge (arrows); (B) DAPI-stained nucleus, with lobulation and cleft; natural side view; (C) distribution of MB microtubules, natural side view. MB-derived microtubules have taken on a zigzag pattern; (D) composite of (B) and (C), showing microtubules localized within the cleft; (E) 90° computer 3D rotation of (C), revealing that the nucleus-associated microtubules form a ring; (F) F-actin (stack), exhibiting pointed projections (arrowheads) and sheet-like F-actin (arrows). Bar, 5 μm.

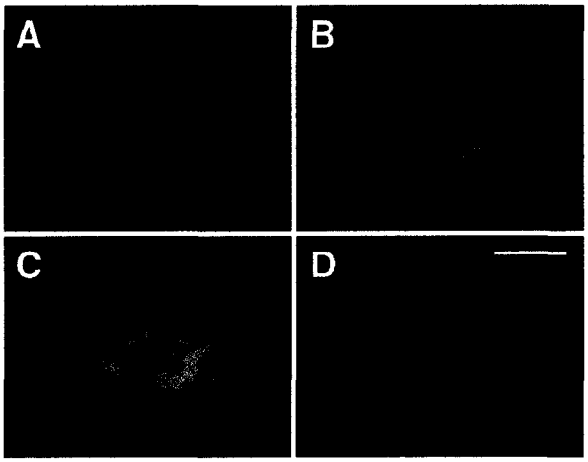

Figure 4-14. Early pancake stage (confocal): (A) Nucleus with 3 lobes; (B) microtubule distribution; (C) composite of (A) and (C), showing microtubule bundles associated with clefts of the lobulating nucleus; (D) F-actin distribution, typical of early cell spreading. Bar, 5 μm.

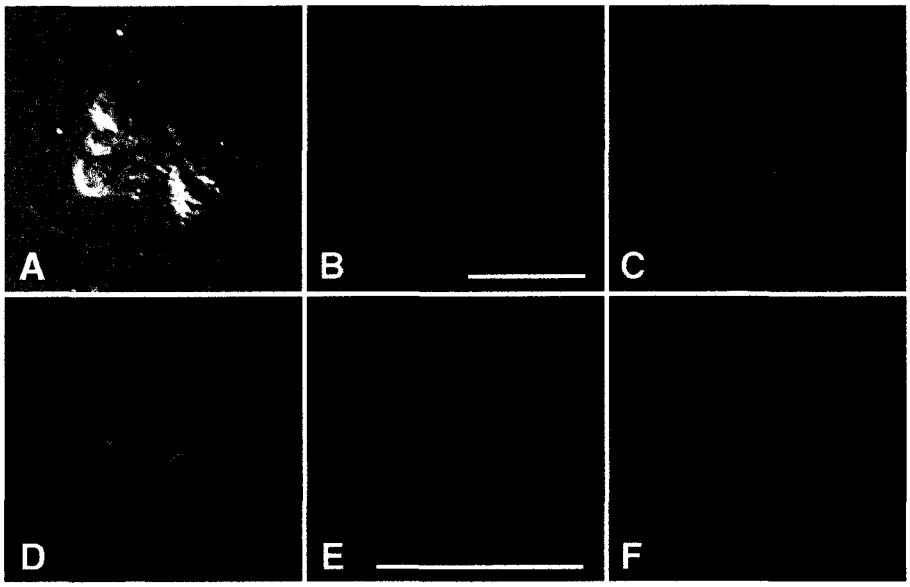

Figure 4-15. Advanced nuclear lobulation and fragmentation in a pancake stage cell (confocal): (A) DIC, showing the cell edge and the lobulating nucleus; (B) DAPI-stained nucleus with three major lobes; (C) distribution of microtubules; (D) composite of (B) and (C), revealing loops of microtubule bundles associated with nuclear lobes; (E) close-up of (D), with major loops of microtubule bundles wrapped around the lobes; (F) F-actin distribution. Bars, 10 μm. (E) is a confocal section and all the others are stacks.

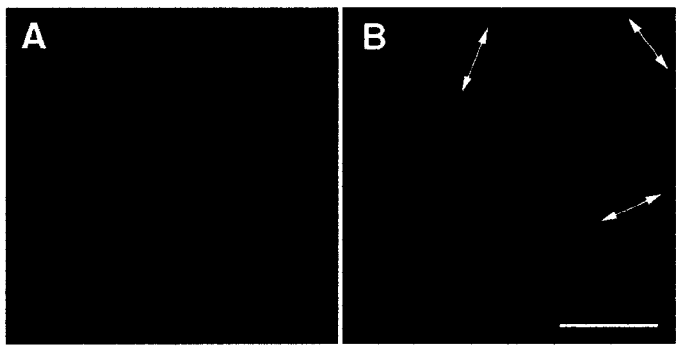

Figure 4-16. Pancakes with and without nuclear lobulation (confocal): (A) DAPI, showing the nucleus of a pancake with no lobes (upper) and of another with four lobes (lower); (B) F-actin, exhibiting stress fibers arranged in geometric (triangular) pattern (upper cell, double headed arrows) and in a less defined pattern (lower cell). Bar, 10 μm

7. Microtubule bundles are also found in the constrictions between nuclear lobes in thin sections.

During the advanced spheroidal stage, thrombocytes were characterized by irregular (blebbing) cell-contour with extensive protrusions (fig. 4-17a). The nucleus in this stage was significantly more distorted than that of the resting cell, with a channel traversing the mid-region. Major cavities, or pockets, contained clusters of microtubules along the length of this channel (fig. 4-17b). The initially spheroidal CS vacuoles became morphologically irregular and significantly sparser, frequently clustered near the cell membrane. During the early pancake stage, thrombocytes became firmly attached to the substrate, such that they survived several aggressive washes, and their basal region became spread laterally (fig. 4-18). Sections through this region revealed highly irregular cell-contour, frequently associated with dense clusters of fibrous projections. Nuclear morphology was also expanded, and was characterized by developing lobes. Bundles of microtubules were frequently found in pockets between these nuclear lobes (e.g., fig. 4-18 inset) and, to a lesser extent, in other peri-nuclear regions. The morphology of CS

vacuoles was similar to those of spheroidal cells and their distribution was usually confined to a region of the cell as a cluster.

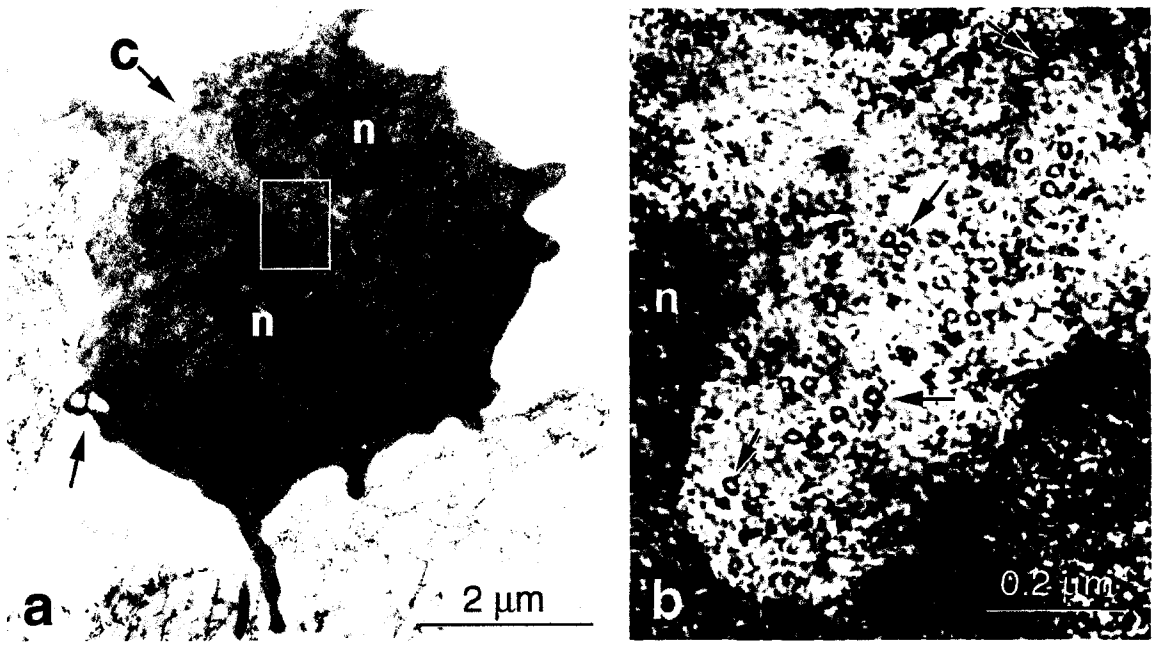

Figure 4-17. Advanced spheroidal stage (TEM): (a) activated thrombocyte, with canalicular remnant (arrow). The nucleus (n) has a channel (arrow "C"); (b) higher magnification view of boxed area in (a). The pocket in the mid-region of the channel is filled with microtubules, many in cross section (examples at arrows).

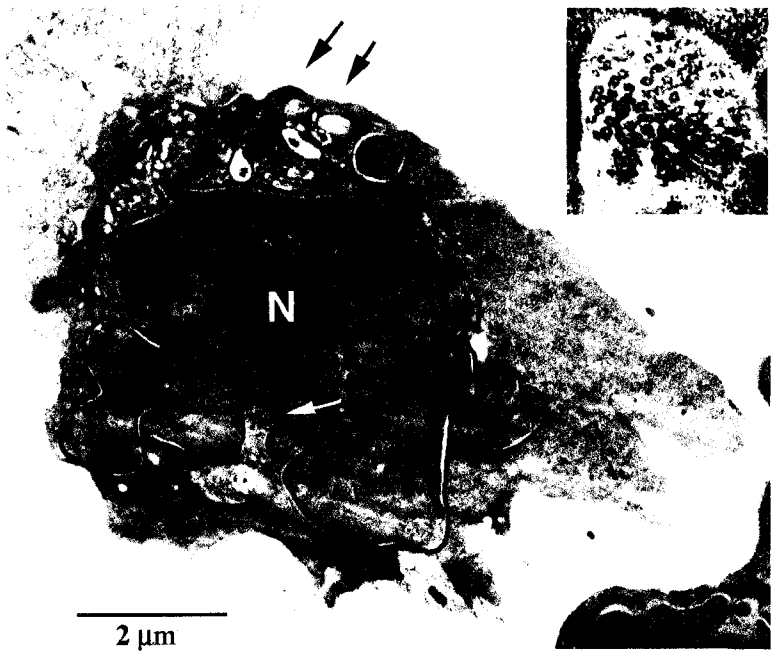

Figure 4-18. Early pancake stage (TEM): Thin section through the basal region of activated cell attached to a flat surface. The outlined nucleus (N) is lobulated, exhibiting a pocket containing a bundle of microtubules in cross-section (white arrow and inset). A group of CS vacuole remnants is located in the upper region of the cell (black arrows).

DISCUSSION

8. The F-actin band is microtubule band specific, rather than erythrocyte specific.

Existence of the F-actin band in thrombocytes indicate that it may be a constant feature of cells possessing the microtubule band, independent of cell cargo. However, our results show that the nature of structural arrangement may be different. In both dogfish and newt erythrocytes, the thickness of the F-actin band matches that of the microtubule band (figs. 2-3; 2-5), whereas in thrombocytes the F-actin is about half the thickness of the microtubule band and the colocalization is restricted to the peripheral microtubule bundles (fig. 4-19).

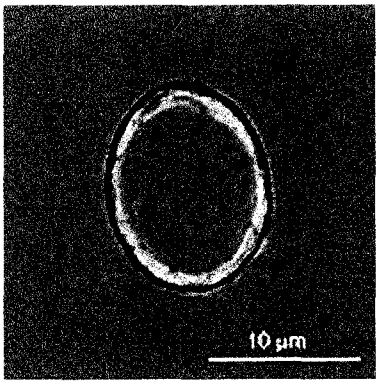

Figure 4-19: Enhanced composite image of fig 4-4 (a) and (b). The darker outer ring represents F-actin distribution and the dark ring represents microtubule distribution.

9. F-actin exhibits peripheral distribution, while microtubules remain central, possibly driving nuclear lobulation during shape change.

While F-actin displays a progressively outward distribution during shape change, MB microtubules exhibit the opposite pattern. Early in activation, the MB accommodates itself into the spheroidal cell shape by buckling or bending (analogous to the seam in a baseball), in effect enclosing the nucleus (fig. 4-9). Subsequently, the major bundle of MB microtubules remains intimately associated with the nucleus as such, and becomes increasingly disorganized as the cell spreads. In all observed cases of cells with a

fragmented nucleus, convoluted bundles of microtubules were found between the migrating nuclear fragments (fig. 4-15D and 4-15H-I) with major bundles wrapped around the neck region between lobes.

This explains the presence of microtubules near nuclear lobes in TEM thin sections reported by Shepro *et al.* (1966). This intimate association of microtubules with nuclear constrictions suggests that they may provide the force required for nuclear lobulation and fragmentation in this system. However, the nature of this driving force and the mechanism of nuclear fragment migration away from the central region remain to be demonstrated.

There is precedence for microtubules exerting a mechanical force to reshape the nucleus. Strongest evidence comes from studies of spermatogenesis in many species, in which manchette microtubules and associated dynein and kinesin motor proteins are believed to be the effector (McIntosh and Porter, 1967; Yoshida *et al.*, 1994; Hall *et al.*, 1992). The intimate association of the MTs with nuclear lobes observed in activated thrombocytes suggests that MTs may provide the force required for nuclear lobulation and fragmentation in this system, but this remains to be tested.

10. Compared to that of mammalian platelets, blebbing and nuclear lobulation are distinguishing features of nucleated thrombocyte shape change.

As observed in the present study, post-activation events in nucleated thrombocytes do parallel those of mammalian platelets with respect to characteristic morphological states and the corresponding time frame. At ~2 minutes after activation, both cell types transform from a planar to a spheroidal state. Cells in this state extend and retract

cytoplasmic projections, presumably securing attachment to the surface, or, potentially, to each other. After attachment, at 3 ~ 4 minutes, both develop radially spreading cytoplasm between the projections referred to as hyalomeres in the platelet sequence (Allen *et al.*, 1979), culminating in a fully spread state at ~10 minutes.

Although the major morphological stages are comparable, one major difference is observed: nucleated thrombocytes develop dynamic blebs concurrent with becoming spheroids (fig. 4-9; 4-10), and these persist for about thirty seconds prior to extending projections. This has not been reported for mammalian platelets. Obviously, presence of the nucleus and its subsequent lobulation and fragmentation are additional distinguishing features in comparison with platelets.

11. Suggested experiment: Purification of thrombocytes may be possible by flow cytometry.

All thrombocyte experiments were carried out using white cell populations rather than pure thrombocyte population. Purification of the thrombocyte population has been attempted based on the method described by Mainwaring and Rowley (1985), using discontinuous Percoll step gradients. However, subjecting white cell suspensions to high "g" forces (>1000) in conjunction with exposure to dense material such as Percoll led to thrombocyte activation, and many times clot formation.

As an alternative method, separation of thrombocytes may be attainable by flow cytometry. This method does not require a probe for cell type recognition since sorting is based on the light scatter properties of cells (cell size and granularity). In zebrafish,

separation of various blood cell types and their precursors by this method seems to be suitable (Traver et al, 2003). Applicability on dogfish thrombocytes remains to be tested.

SUMMARY OF FINDINGS:

(A) A band of F-actin also exists in unactivated thrombocytes.

(B) In this respect, the F-actin band is not red cell specific, but rather marginal band specific.

(C) The F-actin band in thrombocytes is thinner than the microtubule band and colocalizes only with peripheral microtubules.

(D) F-actin-microtubule interaction is lost when thrombocytes undergo shape change.

(E) During activation induced shape change, F-actin has an outward distribution while microtubules remain central, possibly remodeling the nucleus

CHAPTER 5: **F-actin-microtubule functional interaction in thrombocytes**

RESULTS:

1. The MT band in unactivated thrombocyte is cold labile and maintains the cell shape (Pinhasov *et al.*, 2003).

In order to investigate whether thrombocyte microtubule band is sensitive to 0 °C, temperature cycling experiments were performed on white cell suspensions. Prior to chilling such cell suspension consisted of 30~35% thrombocytes identifiable under phase-contrast (fig. 5-1). This was also checked with fluorescence counting of the marginal band microtubules. Then cell suspensions were incubated at 0 °C for different time periods. At the completion of chilling, samples were fixed/lysed, and labeled for usual cytoskeletal components. Examination under phase-contrast revealed a significantly reduced number of ovoid thrombocytes and microtubule labeling showed very few recognizable band structures (fig. 5-2). This indicated that thrombocyte microtubule band was sensitive to low temperature and, if not total disassembly, such sensitivity lead to change of cell shape.

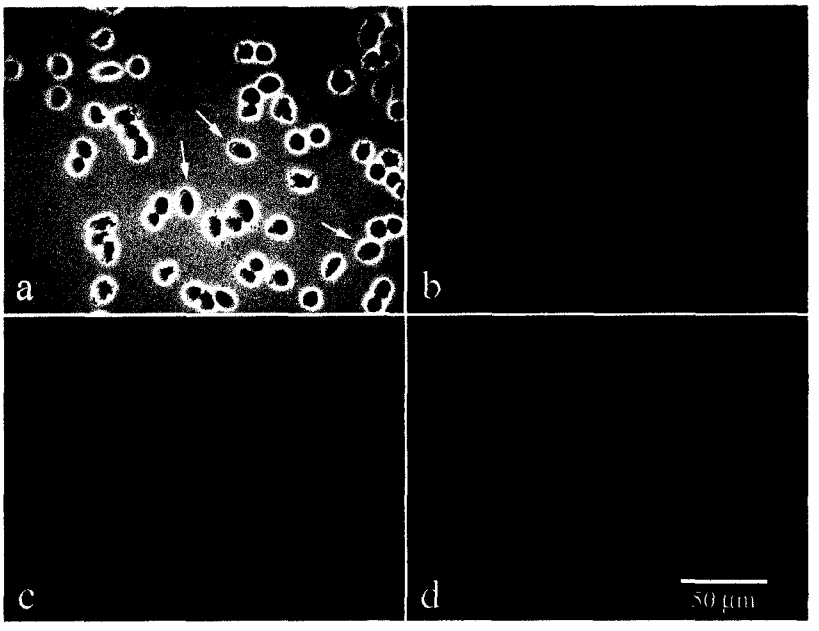

Figure 5-1. Representative population of white blood cells prior to temperature cycling (phase-contrast and epi-fluorescence): (a) mixed white cell types with significant percentage of ovoid thrombocytes (arrows); (b) DAPI stained nuclei; (c) F-actin distribution, with ovoid thrombocytes exhibiting higher intensity than other cells; (d) tubulin distribution revealing thrombocyte marginal bands.

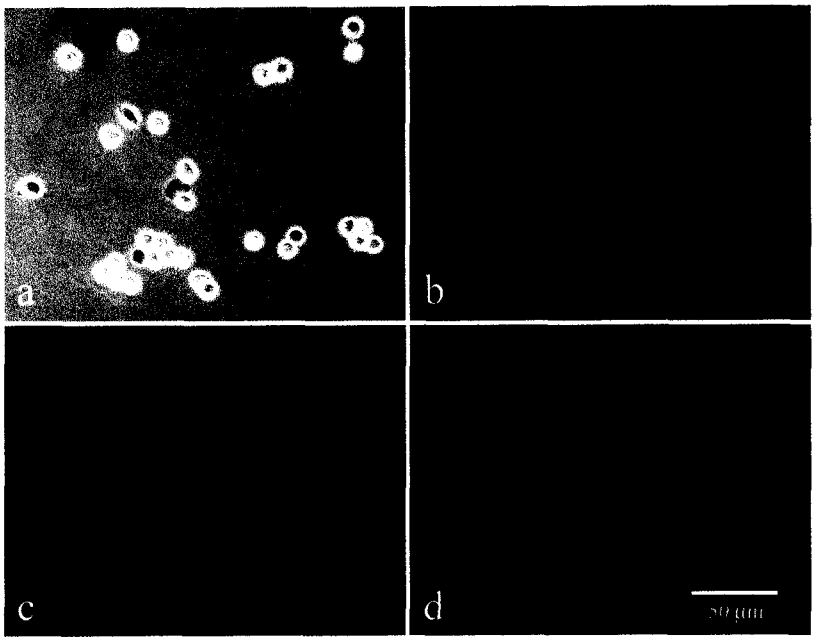

Figure 5-2. Diminished number of ovoid thrombocytes after incubation at 0 °C for 2 hours (phase-contrast and epi-fluorescence); (a) phase-contrast, showing an increased number of highly refractile spheroidal cells; (b) DAPI stained nuclei; (c) F-actin distribution; (d) tubulin staining showing very few recognizable MB.

Detailed examinations of some of the representative cell types present at 0°C revealed an increased number of spheroidal cells under DIC. Microtubule arrangement in these cells was astral or centrosomal. That is, these cells possessed microtubule rays radiating from a brightly labeled central spot (fig. 5-3). F-actin band in these cells was not evident.

When 0°C incubation was carried out in conjunction with 10 μg/ml nocodazole treatment, microtubule disassembly was driven to a greater extent (fig. 5-4). As in the previous case, ovoid thrombocytes were not detected, but there was a great number of spheroidal cells. When labeled for microtubules, a significant number of these spheroidal cells exhibited bright dots with no associated microtubule rays. Closer examination of these dots revealed that they frequently occurred in pairs, reminiscent of centriole pairs. F-actin band in these cells was not distinguishable either.

Figure 5-3. General population of cells after cooling at 0°C for 4 hours without the presence of nocodazole (computer projections of confocal optical sections): (a) cells with spheroid and ovoid shape (DIC); (b) cortical F-actin, possibly affected by cooling and by loss of microtubule organization; (c) disorganizing/disassembling bundles of microtubules frequently occurring with centrosomal and astral arrangement.

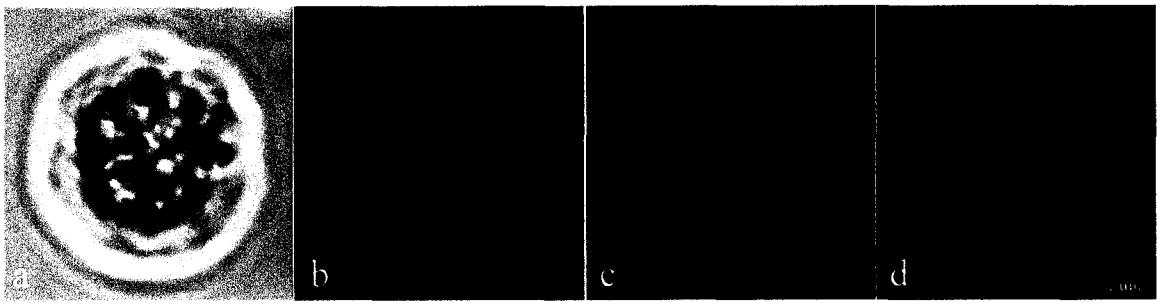

Figure 5-4. Thrombocyte incubated at 0°C with nocodazole (single optical section): (a) DIC image of a contour of a spheroidal thrombocyte; (b) DAPI; (c) dispersed F-actin; (d) pair of brightly fluorescent "dots" which are putative centrosomes.

2. Microtubule band in unactivated thrombocyte reassembles upon re-warming at 22 °C and also drives cell shape recovery

To assess the reversibility of microtubule disassembly, chilled samples were subsequently exposed to 22 °C for different time periods. Samples re-warmed for the same time period as chilling (2 hours) exhibited recognizable thrombocytes under phase-contrast. However, unlike the pre-chilled control cell population, re-warmed thrombocyte population consisted of cells with discoid, singly pointed, doubly pointed, triply pointed, and normal ovoid shapes (fig. 5-5). To quantify the extent of shape recovery, counts were

made over several incubation periods at 22 °C under phase-contrast (fig. 5-6). Prior to chilling, the count of normal ovoid thrombocytes was about ~27% and it declined to about 1~2% after 2 hours at 0°C. There were also variants, discoid in shape, which had the morphology of thrombocytes. These consisted of 10% of white cell population initially and declined slightly to ~8% at 0°C. At 2 hours of re-warming at 22 °C, count of recognizable thrombocytes with ovoid shape increased to ~22%, accompanied with minor percentages of pointed cells. Appearance of these pointed cells indicates that they may be intermediates during shape recovery. But this idea requires further testing. As a side note, thrombocytes with discoid morphology show resistance to temperature cycling treatments. The role of these cells in the grand scheme is not clear, but if these cells are included in the total thrombocyte count (brown line), a complete shape recovery is seen.

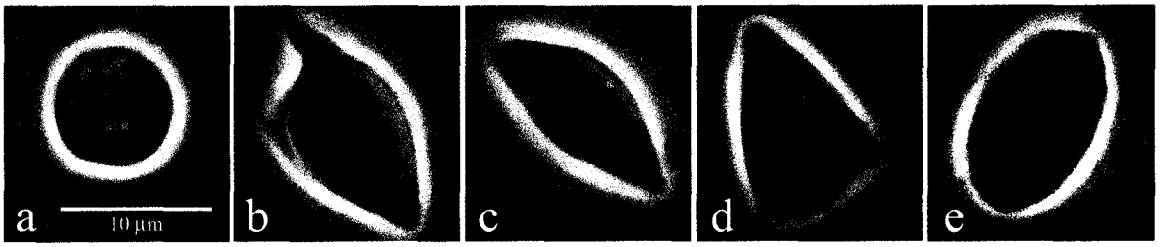

Figure 5-5. Various thrombocyte shapes generated after 2 hours of re-warming under phase-contrast: (a) discoid; (b) singly pointed; (c) doubly pointed; (d) triply pointed; (e) normal ovoid.

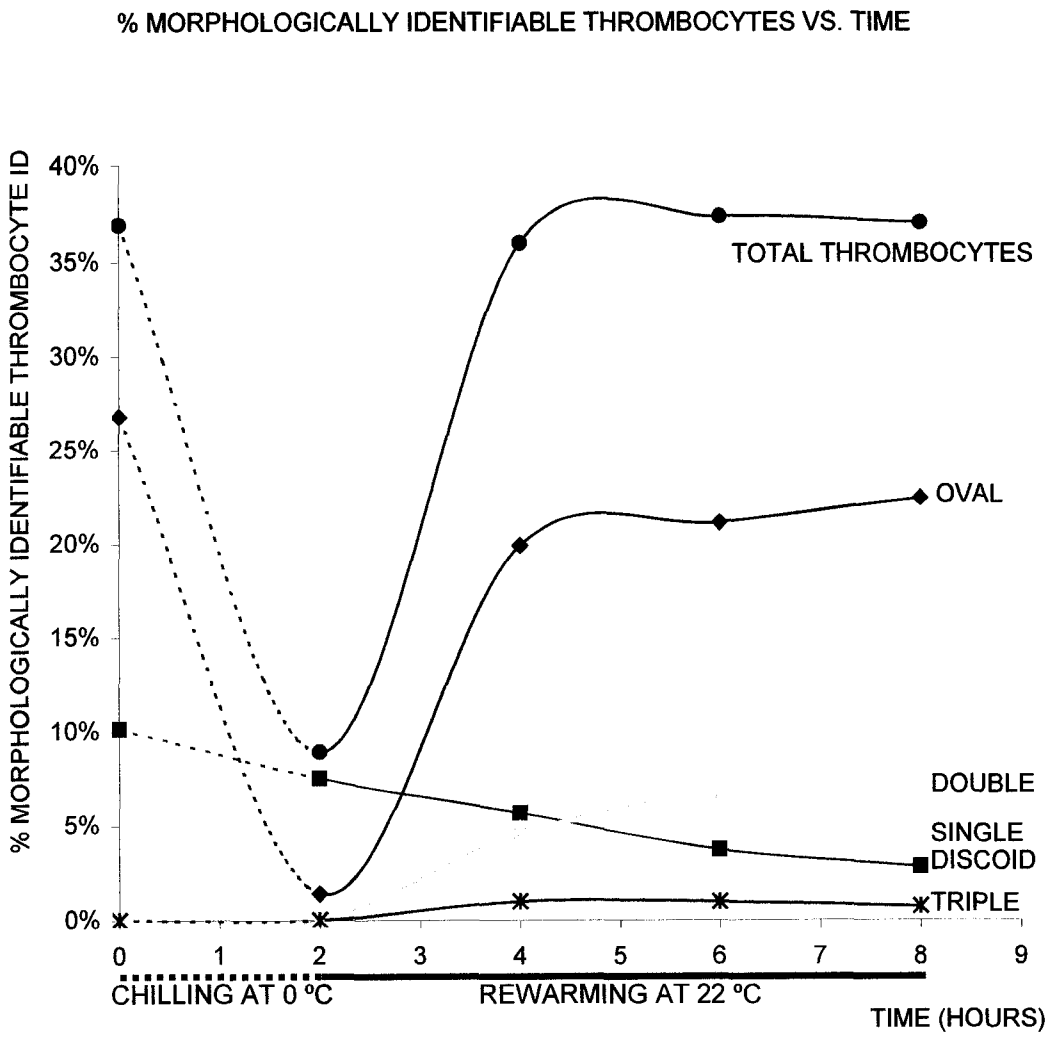

Figure 5-6. % morphologically identifiable thrombocytes (among all white cells by phase-contrast) upon chilling (0 °C) and subsequent rewarming (22 °C). Dotted lines denote incubation at 0 °C for 2 hours and solid lines at 22 °C for time periods after 2 hours. Ovoid thrombocytes (blue, 27% initially) become unrecognizable upon chilling (~1%) but are once again recognizable upon rewarming (>19%). Discoid thrombocytes (red) exhibit decreasing trend regardless of temperature treatment. Doubly-pointed, singly-pointed, and triply-pointed cells, unnoticeable in the initial sample and chilled sample, increase in numbers with increasing time of rewarming. Overall, the total thrombocyte with recognizable shape drops when exposed to 0 °C for 2 hours, but returns to values comparable to initial count upon rewarming (total thrombocytes).

When labeled for cytoskeletal components, recovered cells revealed major MT bundles that defined the cell contour. The pattern of microtubule arrangement in doubly pointed thrombocytes was particularly notable since the ends of microtubule bundles defined the points of these cells (figs. 5-7 and 5-8). Some of these pointed MT bundles also included an inner loop, suggesting that these pointed cells may be intermediates during shape recovery (fig. 5-8d).

Most of the re-warmed thrombocytes were ovoid in shape just like the normal cells (fig. 5-9). Major microtubule bundles in these cells localized in the band region, ovoid in shape (fig. 5-9d). Cells with tighter MT band (i.e., with reduced number of thread-like bundles of microtubules found internal to the major bundle) were also found frequently in the same sample, suggestive of a more advanced stage of re-assembly (fig. 5-10d).

Recovery of the microtubule band was quantified over several incubation periods at 22 °C (fig. 5-11). Initially 35%of cell population exhibited MT bands, identifying them as thrombocytes. Count of MT band decreased to ~5% when incubated at 0 °C for 2 hours. These residual MT bands were not intact ovoid bands observed in normal samples, but were counted as MT bands because they could still be recognized as such. In other words, treatment at 0 °C affected all microtubules, if not by total disassembly, at least by some disorganization. Then, 2 hours of re-warming at 22 °C restored the number of countable MT bands to 28%, showing that MT bands in thrombocytes reassemble upon re-warming. Relating to cell shape count (fig. 5-6), it is evident that the MT band is responsible for maintaining the ovoid shape of thrombocytes in their unactivated state.

F-actin distribution during MT reassembly was not consistent, although cortical F-actin was evident in all thrombocytes examined. In pointed cells, some exhibited brightly

labeled patches of F-actin, seemingly irrelevant to the spatial distribution of the microtubule bundle (fig. 5-7c). Other pointed cells showed bright F-actin labeling colocalizing with the MT bundle in cell contour (fig. 5-8c). Similar inconsistency was observed in ovoid cells. Some ovoid cells exhibited random patches of brightly labeled F-actin, while others seem to reveal a structure reminiscent of a band (figs. 5-9C and 5-10C).

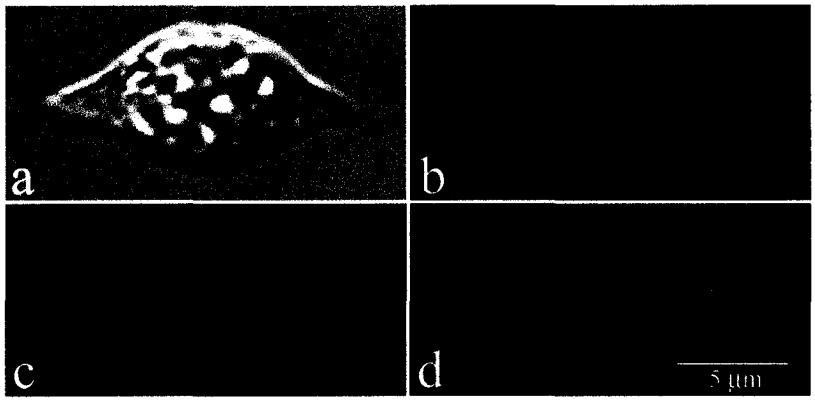

Figure 5-7. Computer-generated optical section stacks showing regeneration of a recognizable thrombocyte after rewarming for 4 hours: (a) shows a DIC image of an elongated thrombocyte with pointed ends on opposite sides; (b) DAPI stained nucleus; (c) Cortical F-actin conforming to the doubly pointed morphology with dispersed bright patches; (d) Reassembling marginal band of microtubules with associated minor bundles.

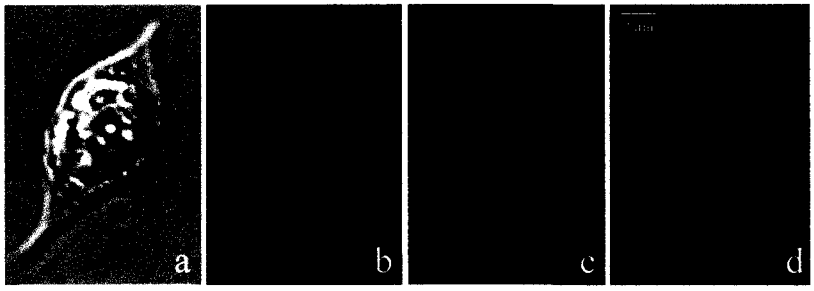

Figure 5-8. Computer generated optical section stacks showing regeneration of a recognizable doubly-pointed thrombocyte after rewarming 4 hours. Thrombocytes with this morphology were atypical, but had interesting cytoskeletal structure. (a) DIC image; (b) DAPI, showing nucleus; (c) F-actin distribution, brightly labeled contour is suggestive of the F-actin band ;(d) microtubule organization, with "tennis racquet" construction at both pointed ends.

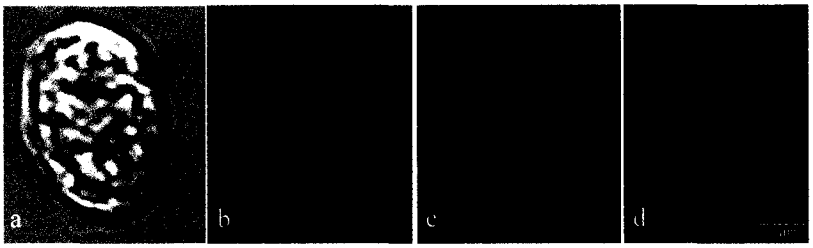

Figure 5-9. Rewarming for 6 hours showing a thrombocyte on its way to complete morphological recovery, correlated with MB reassembly (projection of confocal optical sections): (a) recovering thrombocyte with ovoid shape (DIC); (b) DAPI stained nucleus; (c) cortical F-actin with many bright patches of actin distributed throughout the cell; (d) reassembling band with thread-like bundles of microtubules found internal to the major bundle. Presumably this is an earlier stage than Figure 5-10

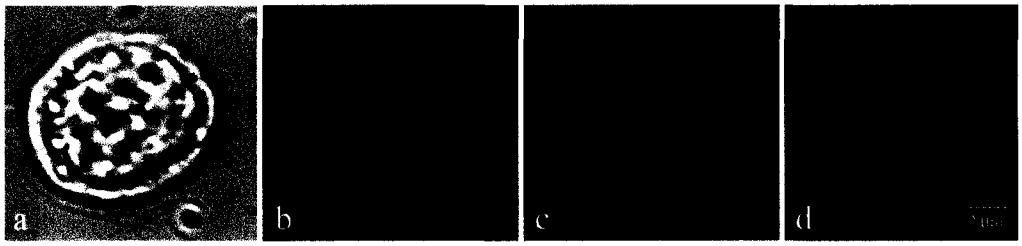

Figure 5-10. Recognizable thrombocyte after 6 hours of rewarming (projection of confocal optical sections): (a) DIC showing rounded, partially flattened contour; (b) DAPI stained nucleus; (c) cortical F-actin defined by the MB shape; (d) reassembled MB with normal appearance is clearly recognizable.

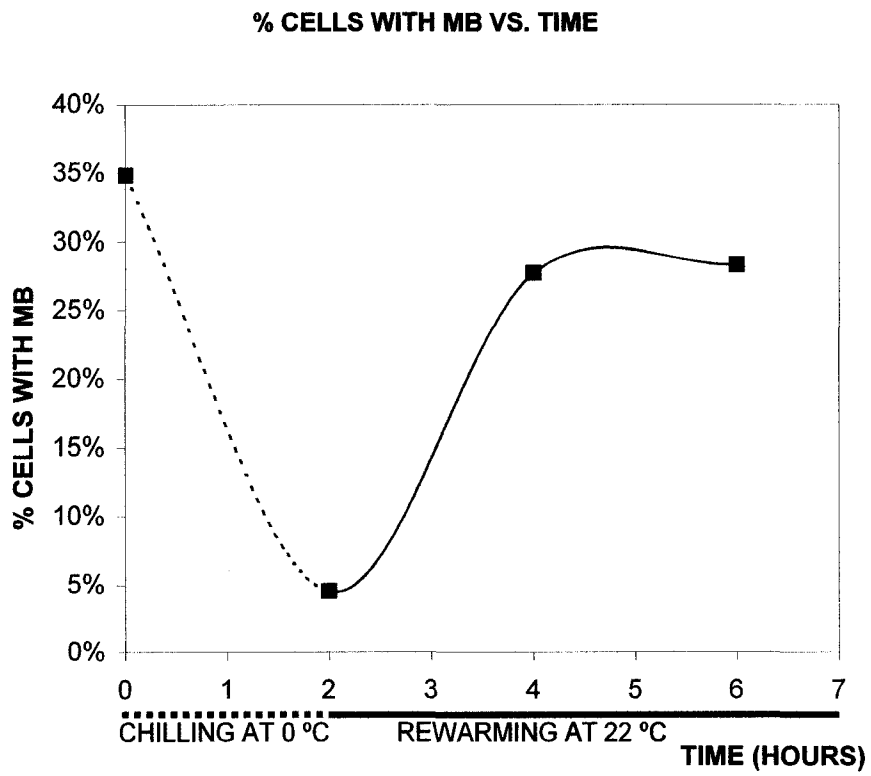

Figure 5-11. % cells with MB upon chilling and rewarming. ~35 % of initial white cell suspension consists of thrombocytes with well-defined MB. Upon exposure at 0 °C for 2 hours, the number of recognizable MBs decreases to ~5% and when rewarmed at 22 °C for >2 hours, the count increases to >28%.

3. The F-actin band is absent in unactivated thrombocytes exposed to 0 °C

While identification of thrombocytes is virtually impossible when sampled at 0 °C because both the cell shape is altered beyond recognition and the microtubule band is disassembled, no cell type exhibited a clear F-actin band. By inference, this indicated that the F-actin band was also affected by low temperature treatment. Also thrombocytes returning to normal shape lacking the F-actin band were observed, indicating that it is cold labile.

4. Pre-exposure of thrombocytes to F-actin disassembly promoting agents blocks normal activation induced shape change.

Cells exposed to 5 μg/ml cytochalasin D for 2 hours or to 1 μM latrunculin B for 1 hour retained their unactivated ovoid morphology, permitting us to test the effects of these inhibitors on shape changes following activation. Cytochalasin D-treated cells failed to undergo thrombin-induced shape changes (fig. 5-12 row A). Cells fixed and permeabilized at 10 minutes of thrombin exposure exhibited a state of MB microtubules similar to that of unactivated thrombocytes. However, F-actin distribution became slightly altered, with patchy cortical actin and a less-well defined MB-associated F-actin band. Treatment with 1 μM latrunculin B for 1 hour produced similar results. Upon thrombin perfusion, cells developed a knob-like extension in one end of the long axis, but progression to the spheroidal stage was never observed. MB microtubules exhibited normal unactivated distribution, while F-actin was more disorganized than that of cells treated with cytochalasin D (fig. 5-12, row B). Cells exposed to solvent controls, 0.5 % DMSO for cytochalasin D and 0.2% DMSO for latrunculin B, progressed to normal thrombin-induced activation, and exhibited microtubule and F-actin distribution characteristic of the early pancake stage (fig. 5-12 row C).

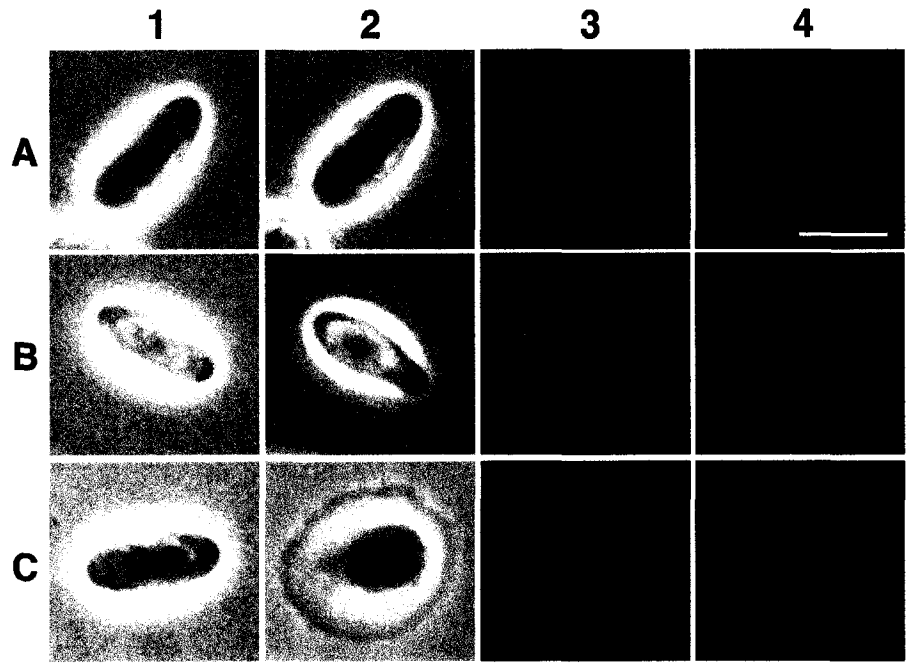

Figure 5-12. Cytochalasin D and latrunculin B inhibit thrombin-induced responses (epifluorescence): (row A) cells pre-incubated in 5 μg/ml cytochalasin D, 2 hours; (row B) 1 μM latrunculin B, 1 hour; (row C) 0.2% DMSO, 1 hour (control); (column 1) phase-contrast, cells prior to attempted activation; (column 2) cells after 10 minutes of thrombin exposure; (column 3) epifluorescence, tubulin distribution in (column 2); (column 4) F-actin distribution in (column 2). Bar, 10 μm.

5. Hyperstabilization of microtubules in activated thrombocytes does not block normal activation induced shape change or nuclear lobulation.

Hyperstabilization of microtubules with taxol does not hinder activation or eventual nuclear fragmentation, suggesting that other cytoskeletal elements may act upon MT band, assuming that MT band drives nuclear fragmentation (fig 5-13). The effect of destabilizing MT band with inhibitors such as nocodazole remains to be investigated, although the requirement for low temperature and the sensitivity of thrombocyte to such treatment results in experimental complication.

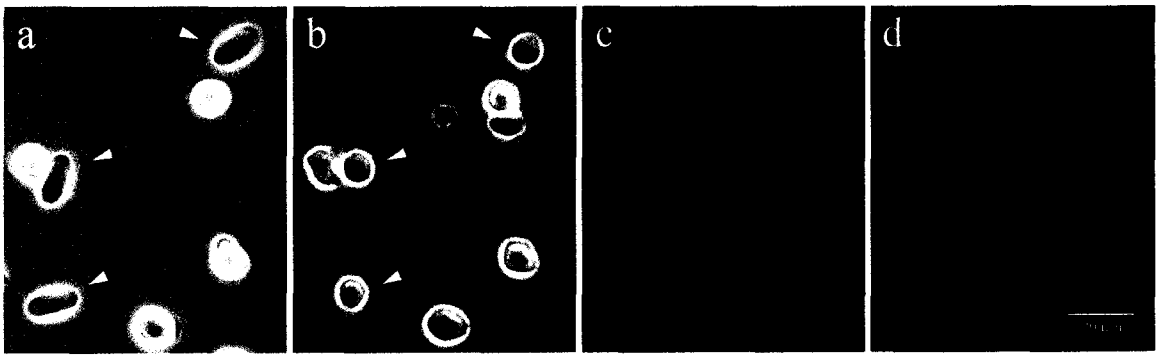

Figure 5-13. Taxol treatment permits activation: (a) cells incubated in 10 μM taxol for 2 hours prior to activation (white arrowheads only, other surrounding cells are not thrombocytes); (b) same cells after 10 minutes of thrombin exposure (phase-contrast); (c) tubulin distribution (FITC epi-immunofluorescence); (d) F-actin distribution (Texas-Red phalloidin epi-fluorescence)

6. Inhibition of non-muscle myosin II blocks post-activational cell shape change.

To test whether marginal band bending was an effector for generation of spheroidal cells or whether it was a secondary result of actin-based motility, myosin II (non-muscle) ATPase inhibitor BDM was utilized. After pre-incubation of thrombocytes with 20 mM BDM for 1hour, thrombin-induced spheroidal cell formation was reduced to 12% from a control level of 96%. This indicated that post-activational cell shape change in thrombocytes might occur through actomyosin-based mechanism.

DISCUSSION AND SUGGESTED EXPERIMENT

7. Function of the microtubule band is to maintain the shape of unactivated thrombocyte.

Results of temperature cycling experiments on unactivated dogfish thrombocytes show that the microtubule band is cold labile. Low temperature induced disassembly of the microtubule band correlated with changes in cell shape. This finding is in agreement with that of chick thrombocytes and mammalian blood platelets (Behnke, 1970), in which

cells became spheroidal from normal disk shape with the loss of the MT band induced by low temperature. Taken a step further, it was shown that the reassembly of dogfish thrombocyte MT band could be achieved with re-warming, and that this correlated with regain of the native cell shape. The appearance of intermediate cell shapes (fig. 5-5) suggests that mature thrombocyte cytoskeleton is similar to that of immature nucleated erythrocytes (chicken, Winkler and Solomon, 1982). Therefore, it was concluded the function of the MT band in thrombocytes is to maintain the shape of unactivated cells. However, this finding may be limited to nucleated thrombocytes since in mature nucleated erythrocytes loss of the MT band does not lead to alteration in cell shape (dogfish, Cohen *et al.*, 1982; frog and chick, Behnke, 1970).

8. The F-actin band in unactivated thrombocytes may enhance stability of the outer MT band.

Most of the F-actin in the unactivated thrombocyte occurs in a cortical layer throughout the cell, and in a specialized ring of F-actin that is associated with the microtubular MB (figs. 4-4; 4-5). Association of F-actin with MBs has also been observed in resting mammalian blood platelets (Debus et al, 1981; Takeuchi et al, 1990), and in non-mammalian vertebrate erythrocytes (Kim *et al.*, 1987; Sanchez and Cohen, 1994; Lee and Cohen, 1998). In addition, F-actin has also been reported in platelets as extensions of MB-associated F-actin with spoke-like arrangement (Takeuchi et al, 1990). Unlike these systems, the F-actin band in unactivated thrombocytes is thinner than that of MT band as determined within the limits of confocal microscopy. Furthermore, the thrombocyte MB itself appears to be composed of inner and outer microtubule bundles, with only the latter colocalizing

with the F-actin band. This suggests that interaction with F-actin may confer increased stability on outer MB microtubules involved in unactivated cell shape maintenance, and that such F-actin-MT interaction is lost when activation triggers rapid cell shape alterations.

In unactivated cells, the MB was enclosed within the cortical meshwork of F-actin (fig. 4-6), an arrangement similar to that found in platelets (White, 1971). This supports MB function as a flexible frame that maintains the shape of unactivated nucleated thrombocytes, with the MB exerting pressure against the cortical F-actin layer. The arrangement of cytoskeletal elements in the unactivated thrombocyte is illustrated diagrammatically in figure 5-14. A similar model has been proposed earlier for nucleated erythrocytes, in which the MB is enclosed within the membrane skeleton (Joseph-Silverstein and Cohen,1984; Cohen *et al.*, 1998). This in turn raises the possibility that MB pressure against the cortical layer of the thrombocyte causes it to be compressed in the plane of contact, accounting for the greater density of F-actin at the MB periphery, i.e., the ring.

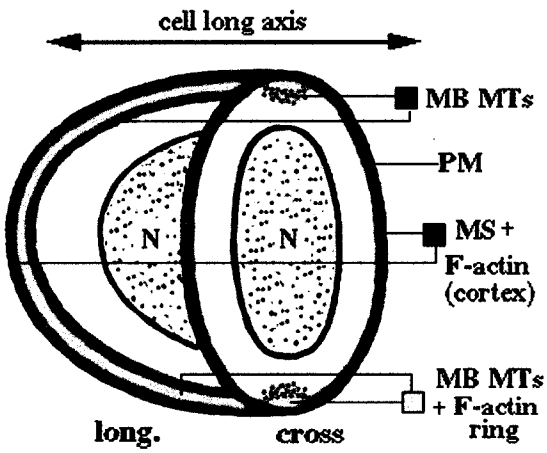

Figure 5-14. Diagrammatic representation of the major cytoskeletal elements in the unactivated thrombocyte. The diagram is a composite of both longitudinal and cross-sectional views. Abbreviations: MB MTs, marginal band microtubules; PM, plasma membrane bilayer; MS, membrane skeleton. The lighter band region (yellow) denotes overlap of MB microtubules with the F-actin ring.

9. F-actin is the major driving force for post-activational cell shape change.

The hypothesis that post-activation stages in nucleated thrombocytes are primarily due to F-actin reorganization is supported by the results. As early as the spheroidal stage, the F-actin band loses colocalization with the buckling MB (fig. 4-8C), and cortical F-actin redistributes into the blebs (fig. 4-9; 4-10). The bent and twisted MB shape at the spheroidal stage raised the possibility that the MB might also be an effector of conversion to the spheroid. However, our tests using cytochalasin D and latrunculin B, both of which inhibit F-actin assembly (Urbanik and Ware, 1989; Spector *et al.*, 1989), showed that unactivated thrombocytes failed to progress to spheroids when exposed to thrombin (fig. 5-12). In addition, the myosin II ATPase inhibitor BDM blocked spheroid formation. Thus, spheroid formation is dependent on F-actin assembly and myosin II function, indicating that bending of MBs is a passive secondary effect. It has been shown that similarly twisted MBs, observed in erythrocytes of blood clams undergoing shape transformation from flattened ellipsoids to spheroids, are not the effector of the transformation (Lema-Foley *et al.*, 1999). Thus, shape transformation in the post-activation stages is dependent upon assembly of F-actin.

Cytochalasin D and latrunculin B are known to cause drastic shape changes in cells in which the F-actin is in dynamic state (Spector *et al.*, 1989). In contrast, observed stability of unactivated cell morphology in the presence of cytochalasin D and latrunculin B indicated that the unactivated thrombocyte contains stable F-actin that is not in dynamic equilibrium with G-actin. This is supported by the observation that a substantial amount of F-actin remains in the cortex after incubation with these inhibitors (fig. 5-12).

Exposure of cells to thrombin would normally convert the stable pre-activation F-actin to a dynamic state, with depolymerization of cortical F-actin maintaining the G-actin pool during reassembly of F-actin elsewhere in the cell. Maintenance of shape in thrombin-exposed cells pre-incubated in CD and LB fits a model in which the inhibitors block de novo synthesis of F-actin from the G actin pool, preventing pool depletion. The altered G-F-actin equilibrium, in turn, would inhibit further disassembly of cortical F-actin.

In platelets, previous studies have shown that cytochalasin D inhibits F-actin assembly upon thrombin activation (Fox and Phillips, 1981). While cytochalasin D-treated dogfish thrombocytes undergo only a very slight shape change (fig. 5-12B2), cytochalasin D-treated platelets do undergo the complete initial cell shape change to spheroids, with a reduction in the number of pseudopods and attenuation of surface convolutions (Casella *et al.*, 1981).

In advanced stages of activation, F-actin distributes outwardly in the form of stress fibers, frequently arranged in geometric patterns, while MTs localize principally in proximity to the nucleus (figs. 4-15F; 4-16B). Platelet cytoskeletal structures resembling stress-fibers have also been reported in some studies (Morgenstern *et al.*, 2001; Tanaka and Itoh, 1998). Thus, in general respects, the spread nucleated thrombocyte cytoskeleton resembles that of activated platelets, in which F-actin spreads outward and microtubules remain in the interior (Debus *et al.*, 1981; Escolar *et al.*, 1986).

10. Activation of nucleated thrombocytes by mammalian thrombin indicates evolutionarily conserved signal transduction pathways.

Activation of mammalian platelets is commonly defined by events such as cell shape change, adhesion, aggregation, and granular exocytosis. Representative agents that induce platelet activation include ADP (Aledort, 1971), thrombin (Haslam, 1964), and the calcium ionophore A23187 (White *et al.*, 1974). Glass surfaces, potentially mimicking damaged vascular endothelia, also induce changes of cell morphology (Baumgartner and Haudenschild, 1972). Our study shows that nucleated thrombocytes undergo morphological changes analogous to mammalian platelets upon contact with a glass surface or, to a much greater extent, exposure to bovine thrombin. Recently, the mechanism of such morphological change has been linked with cell surface receptor-mediated signal transduction. In mammalian platelets, PAR-1 and PAR-4 have been identified as cell surface thrombin-receptors involved in cell aggregation (Kahn *et al.*, 1998). In catfish and zebrafish thrombocytes, an integrin-like complex has been reported as thrombocyte-specific and involved in signaling of aggregation and cell shape alteration (Passer *et al.*, 1997; Jagadeeswaran *et al.*, 1999). Thus, responsiveness of fish thrombocytes to mammalian thrombin indicates the existence of evolutionarily conserved signal transduction pathways.

11. Thrombocytes exhibit population variance in response to activating agent and in nuclear lobulation.

Observations presented here represent the most commonly occurring events. However, variations within the thrombocyte population were also noted. In preparations

involving naturally-induced activation in which whole blood is spread on coverslips without anticoagulant, some thrombocytes were found to progress through post-activation stages more readily than others. For example, variations in early response are evident in figure 4-8A, B. It is conceivable that, during blood withdrawal, fast-progressing cells were those exposed to activating signals to a greater extent than slow progressing ones . However, even in thrombin-induced activation, minor percentages of cells did not respond, supporting the notion of population variability. Variations were also evidenced in nuclear lobulation. Most cells exhibited nuclear lobulation during transition to pancake stages. However, cells in full pancake forms were occasionally found with no apparent nuclear lobulation (e.g., fig. 4-16). Such observations further support population variability and, possibly, existence of thrombocyte subtypes.

12. Nucleated thrombocyte activation: a specialized apoptotic pathway?

Several of the major properties observed in activated nucleated thrombocytes are characteristic of apoptotic cells. These include the initial rounding up into a compact form (apoptotic cell "condensation"), early surface blebbing, and nuclear lobulation and fragmentation. Apoptotic surface blebbing involves actomyosin-based cell motility (Mills *et al.*, 1998), and the observed blebs in thrombocytes are actin-rich (fig. 4-9; 4-10). In addition, in at least some cultured mammalian cells triggered to undergo apoptosis, interaction of microtubules with fragmenting nuclei has been observed (Pittman *et al.*, 1997). Considering that activated thrombocytes are on a pathway leading ultimately to cell death, these similarities raise the possibility that nucleated thrombocyte activation and function may actually be a specialized form of apoptosis.

SUMMARY OF FINDINGS:

(A) Temperature induced disassembly of microtubules results in loss of ovoid shape, evidence that the microtubule band is maintains unactivated thrombocyte cell shape.

(B) Inhibition of F-actin assembly prevents thrombocyte shape change, evidence that the function of F-actin is to drive shape change in activated thrombocytes

(C) Cytoskeletal reorganization in nucleated thrombocytes post activation closely resembles that of mammalian platelets.

CHAPTER 6: **Development of Methods**

1. Fluorescence Localization of Cytoskeletal Proteins in Fibrin-Trapped Cells

Several difficulties arise when fluorescence localization of cytoskeletal proteins is attempted in cells that normally exist in suspension, such as the nucleated erythrocytes used as a model system in this work (e.g., Cohen *et al.*, 1998). Artificially induced attachment of living cells or their cytoskeletons to coverslips or slides with polylysine (Mazia *et al.*, 1975) or other adhesives can distort three-dimensional structure. Material is often lost due to poor or selective adhesion, so that the sample is not representative, and cytoskeletons of pre-selected living cells cannot be readily relocated after labeling. In addition, processing small numbers of cells is difficult.

A new method has been developed that avoids many of these problems. The major steps are: (a) trapping living cells in physiological media within fibrin "clots"; (b) treating the trapped cells with detergents or other agents to produce cytoskeletons; and (c) after fixation, exposing the trapped cytoskeletons to antibodies or other fluorescent probes. In developing the procedure, "blood clam" and amphibian erythrocytes, sea urchin sperm, and sea urchin zygotes were used as test material. It involved trapping the cells within the 3-dimensional matrix of a fibrin clot, which is analogous to a blood clot. However, in this procedure, only the two necessary clotting factors, fibrinogen and thrombin, were used. For clot formation, the mechanism is as in figure 6-1.

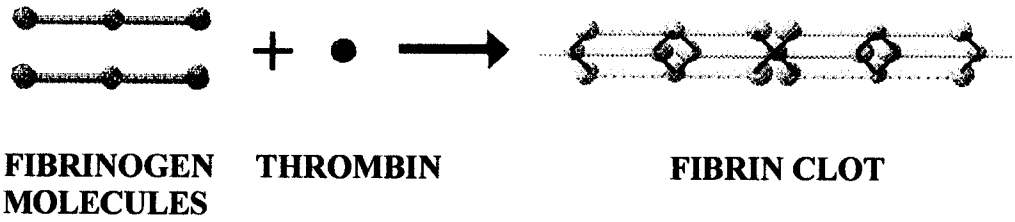

Figure 6-1. Thrombin-induced fibrin polymerization

The enzyme thrombin cleaves off part of the amino terminus of the fibrinogen molecules, forming fibrin. Fibrin in turn self-assembles in a half-staggered, side-by-side array forming a complex network, the fibrin clot.

Living cells were trapped by mixing one volume of a cell suspension in artificial seawater or Ringer's solution with four volumes of the same medium containing 10 mg/ml fibrinogen (Sigma Chemical Co., St. Louis, MO; F8630 from bovine plasma; final conc. = 8 mg/ml). Thrombin (Sigma T4648; from bovine plasma; 50 U/ml frozen stock in Ringer's or artificial seawater) was added to 1 U/ml or, for some amphibian Ringer's solutions, lower concentrations, so that a firm clot formed in about 10 min. Samples (5-25 µl) were delivered to coverslips within this time window, and were usually spread inside self-adhesive plastic rings that remained attached to the coverslips throughout the procedure (Avery #05729 white ring-binder reinforcements, 7 mm interior diameter). In some cases, the suspension was thinly spread without using the rings. To prevent the clots from drying during formation or incubation with probes, the coverslips were kept in moist chambers; for detergent treatment (lysis), fixation, and washes, they were transferred to coverslip staining jars. When seawater was used, the clots were optically clear, whereas in amphibian Ringer's, they were translucent (fig 6-2). This reduction in

clarity interfered with phase contrast to some extent, but did not affect fluorescence microscopy.

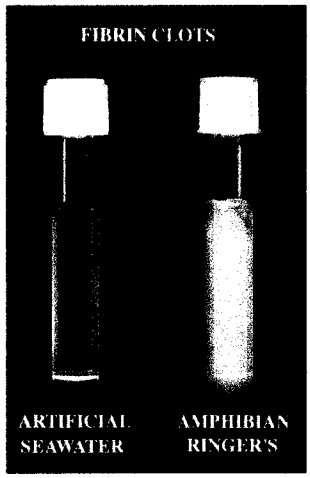

Figure 6-2. Difference in optical clarity of fibrin clots in different physiological media.

Coverslips bearing fibrin-trapped cells were immersed in a cytoskeleton-stabilizing lysing medium containing Triton X100, with or without protease inhibitors (Cohen *et al.*, 1988; Cohen *et al.*, 1996), to produce cytoskeletons within the clot. After 4-8% formaldehyde fixation (either post-lysis, or simultaneously with lysis), the coverslips were washed in PBS and incubated with probes for detection of microtubules and F-actin. These probes included monoclonal anti-α-tubulin and anti-β-tubulin (Sigma T9026, T-4046) as a primary mixture, with FITC-goat anti-mouse IgG (Fab; F-8521) as secondary, FITC-monoclonal anti-β-tubulin (F-2043) for direct labeling, and Texas Red-X phalloidin (Molecular Probes, Eugene OR) for F-actin. It was found that the antibodies penetrated the clots within 1-2 hours, and that both direct and indirect anti-tubulin immunofluorescence was successful. Controls lacking primary antibody were blank, and most clots exhibited little background fluorescence, even though blocking was not performed. General schematic for fibrin trapping of living cells and fluorescence localization of cytoskeletal proteins is shown in figure 6-3.

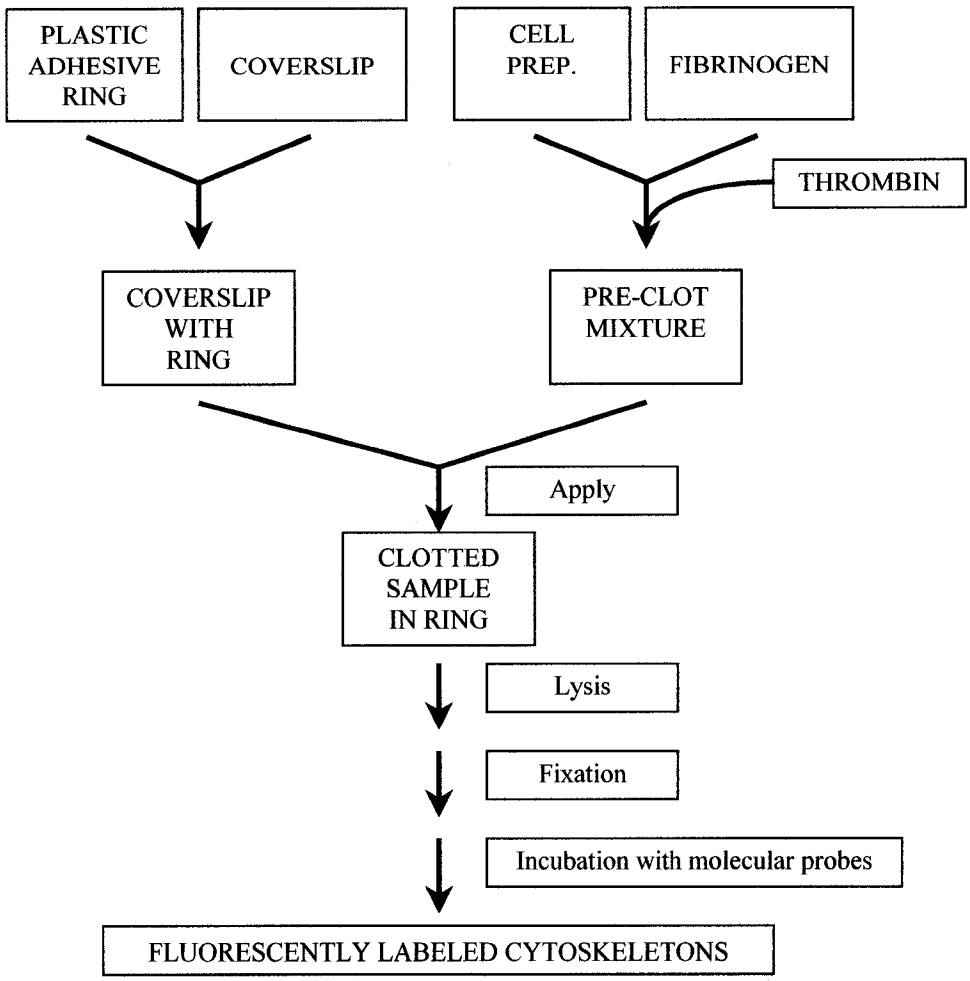

Figure 6-3. General schematic of the fibrin clot method.

Fibrin-trapped specimens were examined by both epifluorescence and confocal fluorescence microscopy; the latter was particularly useful for thicker clots. Tubulin was localized in the marginal bands of both molluscan (*Noetia ponderosa*; fig. 6-4a,a') and amphibian erythrocytes (*Notophthalmus viridescens*, *Ambystoma mexicanum*; not shown), in sea urchin sperm flagella (*Litechinus pictus*; fig. 6-4b,b'), and in mitotic spindles and asters of dividing sea urchin zygotes (*L. pictus*, fig. 6-4c,c'). Sperm distributed throughout the clots showed specific flagellar labeling. In addition, the distribution of F-actin was

examined with Texas Red phalloidin in cytoskeletons of molluscan (*N. ponderosa*, fig. 6-4d,d') and amphibian erythrocytes (*N. viridescens*, fig. 6-4e).

To determine whether the clotting process or the resulting confinement might be detrimental to cells, the development of fertilized sea urchin eggs (*L. pictus*, *Arbacia punctulata*) was monitored in clots incubated in filtered natural seawater contained in coverslip staining jars. The same trapped cells could be repeatedly located and examined during the time preceding lysis (fig. 6-4, f vs. g). Development appeared to progress normally in the clots, with the percentage of dividing cells similar to that in seawater alone. Many ciliated blastulae (fig. 6-4h) rotated within their confined space, and larvae (fig. 6-4i) ultimately escaped from the clot and were found free-swimming in the coverslip jars (2 days at 21.5 °C). Thus, long-term exposure to the clot did not block development.

Although the optimal conditions for various steps remain to be determined for specific cell types, results to date suggest that fibrin trapping will be a useful alternative to methods involving polylysine or other adhesives (Mazia *et al.*, 1975). The images of blood clam erythrocyte cytoskeletons obtained with the new method (e.g., fig. 6-4a,a') are superior, in terms of three-dimensional structure and retention of representative samples to those obtained previously with polylysine. The method has also begun to yield improved data on cytoskeletal organization in blood clam erythrocytes that have undergone a naturally-induced shape transformation (Dadacay *et al.*, 1996). Potential additional advantages include the processing of small cell populations with minimal losses, and the opportunity to observe the same cells before and after lysis and labeling. In addition, though not yet tested, the firmness with which living cells, such as sea urchin

zygotes, are initially trapped suggests that microinjection of antibodies or other probes may be possible prior to processing.

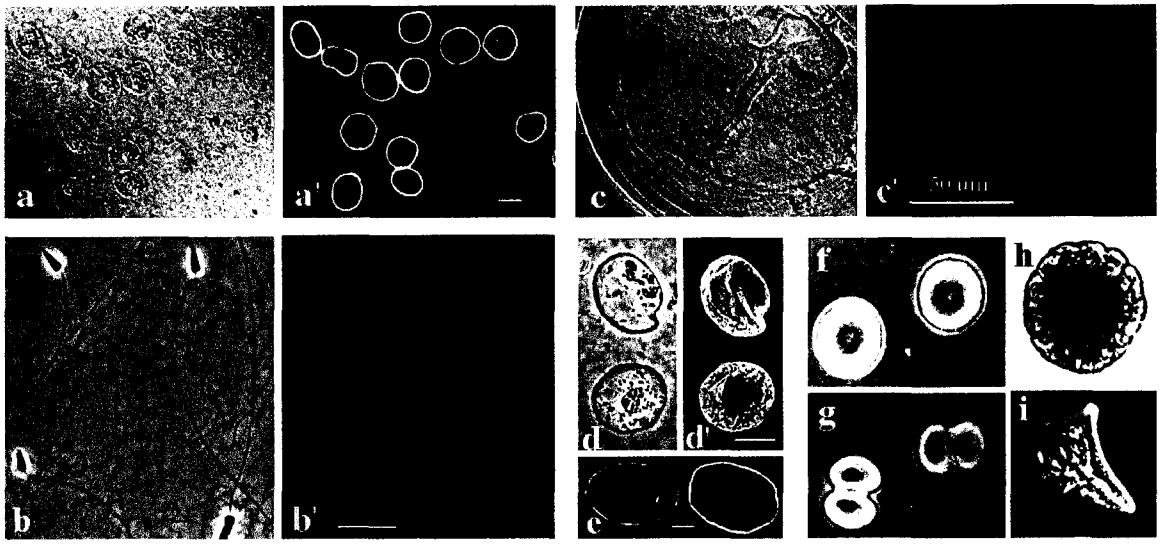

Figure 6-4. Fluorescence localization of cytoskeletal proteins in cells trapped in fibrin clots. Abbreviations: PC phase contrast, DIC differential interference contrast, Fl = fluorescence. (a, a') Clam erythrocytes (*N. ponderosa*); indirect anti-tubulin labeling of marginal bands, DIC-Fl pair. (b, b') Sea urchin sperm (*L. pictus*); indirect anti-tubulin labeling of flagellae, PC-FL pair. (c, c') *L. pictus* zygote, 2-cell stage; indirect anti-tubulin labeling of spindles and asters, DIC-FL pair. (d, d') *N. ponderosa* erythrocytes; Texas Red phalloidin labeling of F-actin. (e) Salamander erythrocytes (*N. viridescens*); Texas Red phalloidin labeling of marginal band-associated F-actin, PC-FL pair. (f, g) Same sea urchin zygotes (*A. punctulata*) viewed before and after first cleavage in clot, PC (h, i) *A. punctulata* at blastula stage, and larva after escape from clot, PC. Bars 10 μm, except as noted.

2. *Rapid Visualization of Microtubules in Blood Cells and Other Cell Types in Marine Model Organisms*

Although specific proteins in living cells can now be labeled routinely with Green Fluorescent Protein, indirect immunofluorescence (IIF) methods for fixed material remain in widespread use (Bikoue *et al.*, 2002). While relatively easy to apply, the standard IIF procedure is lengthy and, for blood cells and other cell types in suspension,

the required attachment of the material to a glass substrate can result in differential adhesion or losses. In addition, the nonmammalian erythrocytes and clotting cells (Mainwaring and Rowley, 1985; Conrad *et al.*, 2001; Lema-Foley *et al.*, 1999; Cohen and Nemhauser, 1985) studied in our laboratory undergo a variety of naturally occurring or experimentally induced alterations to cell morphology. For these cell types, the fixation and permeabilization methods that have produced the best IIF cytoskeletal labeling to date have not preserved the morphology of the living cells very well.

This work had three initial objectives: (a) developing improved methods for morphological preservation and permeabilization of non-mammalian erythrocytes and clotting cells prior to IIF; (b) combining such methods with rapid fluorescence pre-labeling of a mouse primary antibody (use of Zenon^{TM}; 6) to eliminate steps including substrate attachment; and (c) testing the combined approach on cells studied by others, or previously unstudied. Objectives (a) and (b) involved use of dogfish erythrocytes and thrombocytes (*Mustelus canis*), blood ark erythrocytes (*Anadara ovalis*), and horseshoe crab amebocytes (*Limulus Polyphemus*), all of which contain a marginal band (MB) of microtubules. For (c), it involved use of sea urchin sperm (*Arbacia punctulata*) and dividing zygotes (*Lytechinus pictus*) with known microtubule organization, plus spider crab hemocytes (*Libinia emarginata*) not studied previously.

Dogfish erythrocytes were first employed in an experimental survey of variables to develop both sequential and simultaneous methods of rapid fixation and permeabilization (objective a). Standard aldehyde or methanol fixation had produced cross-linked hemoglobin (Hb) that blocked antibody access in earlier studies, and complete detergent lysis prior to fixation distorted cell morphology. Current experiments produced a major

advance: brief formaldehyde prefixation (1%, < 7 min) and detergent extraction (0.4% Triton X-100, 10 min) yielded partial Hb retention and superior preservation of erythrocyte morphology, yet also allowed RF labeling. Similar results were obtained with erythrocytes treated simultaneously with 4% formaldehyde and 0.6% Brij 58 (10 min). The slow extraction rate observed with Brij (compared with Triton) minimized morphological distortion when cells were not pre-fixed.

These methods were then tested on erythrocytes, other blood cells, and additional cell types in combination with Zenon ™ labeling (objectives b and c). Thrombocytes were pre-fixed in 1% formaldehyde in 3% non-pyrogenic NaCl ("saline", ~7 min), then extracted with 0.4% Triton X-100 in PEM (100 mM PIPES, 5 mM EGTA, 1 mM $MgCl_2$ pH 6.8, 10 min). Other cell types were permeabilized and fixed simultaneously in PEM containing 4% formaldehyde, 0.6% Brij 58, plus precautionary protease inhibitors (Sigma P8340 cocktail + 10 mM TAME; amebocytes: TAME only). All preparations were washed in phosphate buffered saline, (PBS, pH 7.2), then incubated in PBS containing mouse monoclonal anti-α and anti-β tubulins (Sigma T9026, T-4026, 1:1 mass mixture) pre-bound with Zenon™ Alexa Fluor 488 F_{ab} (Z-25002, 1: 1 by mass; Molecular Probes). Representative results using a Zeiss standard epifluorescence microscope and Nikon 950 digital camera are shown in Figure 6-5.

MBs were readily visible in dogfish erythrocytes (fig. 6-5a, a'), unactivated dogfish thrombocytes (Fig. lb, b'; c, c'), unactivated *Limulus* amebocytes (granulocytes; fig. 6-5d, d'), and blood ark erythrocytes (fig. 6-5e, e'); moreover, the preservation of blood cell morphology was the best obtained to date. Sea urchin zygote mitotic apparatus was well labeled (fig. 6-5f, f), including such details as crossing astral rays in the equatorial

periphery. Sea urchin sperm flagellar microtubules were brightly labeled (fig. 6-5g, g'), as were MBs discovered in unknown types of spider crab hemocytes (fig. 6-5h, h'). In all cases, microtubules were observed in only 30 min or less after antibody application. Precautionary pre-antibody blocking (PBS-1% bovine serum albumin, 60 min) was performed in some cases, but even without it there was little background. No labeling was observed when fluorescent F_{ab}, was used without anti-tubulin.

How rapidly were microtubules labeled? Perfusion chambers were made on slides scratched so as to enhance flow while retarding cell movement. Fixed dogfish leucocytes were loaded into the chamber and individual identified thrombocytes were viewed during successive perfusion with 0.4% Triton X-100 in PEM (10 min), and PBS (wash). Upon subsequent perfusion with ZenonTmlabeled anti-tubulin, the thrombocyte MB became visible almost immediately (< 30 s; fig. 6-5e, c').

The rapidity of the procedure led us to ask whether all steps might be readily performed by perfusion, while individual pre-selected cells were being continually observed. This possibility was tested with dogfish thrombocytes, which can be activated to initiate clotting functions, adhesion, and shape transformation in saline containing 25U/ml bovine thrombin and 20 mM $CaCl_2$,. Living, unactivated thrombocytes were loaded into the chamber and activated. Then all steps of pre-fixation and extraction, postfixation (4% formaldehyde in PEM, 10 min), wash (PBS), and immunolabeling were performed by perfusion. Microtubule labeling was again rapid and comparable in intensity to that in figure 6-5 (c, c'), confirming feasibility.

These new methods constitute a major practical advance. They now enable us to monitor morphological preservation and examine the cytoskeleton of pre-selected, activating

blood cells at specific stages by perfusion. This process is much more rapid and convenient than was previously possible working with these cells. In addition, for cell populations naturally existing in suspension, all steps can be performed while maintaining them in suspension, bypassing glass adhesion (fig. 6-5). Other important advantages for non-mammalian blood cells are (a) greatly improved preservation of erythrocyte morphology; (b) little non-specific labeling without blocking; (c) sufficient signal intensity even against the labeling antibody background; and (d) reduction of processing time from ~4 h to ~1 h. The same rapid methods are effective with other cell types (Fig. 6-5, f, f'; g, g') and with multiple labeling (e.g., DAPI; fig. 6-5g' inset), indicating that they will be useful to other researchers. As a by-product, they may also be of considerable value in designing time-constrained laboratory exercises for courses.

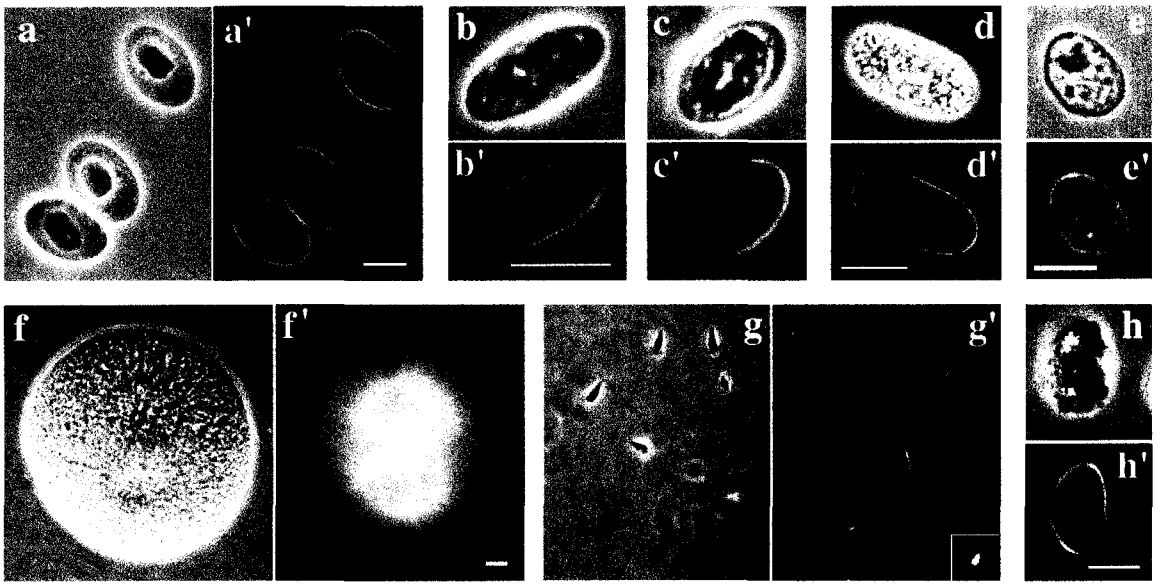

Figure 6-5. Microtubules in various model cell types visualized by rapid fixation and detergent permeabilization followed by Zenon™ immunolabeling. The images are phase contrast – fluorescence pairs, with ' indicating fluorescence. Marginal bands (MBs) are visible in dogfish erythrocytes (a, a'); unactivated dogfish thrombocytes (b, b'; c, c'), *Limulus* amebocytes (d, d'), and blood ark erythrocytes (e, e'). Sea urchin zygote mitotic apparatus (*Lytechinus pictus*; f, f'; fertilization membrane removed by Nitex filtration) and sea urchin sperm flagella (*Arbacia punctulata*; g, g') are also readily labeled. (g', inset): a DAPI-stained sperm nucleus. Also, an unknown type of spider crab hemocyte exhibits distinct MB labeling (h, h'). The thrombocyte MB in c, c' was labeled by on-slide perfusion of the pre-selected fixed cell. Bars = 10 μm.

CHAPTER 7: **Materials And Methods**

A. Erythrocytes

1. Acquisition of dogfish blood: Blood was withdrawn from the visible midline of smooth dogfish (33-40 inch body length), about one-third of the distance from cloacal opening toward the tail using a 10 - 30 ml syringes with 1.5 inch, 22-gauge needles. Immediately, the blood was added to an equal volume of heparinized Elasmobranch Ringer's solution (50 U/ml, final heparin concentration) in order to prevent clotting and activation of thrombocytes (Cohen et al, 1996).

2. Separation of dogfish erythrocytes from white cells: The heparinized blood was centrifuged at ~750 g for 2 minutes to produce an upper layer rich in white cells and a lower layer primarily of erythrocytes. A second centrifugation in sucrose gradient was performed for erythrocytes to remove residual white cells (~1300 g in 0.5 M sucrose).

3. Preparation of Eastern newt erythrocyte cytoskeleton: Blood was obtained by amputating *N. viridescens* tail tip, and either diluted directly into Triton lysis (100mM PIPES, 5 mM EGTA, 1mM MgCl2 [= PEM], containing 10 mM TAME and 0.4% Triton X 100, pH 6.8 with NaOH) medium to produce cytoskeletons, or was collected in amphibian Ringer's solution containing 1% BSA for later lysis. Samples (detergent-produced cytoskeletons) were spread on polylysine-coated coverslips, incubated ~15 min. in moist chambers to allow adhesion, washed in PEM, fixed 30 min. in 4% formaldehyde

in PEM, and washed in PBS. Material was subsequently exposed to probes as described in 7.

4. Trapping of dogfish erythrocyte in fibrin clot: Cells were trapped by mixing the cell suspension in Elasmobranch Ringer's solution with the same medium containing fibrinogen (Sigma F8630; final conc. = 8 mg/ml). Thrombin (Sigma T4648) was added to 1 U/ml (or less in some cases), so that a firm clot formed in ~10 min. Samples were delivered to coverslips within this time window, and were kept in moist chambers during clot formation. Refer to Lee and Cohen (1998) for details.

5. Standard method of lysis and fixation: Fibrin trapped cells were immersed in Triton lysis medium to produce cytoskeletons. The cytoskeletons were fixed for 30 min. in 4% formaldehyde in PEM, and washed in PBS. Fluorescent labeling of actin and tubulin was performed as described in 7.

6. Pre-fixation method: Fibrin trapped cells were exposed to 0.5% formaldehyde in Elasmobranch Ringer's solution for a maximum of 5 minutes (timing is critical since excessive exposure hinders lipid extraction). Subsequently pre-fixed cells were permeabilized in Triton lysis medium, fixed permanently in 4 % formaldehyde in PEM, and fluorescently labeled for actin and tubulin as described in 7.

7. Preparation cytoskeletons in 50% glycerol PEM: Eastern newt (obtained from 5) or dogfish blood cells (obtained from 1 and 2) were treated with Brij lysis medium (0.6%

Brij-58, 10 mM TAME, 1:1000 diluted protease inhibitor cocktail [Sigma P-8340] in PEM adjusted to pH 6.8 with NaOH) to produce cytoskeletons. 15 volumes of cytoskeleton containing lysis medium was then layered onto a triple step glycerol gradient consisting of 8 volume of 25% glycerol, 0.6 Brij in PEM, 14 volume of 40% glycerol, 0.6 Brij PEM, and 2 volume of 50% glycerol in PEM. The cytoskeletons were centrifuged (IEC clinical centrifuge, 5 minutes at speed 7 for small preparation of Eastern newt erythrocyte cytoskeletons or Beckman Accuspin, 10 minutes at 750g for larger preparation of dogfish erythrocyte cytoskeletons) into the 50% layer and stored at 4 °C (Cohen *et al.*, 1998).

8. Isolation of dogfish marginal band: MBs were isolated by exposing cytoskeletons prepared in 8 to 0.05% SDS, 0.2% TritonX-100, 12.5% glycerol in PEM. The isolation reaction was stopped by adding an excess volume of Triton-X while the bands were elliptical in shape (10 µl of 10% Triton-X 100 to 200 µl reaction mixture). The speed of isolation was dependent on the age of stored glycerol cytoskeleton and could be controlled by changing the concentration of SDS and Triton X-100, while maintaining their concentration ratio constant (Sanchez *et al.*, 1990)

9. HMM and S1 labeling: Isolated MBs from 9 were allowed to adhere on polylysine coated coverslips, exposed to 0.5 mg/ml of HMM (Cytoskeleton) or 0.5 mg/ml S1 (Sigma) in PEM, and fixed in 1% glutaraldehyde in PEM. The preparation was mounted on antifade mounting medium (Molecular Probes, Eugene) and examined by epifluorescence microscopy.

10. Actin perturbing agent treatment: Eastern newt erythrocyte cytoskeletons from 8 (in 50% glycerol) were pre-labeled with Texas-Red phalloidin in suspension. Bands were isolated as described in 9 and exposed in separate batches to 0.35 μg/ml latrunculin-B, 5 μg/ml cytochalasin-D, 50 μg/ml gelsolin, and 10 μM mycalolide-B in suspension, or by perfusion through a coverslip during microscopic examination.

11. Elastase treatment: Eastern newt erythrocyte cytoskeletons were pre-labeled and isolated as in 11. The isolated/actin-labeled MBs (elliptical stage) were exposed to 0.5 U/ml elastase (Sigma Chemical Co., St. Louis, MO; Cohen *et al.*, 1998) both in suspension, or by perfusion through a coverslip during microscopic examination.

12. Temperature cycling experiments on dogfish red cells with japlakinolide: The pellet obtained from A2 was resuspended in Elasmobranch Ringer's solution, double the original blood volume for fibrin clots, or ten times the original volume for pointed erythrocyte studies. Cells were trapped by mixing the cell suspension in Elasmobranch Ringer's solution with the same medium containing fibrinogen (Sigma F8630; final conc. = 8 mg/ml). Thrombin (Sigma T4648) was added to 1 U/ml (or less in some cases), so that a firm clot formed in ~10 min. Samples were delivered to coverslips within this time window, and were kept in moist chambers during clot formation (Lee *et. al*, 1998).

Coverslips prepared as above were immersed clot side down in 35X10 mm Petri dishes (Falcon 1008) containing different concentrations of Jasplakinolide or Methanol (0.3%) in Elasmobranch Ringer's solution. Samples were treated at least for 4 hours in

these solutions at 22 °C and subjected to different temperatures. A brief wash in Elasmobranch Ringer's solution was performed to remove excess jasplakinolide or methanol prior to lysis.

13. Lysis and fixation: Fibrin trapped cells from 12 were immersed in Brij or Triton lysis medium (100mM PEM containing 10 mM TAME and 0.6% Brij-58 or 0.4% Triton X 100, pH 6.8 with NaOH) to produce cytoskeletons. The cytoskeletons were fixed for 30 min. in 4% formaldehyde in PEM, and washed in PBS. To probe for tubulin, material was exposed to monoclonal anti-a- and anti-b-tubulin (Sigma T9026, T 4046) as a primary mixture and FITC-goat anti-mouse IgG (Fab; F-8521) secondary. For actin, Texas Red-X phalloidin was applied. After several PBS washes and mounting in Fluoromount, microscopy was performed using a Zeiss epi-fluorescence/phase-contrast microscope equipped with Nikon 950 digital camera.

14. Studies of pointed erythrocytes: Erythrocytes obtained as described above were suspended in Elasmobranch Ringer's solution to ~10% (v/v) working concentration. Following various experimental treatments, samples were fixed in 1% formaldehyde-Ringer's, and results were quantitated by determining the percentage of pointed cells in each sample, counting more than 1000 cells per data point. Counts were repeatable to ~1%. F-actin and tubulin were localized as described above.

B. Thrombocytes

1. Preparation of leucocytes enriched in thrombocytes: One volume (usually 5 ml) of dogfish blood was withdrawn into a syringe containing an equal volume of non-pyrogenic 3% saline as described in A1. 5 ml aliquots of this mixture were centrifuged using an IEC clinical centrifuge at 70 g for 2 minutes. Most erythrocytes sedimented into a pellet, while white cells remained suspended in the supernate. The upper half of the supernate, rich in thrombocytes, was collected. For experiments requiring higher cell density, the supernate was centrifuged at 70 g for 4 minutes in several smaller aliquots (1 – 2 ml), and the pellets were pooled in non-pyrogenic 3% saline to half the original blood volume.

2. Activation by thrombin perfusion: A perfusion chamber slide was devised to observe and capture shape changes of individual selected cell upon exposure to various solutions. It consisted of a detergent-washed 22 X 22 mm coverslip mounted on a 75 x 25 mm glass slide (Fisherbrand Superfrost Plus for improved sample adherence) with a known volume of liquid in between to ensure uniform chamber height. Two edges of the coverslip parallel to slide length were sealed with nail polish, leaving the other edges open. Prior to mounting the coverslip, scratches were made on the slide where the open edges would be placed to facilitate liquid flow. To improve cell adherence, 0.01% poly-lysine was perfused for a minimum of 5 minutes, followed by several washes with non-pyrogenic 3% saline.

A sample of white cell suspension (~15 ml), prepared as described above, or pre-treated with various inhibitors (see below), was loaded into one of the open edges of the

perfusion slide, and allowed ~3 minutes for adherence. While under observation, activation was triggered by perfusing 10 µl of 25 U/ml thrombin solution (Sigma T-4648 bovine thrombin, in 10 mM $CaCl_2$ and 0.5 M NaCl) to an open edge of the coverslip using a narrow micropipette tip and drawing the solution off at the other edge. Usually, 2 - 3 perfusions were required to activate most thrombocytes under the coverslip. Cell activation was recorded using a Zeiss standard 14 phase-contrast microscope equipped with a Cohu CCD video camera (model no. 4915-2110/000).

In some experiments, white cell suspensions were incubated with cytoskeletal inhibitors prior to thrombin exposure. Inhibitors, made up in non-pyrogenic 3% saline, included the following; cytochalasin D (5 µg/ml, 2 hours), latrunculin B (1 mM, 1 hour), 1 mM jasplakinolide for 2 hours, 10 mM phalloidin oleate for 3hours, and 10 mM Taxol for 2 hours. Solvent controls of these were 0.5 % DMSO for cytochalasin D, 0.2% DMSO for latrunculin B and taxol, 0.4% methanol for jasplakinolide, and 2.6% DMSO for phalloidin oleate. At the completion of incubation, samples were loaded in perfusion slides and exposed to thrombin as described above.

At selected time points or morphological stages, perfusion samples were simultaneously fixed and extracted with 2% formaldehyde, 0.6% Brij-58, and 10 mM TAME in PEM for a minimum of 10 minutes.

3. Activation on glass surfaces: Samples activated spontaneously on coverslips were prepared by spreading 100 µl of dogfish whole blood on several detergent-cleaned coverslips. At different time points (6, 12, 20 , and 30 minutes), the coverslips were immersed in 1% formaldehyde in Elasmobranch Ringer's solution (Cavanaugh, 1975;

Babkin *et al.*, 1933) for 10 minutes. Unattached red and white cells other than activated thrombocytes and granulocytes were washed away during fixation. Fixation was followed by several washes in PEM, permeabilization in 0.4 % Triton lysis medium (0.4% Triton X-100, 10 mM TAME, protease inhibitor cocktail [Sigma P-8340] in PEM) for 10 minutes, a wash in PEM, and post-fixation in 4% formaldehyde in PEM for 30 minutes.

4. Fluorescence labeling: After a wash in PBS (phosphate buffered saline, pH 7.2), fixed and samples from above were sequentially labeled for F-actin with 260 nM Texas-Red phalloidin (Molecular Probes, T-7471,); for tubulin with a 50:50 mix of mouse monoclonal anti α- and β-tubulin antibody (Sigma T-9026 and T-4046) as the primary and FITC-goat anti-mouse IgG (Fab; F-8521) as the secondary; and for DNA with 3 μM DAPI (Sigma D-9542). PBS was used as the wash medium for all treatments. Alternatively, samples were triple-labeled in PBS containing mouse monoclonal anti-α and anti-β tubulins pre-bound with Zenon™ Alexa Fluor 488 F_{ab} (Z-25002, 1:1 by mass; Molecular Probes), 260 nM Texas-Red phalloidin, and 3 μM DAPI for a minimum of 10 minutes, followed by a wash in PBS. Labeled samples were examined using either a Zeiss epi-fluorescence microscope equipped with a Nikon 950 digital camera, or a Zeiss LSM 510 confocal microscope.

5. Sample preparation for electron microscopy: For unactivated thrombocytes, the white cell suspension was prepared as described, except that blood was withdrawn into 3% NaCl containing 50 U/ml (final) heparin. The cell suspension, containing mostly unactivated thrombocytes, was fixed in 1% glutaraldehyde in 3% NaCl at 22 °C for 1

hour, followed by two washes (IEC, 1120 g for 2 minutes) in Sorensen's phosphate buffer (0.067 M phosphate at pH 7.4). The suspension was subsequently concentrated in 1/25 of the original volume (i.e., 0.2 ml of Sorensen's phosphate buffer, if the original volume of fixed WBC suspension was 5 ml), trapped in 1% low-melt agarose (solidifying T = 40 °C), and fixed in 1% OsO_4 in the same buffer for 1 hour. This was followed by washes in phosphate buffer, dehydration in an ethanol series, infiltration with Epon-propylene oxide, and embedding in Epon.

For activated thrombocytes, the white cell suspension was prepared directly from whole blood. 1 ml of this suspension was applied to a single welled Permanox chamber slide (Lab-Tek, Cat # 177410) and cells were allowed to settle for 30 minutes. The excess cell suspension was removed and activation was induced by exposing cells to 1 ml of 25 u/ml thrombin in 0.5 M NaCl and 20 mM $CaCl_2$ for 30 minutes. The sample was then fixed in 1% glutaraldehyde in 3% NaCl for 60 minutes, washed several times in Sorensen's phosphate buffer, and post-fixed in 1% OsO_4 in the same buffer for 1 hour. The fixed sample was dehydrated in an ethanol series, infiltrated with Epon-ethanol, and flat-embedded in epon. Pieces of flat embedments were glued onto the tip of Epon capsule blanks to obtain face-view sections.

Thin sections of both unactivated and activated samples were obtained using an MT-2 ultramicrotome (DuPont-Sorvall Instruments) with diamond knife, stained with saturated uranyl acetate in 50% ethanol followed by Reynold lead citrate, and examined in the Hitachi H600 TEM at 75 kV.

6. Temperature cycling: White cell suspension obtained as above was dispensed into sterile siliconized 2 ml microfuge tubes in aliquots of 1 ml, and these tubes were incubated in respective temperatures. Incubation samples include initial control at 22 °C, 2 hours at 0 °C, 2 hours at 0 °C and rewarmed for 2, 4, and 6 hours. All temperature variations were accompanied by 22 °C control. To minimize possibility of clotting, samples at 22 °C were incubated with slow rotation (which also prevents sedimentation), while samples at 0 °C were incubated in ice slurry with occasional (every ~ 20 minutes) turning to keep cells suspended. At the completion of incubation, samples were fixed in 2% paraformaldehyde in 3% saline. 10 μg/ml nocodazole (0.5% DMSO) in 3% NaCl was used for some cooling experiments.

BIBLIOGRAPHY

Aledort, L. M. 1971. Platelet aggregation. In: Johnson, SA, editor. *The Circulating Platelet*. London: Academic Press. 259.

Allen, R. D., L. R. Zacharski, S. T. Widirstky, R. Rosenstein, L. M. Zaitlin, and D. R. Burgess. 1979. Transformation and motility of human platelets: details of the shape change and release reaction observed by optical and electron microscopy. *J. Cell Biol.* 83:126-142.

Amato, P. A. and R. F. Loizzi. 1981. The identification and localization of actin and actin-like filaments in lactating guinea pig mammary gland alveolar cells. *Cell Motil.* 1:329-347.

Arikawa, K., and D. S. Williams. 1989. Organization of actin filaments and immunocolocalization of alpha-actinin in the connecting cilium of rat photoreceptors. *J. Comp. Neurol.* 288:640-646.

Babkin, B. P., D. J. Bowie, and J. V. V. Nichols. 1933. Structure and reactions to stimuli of arteries (and conus) in the elasmobranch genus *Raja*. *Contr. Canad. Biol. & Fish. N. S.* 8:209-225.

Baumgartner, H. R., and C. Haudenschild. 1972. Adhesion of platelets to subendothelium. *Ann. N. Y. Acad. Sci.* 201:22-36.

Bearer, E. L., J. M. Prakash, and Z. Li. 2002. Actin dynamics in platelets. *Int. Rev. Cytol.* 217:137-182.

Bearer, E.L. and T. S. Reese. 1999. Association of actin filaments with axonal microtubule tracts. *J. Neurocytol.* 28: 85-98.

Bearer, E. L., M. L. Schlief, X. O. Breakefield, D. E. Schuback, T. S. Reese, and J. H. LaVail. 1999. Squid axoplasm supports the retrograde axonal transport of herpes simplex virus. *Biol. Bull*. 197:257-258.

Behnke, O. A comparative study of microtubules of disk-shaped blood cells. *J. Ultrastruct. Res.* 1970; 31:61-75.

Bertram, E.M., A. R. Jilbert, and I. Kotlarski. 1998. Characterisation of duck thrombocytes. *Res. Vet. Sci.* 64:267-270.

Bikoue, A., G. Janossy, and D. Barnett. 2002. Stabilised cellular immuno-fluorescence assay: CD45 expression as a calibration standard for human leukocytes. *J. Immunol. Methods.* 266:19-32.

Bubb, M. R., I. Spector, B. B. Beyer, and K. M. Fosen. 2000. Effects of jasplakinolide on the kinetics of actin polymerization. An explanation for certain in vivo observations. *J. Biol. Chem.* 275:5163-5170.

Casella, J. F., M. D. Flanagan, and S. Lin. 1981. Cytochalasin D inhibits actin polymerization and induces depolymerization of actin filaments formed during platelet shape change. *Nature.* 293:302-305.

Cavanaugh, G. M., editor. 1975. *Formulae And Methods VI of the Marine Biological Laboratory Chem Room 6th edition.* Woods Hole, Mass: The Marine Biological Laboratory,

Cohen, W. D. 1978. Observations of the marginal band system of nucleated erythrocytes. *J. Cell Biol.* 78:260-273.

Cohen, W. D. 1991. The cytoskeletal system of nucleated erythrocytes. *Int. Rev. Cytol.* 130: 37-84.

Cohen, W. D., D. Bartelt, R. Jaeger, G. Langford, and I. Nemhauser. 1982. The cytoskeletal system of nucleated erythrocytes. I. Composition and function of major elements. *J. Cell Biol.* 93: 828-838.

Cohen, R. S., S. K. Chung, and D. W. Pfaff. 1985. Immunocytochemical localization of actin in dendritic spines of the cerebral cortex using colloidal gold as a probe. *Cell Mol. Neurobiol.* 5: 271-84.

Cohen, W. D., M. F. Cohen, C. H. Tyndale-Biscoe, J. L. VandeBerg, and G. B. Ralston. 1990. The cytoskeletal system of mammalian primitive erythrocytes: studies in developing marsupials. *Cell Motil. Cytoskeleton.* 16:133-45.

Cohen, W. D., and I. Nemhauser. 1980. Association of centrioles with the marginal band of a molluscan erythrocyte. *J Cell Biol.* 86:286-291.

Cohen, W. D., and I. Nemhauser. 1985. Chapter 1:3-49 in *Blood Cells of Marine Invertebrates*. W. D. Cohen, ed., New York: Alan R. Liss, Inc.

Cohen, W. D., I. Sanchez, N. Rayos, A. Dadacay. 1996. Utility of dogfish erythrocytes for studies of the cytoskeleton and cellular morphogenesis. Marine Models Electronic Record, Biol Bull Publications (online: http://www.mbl.edu/BiologicalBulletin/MMER/COH/CohTit.html),

Cohen, W. D., Y. Sorokina, and I. Sanchez. 1998. Elliptical versus circular erythrocyte marginal bands: isolation, shape conversion, and mechanical properties. *Cell Motil. Cytoskeleton.* 40:238-248.

Conrad, M. L., R. L. Pardy, and P. B. Armstrong. 2001. Response of the blood cell of the American horseshoe crab, *Limulus polyphemus*, to a lipopolysaccharide-like molecule from the green alga *Chlorella*. *Biol Bull.* 201:246-247.

Cramer L. P., and T. J. Mitchison. 1995. Myosin is involved in postmitotic cell spreading. *J. Cell Biol.* 131:179-189.

Dadacay, A-V. M., J. C. Huerta, C. J. Theiner, S. Swarnakar, and W. C. Cohen. 1996. Reversible Alteration of Molluscan Erythrocyte Morphology by a Natural Hemolymph Activity. *Biol. Bull.* 191:276-277.

Daimon, T., and K. Uchida. 1985. Ultrastructural evidence of the existence of the surface connected canalicular system in the thrombocyte of the shark (*Triakis scyllia*). *J. Anat.* 141:193-200.

DaMatta, R. A., S. H. Seabra, and W. deSouza. 1998. Further studies on the phagocytic capacity of chicken thrombocytes. *J. Submicrosc. CytoL. PathoL.* 30:271-277.

Debus E, K. Weber, and M. Osborn. 1981. The cytoskeleton of blood platelets viewed by immunofluorescence microscopy. *Eur. J. Cell Biol.* 24:45-52.

Eleftheriou, E. P., and B. A. Palevitz. 1992. The effect of cytochalasin D on preprophase band organization in root tip cells of *Allium*. *J. Cell Sci.* 103:989-998.

Endo, E., H. Fujimoto, A. Ishimori, N. Matsuura, J. Khato, and T. Takahashi. 1984. In vitro test of phagocytic ability of human platelets using colloidal carbon. *Tohoku J. Exp. Med.* 142:131-139.

Escolar, G., M. Krumwiede, and J. G. White. 1986. Organization of the actin cytoskeleton of resting and activated platelets in suspension. *Am. J. Pathol.* 123:86-94.

Euteneuer, U., and M. Schliwa. 1985. Evidence for an involvement of actin in the positioning and motility of centrosomes. *J. Cell Biol.* 101:96-103.

Fawcett, D. W., and F. Witebsky. 1964. Observations on the ultrastructure of nucleated erythrocytes and thrombocytes with particular reference to the structural basis of their discoidal shape. *Z. Zellsforsch Mirosk. Anat.* 62:785-806.

Filanoski, B. 2002. ZenonTM Technology Bulletin, Molecular Probes, Inc., Eugene OR.

Forer, A., and J. D. Pickette-Heaps. 1998. Cytochalasin D and latrunculin affect chromosome behaviour during meiosis in crane-fly spermatocytes. *Chromosome Res.* 6:533-549

Fox, J. E. B., and D. R. Phillips. 1981. Inhibition of actin polymerization in blood platelets by cytochalasins. *Nature.* 292:650-652.

Gavin, R.H. 1977. The oral apparatus of *Tetrahymena pyriformis*, strain WH-6. IV. Observations on the organization of microtubules and filaments in the isolated oral apparatus and the differential effect of potassium chloride on the stability of oral apparatus microtubules. *J. Morphol.* 151:239-257.

Gavin, R. H. 1997. Microtubule-microfilament synergy in the cytoskeleton. *Int. Rev. Cytol.* 173: 207-242.

Haslam, R. J. 1964. Role of adenosine diphosphate in the aggregation of human blood-platelets by thrombin and by fatty acids. *Nature.* 202:765-767.

Hall, E. S., J. Eveleth, C. Jiang, D. M. Redenbach, and K. Boekelheide. 1992. Distribution of the microtubule-dependent motors cytoplasmic dynein and kinesin in rat testis. *Biol. Reprod.* 46:817-828.

Henderson, E., P. G. Haydon, and D. S. Sakaguchi. 1992. Actin filament dynamics in living glial cells imaged by atomic force microscopy. *Science.* 257: 1944-1946.

Hill, D. J., D. H. Griffiths, and A. F. Rowley. 1999. Trout thrombocytes contain 12- but not 5-lipoxygenase activity. *Biochim. Biophys. Acta.* 1437:63-70.

Hird, S. N., and J. G. White. 1993. Cortical and cytoplasmic flow polarity in early embryonic cells of *Caenorhabditis elegans*. *J. Cell Biol.* 121:1343-1355.

Hoey, J. G., and R. H. Gavin. 1992. Localization of actin in the Tetrahymena basal body-cage complex. *J. Cell Sci.* 103: 629-641.

Huxley, H. E. 1963. Electron microscope studies on the structure of natural and synthetic protein filaments from striated muscle. *Jour. Mol. Biol.* 7:281-308.

Jagadeeswaran, P., J. P. Sheehan, F. E. Craig, and D. Troyer. 1999. Identification and characterization of zebrafish thrombocytes. *Br. J. Haematol.* 107:731-738.

Janmey, P. A., U. Euteneuer, P. Traub, and M. Schliwa. 1991. Viscoelastic properties of vimentin compared with other filamentous biopolymer networks. *J. Cell Biol.* 113:155-160.

Joseph-Silverstein, J., and W. D. Cohen. 1984. The cytoskeletal system of nucleated erythrocytes. III. Marginal band function in mature cells. *J. Cell Biol.* 98:2118-2125.

Kadota, A., and M. Wada. 1995. Cytoskeletal aspects of nuclear migration during tip-growth in the fern *Adiantum protonema* cell. *Protoplasma.* 188:170-179.

Kahn, M. L., Y. W. Zheng, W. Huang, V. Bigornia, D. Zeng, S. Moff, R. V. Jr. Farese, C. Tam, and S. R. Coughlin. 1998. A dual thrombin receptor system for platelet activation. *Nature.* 394:690-694.

Kann, M. L. and J. P. Fouquet. 1989. Comparison of LR white resin, Lowicryl K4M and Epon postembedding procedures for immunogold staining of actin in the testis. *Histochemistry.* 91: 221-226.

Kim, S., M. Magendantz, W. Katz, and F. Solomon. 1987. Development of a differentiated microtubule structure: formation of the chicken erythrocyte marginal band in vivo. *J. Cell Biol.* 104:51-59.

Kowit, J. D., R. W. Linck, and D. M. Kenney. 1988. Isolated cytoskeletons of human blood platelets: dark-field imaging of coiled and uncoiled microtubules. *Biol. Cell.* 64:283-291.

Lee, K-G, A. Braun, I. Chaikhoutdinov, J. DeNobile, M. Conrad, and W. Cohen. 2002. Rapid visualization of microtubules in cells of marine model organisms. *Biol. Bull.* 203:204-206.

Lee, K-G., and W. D. Cohen. 1998a. Co-localization of F-actin and marginal band tubulin in the cytoskeleton of salamander erythrocytes. 38th ASCB annual meeting.

Lee, K-G., Z. Koroleva, and W. D. Cohen. 1999. Association of F-actin with marginal bands of both erythrocytes and thrombocytes. 39th ASCB annual meeting.

Lee, K-G., T. Miller, A. Williams, and W. D. Cohen. 2001. Evidence of Actin-Microtubule Interaction in Erythrocyte Marginal Bands. 41st ASCB annual meeting.

Lee, K-G., N. Mohan, Z. Koroleva, L.-F. Huang, and W. D. Cohen. 1998b. Fluorescence localization of cytoskeletal proteins in fibrin-trapped cells. *Biol. Bull.* 195: 211-212.

Lema-Foley, C., K. G. Lee, T. Parris, Z. Koroleva, N. Mohan, P. Noailles, W. D. Cohen. 1999. Reversible alteration of morphology in an invertebrate erythrocyte: properties of the natural inducer and the cellular response. *Biol. Bull.* 197:395-405.

Lin, C. H., and P. Forscher. 1993. Cytoskeletal remodeling during growth cone-target interactions. *Cell Biol.* 121:1369-83.

Lloyd-Evans, P., S. E. Barrow, D. J. Hill, L. A. Bowden, G. E. Rainger, J. Knight, and A. F. Rowley. 1994. Eicosanoid generation and effects on the aggregation of

thrombocytes from the rainbow trout, *Oncorhynchus mykiss*. *Biochim. Biophys. Acta.* 1215:291-299.

Mainwaring, G., and A. F. Rowley. 1985. Separation of leucocytes in the dogfish (*Scyliorhinus canicula*) using density gradient centrifugation and differential adhesion to glass coverslips. *Cell Tissue Res.* 241:283-290.

Mantur, M., N. Wolosowicz, J. Prokopowicz, and R. Kemona. 1986. System for testing the phagocytic capacity of human blood platelets. *Folia. Haematol. Int. Mag. Klin. Morphol. Blutforsch.* 113:685-689.

Mazia, D., G. Schatten, and W. Sale. 1975. Adhesion of cells to surfaces coated with polylysine. Applications to electron microscopy. *J. Cell Biol.* 66:198-200.

McGough, A., W. Chiu, and M. Way. 1998. Determination of the gelsolin binding site on F-actin: implications for severing and capping. *Biophys. J.* 74: 764-772.

McIntosh, J. R., and K. R. Porter. 1967. Microtubules in the spermatids of the domestic fowl. *J. Cell Biol.* 35:153-173.

Mills, J. C., N. L. Stone, J. Erhardt, and R. N. Pittman. 1998. Apoptotic membrane blebbing is regulated by myosin light chain phosphorylation. *J. Cell Biol.* 140:627-636.

Mineyuki, Y., and B. A. Palevitz. 1990. Relationship between prophase band organization, F-actin and the division site in *Allium*. Fluorescence and morphometric studies on cytochalasin-treated cells. *J. Cell Sci.* 97:283-295.

Morgenstern, E., M. Daub, and R. Dierichs. 2001. A new model for in vitro clot formation that considers the mode of the fibrin(ogen) contacts to platelets and the arrangement of the platelet cytoskeleton. *Ann. N.Y. Acad. Sci.* 936:449-455.

Mooseker, M. S., and L. G. Tilney. 1975. Organization of an actin filament-membrane complex. Filament polarity and membrane attachment in the microvilli of intestinal epithelial cells. *J. Cell Biol.* 67: 725-743.

Nachmias, V. T. 1980. Cytoskeleton of human platelets at rest and after spreading. *J. Cell Biol.* 86:795-802.

Nemhauser, I., J. Joseph-Silverstein, and W. D. Cohen. 1983. Centrioles as microtubule-organizing centers for marginal bands of molluscan erythrocytes. *J. Cell Biol.* 96: 979-989.

Ostap, E. M. 2002. 2,3-Butanedione monoxime (BDM) as a myosin inhibitor. *J. Muscle Res. Cell Motil.* 23:305-308.

O'Toole, E. T., R. R. Hantgan, J. C. Lewis. 1994. Localization of fibrinogen during aggregation of avian thrombocytes. *Exp. Mol. Pathol.* 61:175-190.

Passer, B. J., C. H. Chen, N. W. Miller, and M. D. Cooper. 1997. Catfish thrombocytes express an integrin-like CD41/CD61 complex. *Exp. Cell Res.* 234:347-353.

Pellizzon, C. H. and L. O. Lunardi. 2000. Endocytic activity in the thrombocytes of the turtle *Phrynopys hilarii* (freshwater South American species). *J. Submicrosc. Cytol. Pathol.* 32:651-656.

Pica, A., A. Lodato, M. C. Grimaldi, and F. Della Corte. 1990. Morphology, origin and functions of the thrombocytes of *Elasmobranchs*. *Arch. Ital. Anat. Embriol.* 95:187-207.

Pinkhasov, R. M., K. G. Lee, and W. D. Cohen. 2003. Marginal band function in unactivated nucleated thrombocytes 43rd ASCB annual meeting.

Pittman, S., M. Geyp, M. Fraser, K. Ellem, A. Peaston, and C. Ireland. 1997. Multiple centrosomal microtubule organising centres and increased microtubule stability are early features of VP-16-induced apoptosis in CCRF-CEM cells. *Leuk. Res.* 21:491-499.

Ramachandran, I., M. Terry, and M. B. Ferrari. 2003. Skeletal muscle myosin cross-bridge cycling is necessary for myofibrillogenesis. *Cell Motil. Cytoskeleton.* 55:61-72.

Reed, W., J. Avolio, and P. Satir. 1984. The cytoskeleton of the apical border of the lateral cells of freshwater mussel gill: structural integration of microtubule and actin filament-based organelles. *J. Cell Sci.* 68:1-33.

Riparbelli, M. G., and G. Callaini. 1995. Cytoskeleton of the *Drosophila* egg chamber: new observations on microfilament distribution during oocyte growth. *Cell Motil. Cytoskeleton.* 31:298-306.

Rowley, A. F., T. C. Hunt, M. Page, and G. Mainwaring. 1988. Fish. In: A. F. Rowley, and N. A. Ratcliffe, editors. *Vertebrate Blood Cells.* Cambridge: Cambridge University Press, 19-127.

Ruhrberg, C. and F. M. Watt. 1997. The plakin family: versatile organizers of cytoskeletal architecture. *Curr. Opin. Genet. Dev.* 7:392-397.

Saito, S., S. Watabe, H. Ozaki, N. Fusetani, and H. Karaki. 1994. Mycalolide B, a novel actin depolymerizing agent. *J. Biol. Chem.* 269: 29710-29714.

Sakamoto, H., M. Ueno, W. Yangbong, R. Khatun, S. Tanaka, I. Miyabe, Y. Ogawa, and M. Onodera. 2000. Glycoprotein Ibalpha-bound thrombin functions as a serine

protease to producemacromolecular activators of phagocytosis from platelets. *Biochem. Biophys. Res. Commun.* 270:377-382.

Sanchez, I., and W. D. Cohen. 1994a. Localization of tau and other proteins of isolated marginal bands. *Cell Motil Cytoskeleton.* 27: 350-360.

Sanchez, I., and W. D. Cohen. 1994b. Assembly and bundling of marginal band microtubules protein: role of tau. *Cell Motil. Cytoskeleton.* 29:57-71.

Sanchez, I., L. H. Twersky, and W. D. Cohen. 1990. Detergent-based isolation of marginal bands of microtubules from nucleated erythrocytes. *Eur. J. Cell. Biol.* 52:348-358.

Sanger, J. M. and J. W. Sanger. 1980. Banding and polarity of actin filaments in interphase and cleaving cells. *J. Cell Biol.* 86:568-575.

Schwer H. D., P. Lecine, S. Tiwari, J. E. Jr. Italiano, J. H. Hartwig, and R. A. Shivdasani. 2001. A lineage-restricted and divergent beta-tubulin isoform is essential for platelet biogenesis, structure and function. *Curr. Biol.* 11:579-586.

Selden, L.A., L. C. Gershman, and J. E. Estes. 1980. A proposed mechanism of action of cytochalasin D on muscle actin. Biochem Biophys Res Commun. 95:1854-1860.

Senderowicz, A.M., G. Kaur, E. Sainz, C. Laing, W. D. Inman, J. Rodriguez, P. Crews, L. Malspeis, M. R. Grever, and E. A. Sausville. 1995. Jasplakinolide's inhibition of the growth of prostate carcinoma cells in vitro with disruption of the actin cytoskeleton. *J. Natl. Cancer Inst.* 87:46-51.

Shepro, D., F. A. Belamarich, and R. Branson. 1966. The fine structure of the thrombocyte in the dogfish (*Mustelus canis*) with special reference to microtubule orientation. *Anat. Rec.* 156:203-214.

Silverman-Gavrila, R. V., and A. Forer. 2003. Myosin localization during meiosis I of crane-fly spermatocytes gives indications about its role in division. *Cell Motil. Cytoskeleton.* 55:97-113.

Spector, I., N. R. Shochet, D. Blasberger, and Y. Kashman. 1989. Latrunculins--novel marine macrolides that disrupt microfilament organization and affect cell growth: I. Comparison with cytochalasin D. *Cell Motil. Cytoskeleton.* 13:127-144.

Strome, S. 1993. Determination of cleavage planes. *Cell.* 72:3-6.

Takakuwa, R., Y. Kokai, T. Kojima, T. Akatsuka, H. Tobioka, N. Sawada, and M. Mori. 2000. Uncoupling of gate and fence functions of MDCK cells by the actin-depolymerizing reagent mycalolide B. *Exp. Cell Res.* 257: 238-244.

Takeuchi, K., K. Kuroda, M. Ishigami, and T. Nakamura. 1990. Actin cytoskeleton of resting bovine platelets. *Exp. Cell Res.* 186:374-380.

Tanaka, K., and K. Itoh. 1998. Reorganization of stress fiber-like structures in spreading platelets during surface activation. *J. Struct. Biol.* 124:13-41.

Traver, D., B. H. Paw, K. D. Poss, W. T. Penberthy, S. Lin, and L. I. Zon. 2003. Transplantation and in vivo imaging of multilineage engraftment in zebrafish bloodless mutants. *Nat. Immunol.* 4:1238-1246.

Urbanik, E., and B. R. Ware. 1989. Actin filament capping and cleaving activity of cytochalasins B, D, E, and H. *Arch. Biochem. Biophys.* 269:181-187.

Vinckier, A., I. Heyvaert, A. D'Hoore, T. McKittrick, C. Van Haesendonck, Y. Engelborghs, and L Hellemans. 1995. Immobilizing and imaging microtubules by atomic force microscopy. *Ultramicroscopy.* 57:337-343.

Wang, X., C. A. Herman. 1997. Eicosanoid synthesis by purified thrombocytes and erythrocytes from warm- and cold-acclimated American bullfrogs (*Rana catesbeiana*). *Gen. Comp. Endocrinol.* 106:138-144.

Waugh, R. E., and G. Erwin. 1989. Flexural rigidity of marginal bands isolated from erythrocytes of the newt. 108:1711-1716.

Waugh, R. E., G. Erwin, and A. Bouzid. 1986. Measurement of the extensional and flexural rigidities of a subcellular structure: marginal bands isolated from erythrocytes of the newt. *J. Biochem. Eng.* 108: 201-207.

Weisenhorn, A. L., B. Drake, C. B. Prater, S. A. Gould, P. K. Hansma, F. Ohnesorge, M. Egger, S. P. Heyn, and H. E. Gaub. 1990. Immobilized proteins in buffer imaged at molecular resolution by atomic force microscopy. *Biophys. J.* 58:1251-1258.

White, J. G. 1971. Platelet morphology. In: S. A. Johnson, editor. *The Circulating Platelet.* London: Academic Press, 46.

White, J. G., and C. C. Clawson. 1980. The surface-connected canalicular system of blood platelets -- a fenestrated membrane system. *Am. J. Pathol.* 101:353-364.

White, J.G., and C. C. Clawson. 1982. Effects of small latex particle uptake on the surface connected canalicular system of blood platelets: a freeze-fracture and cytochemical study. *Diap. Histopathol.* 5:3-10.

White, J. G., Rao, G. H. R., Gerrard, J. M. 1974. Effects of the ionophore A23187 on blood platelets. I. Influence on aggregation and secretion. *Am. J. Pathol.* 77:135.

Winckler, B., and F. Solomon. 1982. A role for microtubule bundles in the morphogenesis of chicken erythrocytes. *Proc. Natl. Acad. Sci. U. S. A.* 88: 6033-6037.

Yoshida, T., S. O. Ioshii, K. Imanaka-Yoshida, and K. Izutsu. 1994. Association of cytoplasmic dynein with manchette microtubules and spermatid nuclear envelope during spermiogenesis in rats. *J. Cell Sci.* 107:625-633.

Zucker, M. B., and V. T. Nachmias. 1985. Platelet activation. *Arteriosclerosis.* 5:2-18.

PUBLICATIONS

Lee, K-G., N. Mohan, Z. Koroleva, L.-F. Huang, and W. D. Cohen. 1998b. Fluorescence localization of cytoskeletal proteins in fibrin-trapped cells. *Biol. Bull.* 195: 211-212.

Lee K-G, A. Braun, I. Chaikhoutdinov, J. DeNobile, M. Conrad, and W. Cohen. 2002. Rapid visualization of microtubules in cells of marine model organisms. *Biol. Bull.* 203:204-206.

Lee, K.-G., T. Miller, I. Anastassov, and W. D. Cohen. 2004. Shape transformation and cytoskeletal reorganization in activated non-mammalian thrombocytes. *Cell Biol. Int.* 28:299-310.